A PORTABLE ELECTROCHEMICAL BIOSENSOR FOR DETECTION OF LISTERIA MONOCYTOGENES

by

OR ZOLTI

(Under the Direction of Ramaraja P. Ramasamy)

ABSTRACT

Foodborne pathogens are infectious biological agents such as bacteria or viruses present in food or water that cause mild to severe diseases, that could lead to hospitalization, or even death. Food borne diseases have a significant impact on public health, nation's healthcare infrastructure and the economy. It is important to diagnose and detect these pathogens early in the food distribution and supply chain in order to avoid expensive recalls and major outbreaks. Among these pathogens, *Listeria monocytogenes* is the cause of 23 % of all foodborne pathogen outbreaks in the United States since 2019 and caused hospitalization of 93 % in confirmed cases. At present, culture-based microbiological or molecular diagnostic methods are used that require laboratory tests and take anywhere from two to five days for results. Biosensors could present an alternative to conventional laboratory-based methods for rapid and early detection of the pathogens. The dissertation focuses on the development of an electrochemical biosensor on a portable diagnostic platform that is capable of detecting *Listeria monocytogenes* in both buffer and in simple food-matrix such as chicken broth. The detection approach was an electrochemical biosensor, with bacteriophage as recognition molecule immobilized on a carbon nanotube modified glassy carbon (GC) and a portable screen printed (SP) electrodes. The detection signal was generated through an

electrochemical impedance spectroscopy (EIS) and was done under stationary and flow conditions with sample volumes of up to 100 µL. The biosensors showed very high sensitivity and selectivity with a limit of detection below 10 CFU/mL in pure samples. The dissertation research demonstrates the feasibility of this biosensor for use in food diagnostics as well as provide a scientific foundation for development of similar electrochemical sensing platform for detection of other bacterial cells.

INDEX WORDS: Electrochemical biosensor, Food safety, Bacteriophage, Microfluidics, Impedance spectroscopy, *Listeria monocytogenes*, Rapid diagnostics, Carbon Nanotubes, Electrochemistry.

A PORTABLE ELECTROCHEMICAL BIOSENSOR FOR DETECTION OF LISTERIA MONOCYTOGENES

by

OR ZOLTI

BS, Ben-Gurion University in the Negev, Israel, 2014

MS Materials Science and Engineering, Tel-Aviv University, Israel, 2017

A Dissertation Submitted to the Graduate Faculty of The University of Georgia in Partial Fulfillment of the Requirements for the Degree

DOCTOR OF PHILOSOPHY

ATHENS, GEORGIA

2023

A PORTABLE ELECTROCHEMICAL BIOSENSOR FOR DETECTION OF LISTERIA MONOCYTOGENES

by

OR ZOLTI

Major Professor:	Ramaraja P. Ramasamy
Committee:	William S. Kisaalita
	Eric Freeman
	Leidong Mao
	Jose I. Reyes de Corcuera

Electronic Version Approved:

Ron Walcott
Vice Provost for Graduate Education and Dean of the Graduate School
The University of Georgia
May 2023

DEDICATION

Dedicated to my family and friends

Who is a wise man? He who learns from every man. As is stated (Psalms 119:99): "From all my teachers I have grown wise"; Who is a Hero? He who controls his impulses. As is stated (Proverbs 16:32), "Better one who is slow to anger than one with might, one who rules his spirit than the captor of a city."; Who is a rich man? He who is happy with his portion. As is stated (Psalms 128:2): "If you eat of toil of your hands, fortunate are you, and good is to you"; "fortunate are you" in this world, "and good is to you" in the World to Come; Who is an honorable man? He who honors his fellow man; As is stated (I Samuel 2:30): "For to those who honor me, I accord honor; those who scorn me shall be demeaned;".

—**Rabbi Simeon Ben Zoma** (Pirkei Avot, Chapter 4a)

ACKNOWLEDGEMENTS

I want to thank my advisor, Dr. Ramasamy, for his guidance, mentorship, and help throughout the degree. Dr. Ramasamy's guidance, kindness, and continuous support during these years helped me to improve my capabilities and to develop real passion for research.

I want to thank my committee members, Dr. William Kisaalita, Dr. Leidong Mao, Dr. Eric Freeman, and Dr. Jose Reyes de Corcuera for their advice, support, and suggestions. Your availability at different stages of my Ph.D. along with your constructive advice and criticism have been proven priceless in the road to achieve this degree.

I highly appreciate Dr. Francisco Diez-Gonzalez, Director Center for food safety, Dr. Nikki Shariat, Assistant Professor, Department of Population Health, and Dr. Christine Szymanski, Professor Department of Microbiology, for kindly providing the *Listeria monocytogenes* Scott A, *Salmonella enterica* subsp. enterica serotype Typhimurium 291RH, and *Escherichia coli* O157:H7, respectively.

I thank the help of Dr. Jason Locklin, Dr. Evan White, Mr. Ryan Maynard, Mr. Ethan Stinchcomb, Ms. Caitlin Cato, and Dr. Kun Yao for their help, guidance, and their expertise that allowed this work to be completed.

I want to express my appreciation for my current and past lab members: Dr. Yi Fang, Dr. Hamid Asadi, Dr. Baviththra Suganthan, Ms. Alyssa Ghuman, Mr. Sanket Nagdeve, Ms. April A. Rains, Mr. Austin Duncan, Ms. Dilmeet Kaur, Mr. Sankaranarayanan Venkatakrishnan, Ms. Alexa T. Hansen, Ms. Anna Baber, and Mr. Dominik Groh. Having you in the lab made it feel less like a job and more like a family. For advice, conversations, jokes, coffee, and many more experiences

in the last five years. You are amazing people and I hope you will continue to succeed in all your future endeavors.

And last but not least to my family and friends around the world, for the support, push, and kindness. I wouldn't have been able to finish this work without you.

TABLE OF CONTENTS

Page

LIST OF TABLES

Page

LIST OF FIGURES

Page

CHAPTER 1

THEORETICAL BACKGROUND

1.1. Foodborne Pathogens

Foodborne pathogens are bacteria, viruses, fungi, and parasites that can be found in food or water items and cause disease after consumption. An outbreak of foodborne disease is defined by the center of disease control and prevention (CDC) as at least two cases of similar illness resulting from the consumption of food from the same source [1]. There are over 200 different kinds of food related diseases, while their severity is increase among children, the elderly, and immunocompromised individuals [2]. Foodborne disease cost in the United States is estimated by the federal government to 17.6 billion dollars annually [3]. According to the world health organization (WHO) almost one in ten people in the world will fall ill due to foodborne pathogens. The WHO also mentions that foodborne illness impede global socioeconomic development to the strain on healthcare systems and the effect on tourism and trade [4]. Most infections of foodborne pathogens in the United States are due to low hygiene practices in the production factory or kitchen. Foodborne pathogens can be found on working surfaces, different kitchen appliances, refrigeration units, and shelves [5].

The most common foodborne pathogen that causes diseases are bacteria. The foodborne bacteria exist in a variety of shapes, types and prototypes. Some of the bacteria are psychrotrophs and can multiply in temperatures of down to 4 ^{o}C like *Listeria monocytogenes* and *Yersinia enterocoliticia*. Alternatively, some of the bacteria form spores, like *Clostridium botulinum*, or producing heat resistant toxins, like *Staphylococus aureus*, which make them highly heat-resistant.

Overall their optimum growing temperature is 30 ºC to 40 ºC [6]. Viruses are another cause for foodborne illness, and there are over 100 types that can cause it. The most common foodborne viruses are Norovirus and Hepatitis A. which mostly transmit via shellfish due to human fecal contamination in their native waters and are less affected than bacteria to depuration cleaning processes that intended to remove them, another reason for their infectivity through shellfish is that human consume shellfish with their digestive track and mostly raw or undercooked [7,8]. Foodborne parasites are organisms that are bigger than bacteria but unlike bacteria do not reproduce inside food, only inside a host. They can be transmitted from animals to humans, humans to humans, or humans to animals. The most common foodborne parasites are *Cyclospora Cayetanensis* and *Toxoplasma gondii* and they are mostly common in low and middle income countries [9]. In the last two years in the US there have been outbreaks of *Listeria monocytogenes* (mushrooms, deli meats, dairy), *Salmonella spp*. (sprouts and fish), Norovirus (oysters), *E. coli* O157:H7 (beef, ready to eat foods, spinach) and *Salmonella spp.* (peanut butter) [10].

1.2. Biosensors:

The illness and outcomes of foodborne pathogens are affecting the whole world, and hence the detection of pathogens, pollutants, hazardous biomolecules, and other harming agents is a crucial part of dealing with the issue. The gold standard for foodborne pathogens detection is culture-based methods. Samples are taken at specific control points during the manufacturing and distribution process, cultivated on a nutrient-filled medium, plated, and tested with visual, biochemical, and immunological means before and after enrichment. Although very accurate, this method is not ideal due to the long processing time, sample transportation, robustness, and expensive skilled labor and equipment [11–15]. To overcome these shortcomings, the industry needs a faster and cost-efficient detection method with similar or even better sensitivity to comply

with modern food and safety standards [16–18]. These concerns have encouraged researchers to improve current methods and develop new analytical methods.

Biosensors are analytical devices measuring a specific biological analyte or reaction by utilizing a biorecognition molecule to generate a signals [19,20]. They exhibit very high sensitivity and specificity in a simple to use platform [21]. They are incorporated in many different fields such as: drug discovery, food safety, process control, and environmental monitoring. In the food industry biosensors are in use to detect foodborne pathogens in food samples and to verify the freshness of different produce products by analyzing volatile organic compounds that they release once spoiled [22]. Biosensors consist of biorecognition molecule, a nanomaterial (not always), a transducer that translate those reactions from a readable quantifiable signal, a signal manipulator that amplify the signal and filter out some of the noise, a computing unit that analyze the signals and produces the wanted results, and a display that show these results to the user. All of these components are presented in Figure 1.

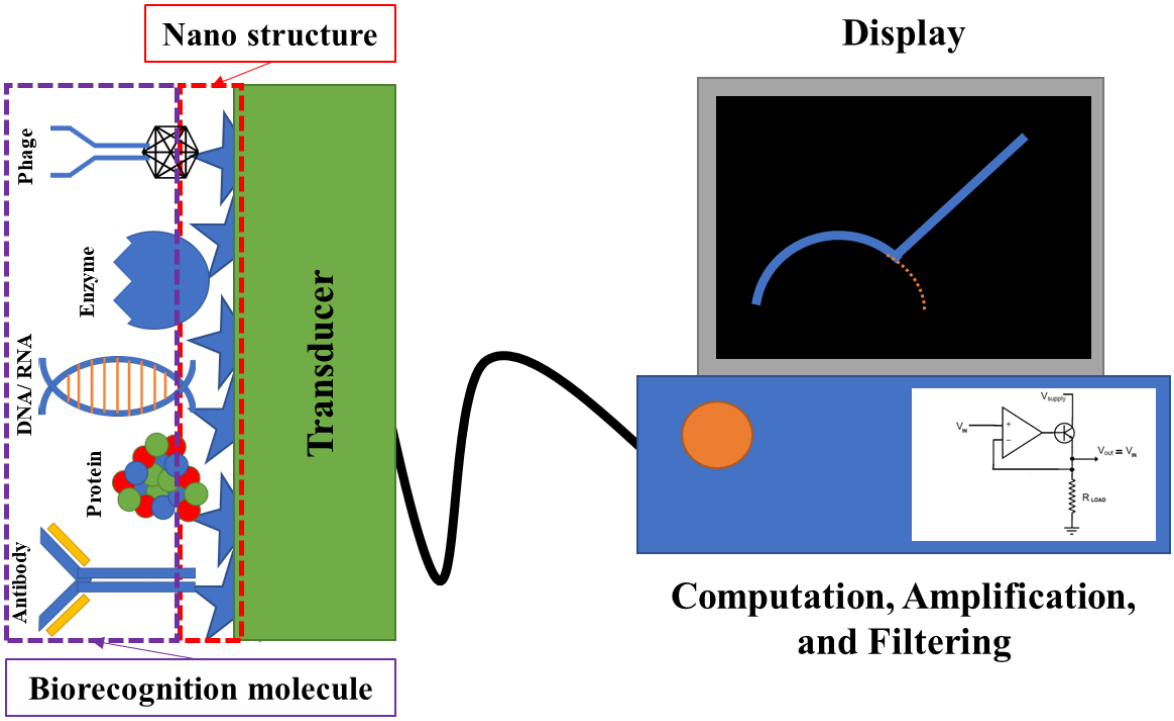

Figure 1: Biosensor components

Biorecognition molecules can be antibody, proteins, nucleic acids (RNA, DNA), enzymes, bacteriophages, and many others. When the target analyte is interacting with the biorecognition element it forms an analog continuous signal according to the amount of detection events that happen. In some cases, the biorecognition elements will be connected to the surface of the transducer through a nanostructure like nanowires, nanotubes, or other to increase the surface area and allow more biorecognition molecules and therefore more interactions between target analyte and biorecognition elements. The transducer is turning the analog signal from the interaction and translate it to an electrochemical, electric, magnetic, optical, colorimetric or gravimetric signal to enable qualitative or quantitative detection.

There are many parameters that make biosensors comparable: sensitivity, selectivity, detection range, reliability, areas of linearity, signal-to-noise ratio, limit of detection, limit of quantification, and time of detection. Sensitivity is comprised of two main terms. The first term in

threshold which describes the lowest concentration of analyte the biosensor can reliably find, and the second is the resolution that determine the minimal change in concentration the biosensor can differentiate this is the major factor in choosing a transducer. Selectivity is the ability of the sensor to reliably detect its target and stay unresponsive to other contaminants or pseudo-analytes this variable is the major factor when choosing a biorecognition molecule. The detection range is the range of concentrations in which the biosensor can produce a signal from a detection event this range is usually determined by one or more linear correlation areas in which the change in concentration linearly change the output signal the slope of the linear correlation is a quantifiable measure of the resolution. Reliability is the parameter that describes the ability of the biosensor to give the same signal from two or more detection attempts under the same conditions. Signal-to-noise ratio is a parameter that describe the variability of the output signal around the average detection measurement with or without the presence of target analyte. Limit of detection is the lowest concentration of analyte the biosensor can reliably detect, and limit of quantification is the lowest concentration the biosensor can reliably quantify. There are multiple ways to determine both limits.

The biosensors market is a very profitable global arena with a market size of US$ 27.5 billion in 2021 and a projection of reaching ~US$ 50 billion by 2030, as seen in Figure *2*, with a compound annual growth rate (CAGR) of 7.7-8 % according to market reports of 2022. Many large companies operating and developing the biosensors market, among them Bio-Rad Laboratories Inc., Abbott Laboratories, Biosensors International Group Ltd., DuPont Biosensor Materials, Johnson & Johnson, and many other. The major transducers used in the biosensor industry as of 2022 are electrochemical, thermal, optical, and piezoelectric while electrochemical biosensors have the largest revenue with 71 % of the market and optical biosensors are reported as

the fastest growing. While point of care (POC) biosensor devices are reported to have the largest share of the market with 50 %, the reports also show that the food industry is the fastest growing, where the major detection targets are foodborne pathogens in food processing plants and in preservatives [23–25].

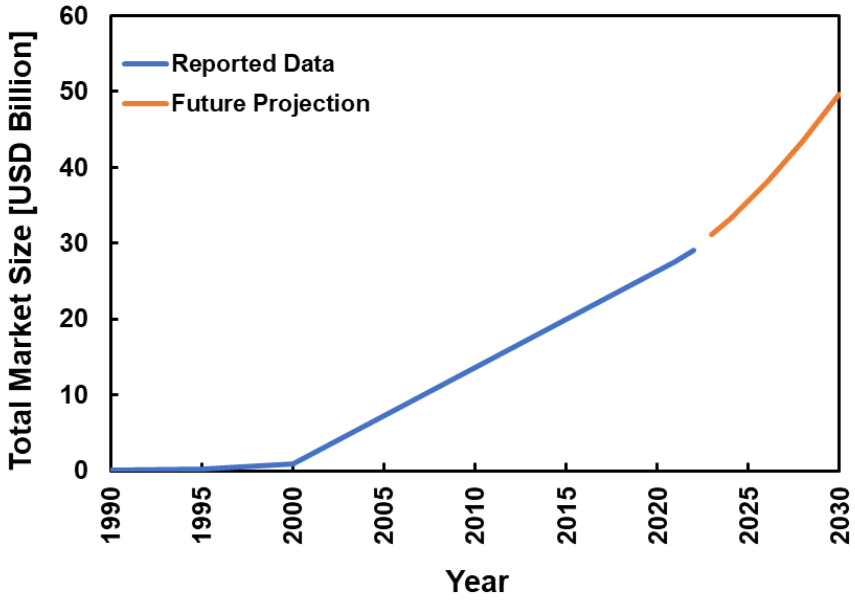

Figure 2: Biosensor Global Market Annual Growth

1.2.1. Transduction Methods of Biosensors

There are many different types of transducers for biosensors, the most common are electrochemical, thermal, optical and piezo-electric. Piezo-electric transducer translating the mass change due to the bonding of the target analyte with the biorecognition molecule into a change in the frequency of a crystal resonance. The frequency of the oscillation decrees as the surface mass increase that can be measured and quantified. Piezo-electric transducers are compatible with liquid and volatile samples and piezo-electric biosensors have been reported to detect foodborne pathogens with a LOD of 8000 CFU/mL without nanostructures and down to 20 CFU/mL when gold nanoparticles were integrated [23,26].

Optical transducers translate the binding on the surface into an optical signal that can be measured. The optical signal can be reflectance, absorbance, luminescence or fluorescence and is mostly collected with the use of optical fibers or waveguides. Optical transducers are not susceptible to electric or magnetic fields and are compatible to liquid and volatile samples. The sensitivity of optical biosensors is down to a single molecule [27,28].

Thermal transducers utilize the heat absorption or evolution due to the interaction between the target analyte and the biorecognition molecule. This method is monitoring the temperature within the sample. The heat change can be measured directly or by monitoring the change in temperature of the circulating fluid following the reaction [29,30].

The most common and the focus of this work are electrochemical transducers. Electrochemical transducers translate the interaction between the target analyte and the biorecognition molecule into electric signals. They possess very high sensitivity, low detection limit, simplicity of use, and quick detection time. Electrochemical transducers require liquid samples, they are compatible with miniaturization which is emphasized by their ability to work with extremely low sample volumes. An electrochemical transducer can work in different modes according to electric signal it monitors. Potentiometric transducers measure the change in electric potential between the working electrode where the interaction happen to a reference electrode. Amperometric transducers will measure the electric current between the work and a counter electrode due to a reduction-oxidation of an electroactive couple. Impedimetric transducers measure the resistance and capacitance changes of the surface of interaction between the analyte and the biorecognition molecule under an alternating current at a single or multiple frequencies [31–33].

1.2.2. Biorecognition Molecules

The biorecognition molecules can be either natural or synthetic. Natural biorecognition molecules are the kind that can be naturally found in nature and the main ones used are enzymes, antibodies, nucleic acids, and bacteriophages. Enzymes are biocatalysts that specifically find their substrates and catalyze their transformation and come with a variation of some physicochemical parameters into different molecules. Naturally every cellular metabolic process requires enzymes to allow the quick reaction. Enzymes in biosensors will be immobilized close to the transducer, and the transduction will monitor the changes in either substrate, products, or the physical characteristics in the sample (heat, magnetism, etc.). Enzymes suffer from low stability due to their proteic nature. They are susceptible to environmental changes which may cause their activity to go down [34,35].

Antibodies are large proteins used by the immune system to find and defuse pathogens in the body, while each antibody is specific to a specific threat and therefore are designed by nature to be a specific biorecognition receptor. In a biosensor, the antibody will be immobilized near the transducer and will strongly attach to their target upon collision. This attachment can be monitored and translated by the transducer. The biggest disadvantages of antibodies are their susceptibility to environmental conditions and the difficulty to immobilize them in the needed orientation [36–38].

Nucleic acids are naturally occurring biopolymers that make the genetic material and act as the primary information source of the cell. There are two major classes of nucleic acids and they are deoxyribonucleic acid (DNA) and ribonucleic acid (RNA). The main difference between the two is sugar molecule, where if it is deoxyribose, the chain will be DNA and if it is ribose, it will be RNA. The detection with nucleic acids as a biorecognition molecule is done by using a single

helix, a detecting probe, to attach only to its complementary probe sequence existing in the sample, by forming a series of hydrogen bonds. The specificity arises from the ability of the nucleotides to form these bonds only with the right counterpart, and hence for a specific sequence only the corresponding sequence can fit. The attachment of the two probes is called hybridization and in most cases for a successful detection at least 10^6 of the target probes should exist in the sample. To overcome this issue and detect at lower concentrations, there are different possible amplification steps the target sequence will go through before detection. Some other limitations of nucleic acid-based biosensors might be, the need for sample preparation, their inability to distinguish between live and dead targets, and the need for denaturation of the detection probe that naturally exist as a double strand and not as the single strand as needed for hybridization to happen [39,40].

Bacteriophages are viruses that target and infect bacteria. Due to their nature, as are antibodies, they are a naturally evolved biorecognition elements for their target bacteria and in nature regulates the microbial balance. Phages are very specific, reproduce quickly, and can survive in a wider range of environmental conditions that most other biorecognition molecules. Bacteriophage will only attach to live host, and hence are capable to distinguish between live and dead bacteria, they are also safe for humans, and are ubiquitous in nature. The biggest challenge of phage-based biosensors is to attach them in the right orientation to allow the capture of the target bacteria [41–43].

1.2.3. Nanomaterials use in Biosensors

Nano materials or nanostructures are defined by having at least one dimension that is smaller than 100nm, up to 15 X 10^3 atoms. Their dimensions give them physical and chemical properties that are unmatched by bigger structures. By having such small dimensions, nanomaterials exhibit unparallelly high surface to volume ratio. This quality made them extremely attractive for sensing transduction applications since by immobilizing them on the surface can increase tremendously the active detection area without increasing the planar size of the probe. Nanomaterials also improve the miniaturization, sensitivity, and specificity. In electrochemical biosensing the main nanomaterials that are used are carbon based (carbon nanotubes, graphene, etc.) and metal-oxide nanoparticles [44,45].

Carbon nanotubes (CNT) are nanomaterial that has a nanometric diameter and is composed of hexagonally connected carbons. The main two categories of CNT are single- and multi-wall and the difference relates to the amount of coaxial rolled layers. Both types of CNT are commonly used in biosensors due to their unique electrical and mechanical properties. CNT nanometric dimension is their diameter while their length can reach tens of microns [46].

Graphene is a two-dimensional sheet of hexagonally joint carbon atoms. Graphene and graphene structures like graphene-oxide and reduced graphene-oxide have unique physical and chemical properties. Graphene structures are usually used as they are or as part of nanocomposite with metallic nanoparticles. Graphene structures have shown to have great conductivity in their plane, but less so between two different sheets along the z-axis. Their biggest advantage in biosensing is that they do not have any “dead-zones”, which means that all of their surface is open for interaction or immobilization [47].

Metal-oxide nanoparticles have various electrical and photochemical properties that are affected by their size, surface area, and stability. Their advantages are biocompatibility, no ohmic loses in low currents due to their intrinsic n-type nature, and the ease of immobilizing different biorecognition molecules due to the abundant hydroxyl functional groups on their surface. They also have some major disadvantages such as organic-inorganic interfaces, reducing electron-hole recombination, and low stability at humid conditions [48,49].

1.3.Signal Analysis:

ECBS are very sensitive and specific but due to the logarithmic nature of pathogen concentrations pose a challenge in assessing some important parameters like, noise level, areas of linearity in the calibration curve, correctly finding the limit of detection (LOD), limit of Quantitation, and recovery rate [50]. Noise level of a sensor regards the variability of the measured signal due to anything other than the concentration of the target analyte [51], more about the calculation and assessment of noise levels and signal to noise ration can be found in appendix H. The area of linearity in the calibration curve is also known as the linearity of the sensor, reflects a sensor's response to changes in target analyte concentration in a constant rate for a specific concentration range. Linearity is very desirable at as large as possible concentration range but all sensors tend to have deviation from linearity [52–54]. The limit of detection is a sensor's characteristic that determines the lowest concentration of target analyte that can be reliably detected, it is calculated from the linear region of the calibration curve through various statistical analysis approaches [55,56]. The limit of quantitation is the lowest concentration of target analyte that can be quantitated with any degree of certainty. LOQ, like LOD, can be calculated using different accepted approaches although it is important to use the same method for the calculation of both [57,58]. The recovery rate of a sensor points to its capability to predict an unknown

concentration in a sample and measures the percentage of accuracy of a signal obtained by a controlled concentration [59].

1.3.1. Areas of Linearity:

The accuracy of the biosensor's response is determined by the linearity of the signal's values within the reliable detection range. The linearity of a biosensor will also define it's resolution and in some cases its limit of detection and hence is one of the most important performance characteristics of a biosensor [19,52–54]. There are various methods of determining areas of linearity like: ANOVA lack-of-fit, Mandel's test, and significance of quadratic term. In addition, there are some more commonly used although not as accurate numerically parameters such as correlation coefficient, standard deviation of regression, standard deviation of the slope, quality coefficients, and back calculated concentration relative error. The main challenge is to choose the right method since using different methods might give different and sometime contradicting results [60,61]. To measure the quality of the linear fitting, calibration residual plots are necessary along with confidence levels [62].

The first method of determining linearity is called linearity confidence test and is done via calibration plot and coefficients of correlation and determination method. The initial step in determining an area of linearity according to this method is to inspect the calibration curve. Although the correlation coefficient is widely used, it is not a good parameter for the determination of linearity since it is the ratio of variability explained by the model with regard to the total variability [61]. Alternatively, one should evaluate the existence of the experimental data within the confidence limits of the fitted model. The regression line is affected by each calibration point, and their individual leverage on it must be taken into account. The leverage is defined as the

amount of which the predicted value will change if the measured value was changed by one unit on the y-axis, as seen in eq. (10):

$$(1) \quad h_i = \frac{1}{n} + \frac{(x_i - \bar{x})^2}{\sum_{i=1}^{n}(x_i - \bar{x})^2}$$

Where h_i is the leverage score, n is the number of points, x_i is a known concentration of analyte, and $\bar{x}$ is the average concentration. This value is used to obtain the standard error of each measurement point at concentration x_i according to eq. (11):

$$(2) \quad s_{\hat{y}} = s_{y/x} \cdot \sqrt{h_i}$$

Where $s_{\hat{y}}$ is the standard error and $s_{y/x}$ is the residual standard deviation. The coefficient interval can be obtained from eq. (12):

$$(3) \quad CI = \hat{y} \pm t_{crit} \cdot s_{\hat{y}}$$

Where CI is the coefficient interval and t_{crit} is the t-student value for the required α and 2 degrees of freedom. The confidence region of the calibration curve is obtained by using the calculated CI against the concentration as seen in eq. (13):

$$(4) \quad PI = \hat{y} \pm t_{crit} \cdot s_{y/x} \cdot \sqrt{\frac{1}{m} + h_i}$$

Where m is the number of replicates used to obtain the mean signal for each calibration point. To assure the model fits the data, all points must be inside the region. The second approach is the residual plot method. This method can help detect outliers, influence points, lack of fit, and uneven variance. A residual is the error between the predicted value and the observed value. It is calculated according to eq. (14):

$$(5) \quad e_i = y - \hat{y}$$

In a good correlation function, the residuals will be normally distributed around y=0. The third method to calculate linearity is done via the response factor plot. In this method, a signal to concentration plot against standards with known concentration is plotted. The model of the computed response factors is traced as a central line along the calibration range along with two lines that are ±α (in percentage), according to the required confidence level, away from the median. As long as all the points lay between these outer lines, linearity can be assumed. The fourth method to find linearity is percent relative error (%RE) of back calculated concentrations. After a model have been used to fit the data, the calibration function is then used to back calculate the concentration from a given y value. The difference between the calculated value and the actual concentration is the error associate to the concentration of each standard when it is predicted by this model. Dividing this value by the actual concentration will give the %RE and all points within the linear range should be between ±15% to assume linearity [63,64]. An Example to each of the linearity confidence models is shown in Figure 3. As seen, although the coefficient of determination of this data is R^2=0.99 some of the points are outside the range of linearity with confidence of 95 %.

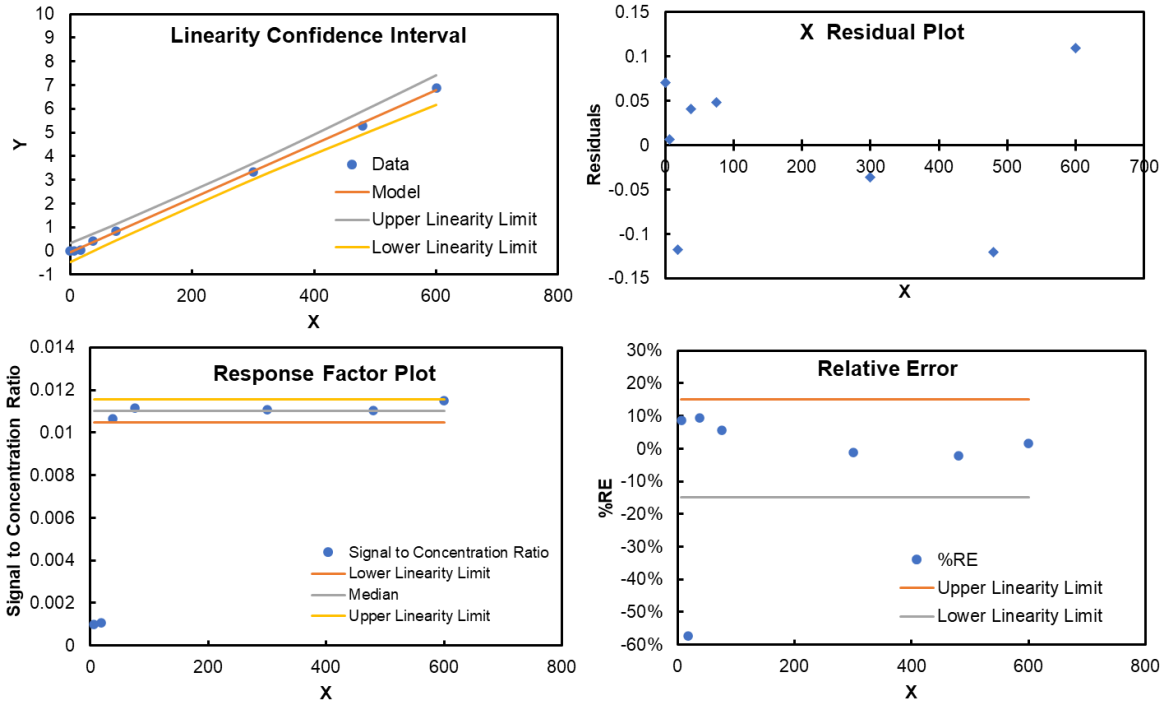

Figure 3: The different linearity models for a random series with a coefficient of determination (R^2=0.99) and for each method the confidence level was set to $\alpha = 0.05$.

1.3.2. Finding the Limits of Detection and Quantification:

The simplest used to assess the LOD is the value of the lowest point on the linear dynamic range. It is a simple approach and tend to overestimate the LOD [65,66]. Another approach is to determine the LOD according to the signal to noise ratio. In this method the ratio of a signal obtained from a known low concentration is divided by the standard deviation of the signal obtained from the blank solution. The LOD is the lowest concentration tested for which this ratio was 3 or above, this method is also known as the 6σ approach [67,68]. Next, the approach adopted by the International Union of Pure and Applied Chemistry (IUPAC) determines that the LOD is

determined by mean value and the standard deviation of the response to the blank solution along with the according to eq (15):

$$(6) \quad X_{LOD} = \overline{X}_{blank} + k\sigma_{blank}$$

Where X_{LOD} is the response value of the LOD concentration, X_{blank} is the mean response to the blank solution, k is numerical factor of the confidence level desired (3.3 for LOD and 10 for LOQ), and σ_{blank} is the standard deviation of the response to the blank solution. The value is then plugged into the equation of the calibration curve linear regime. It might provide LOD that is lower than the lowest point of the linear dynamic range [69,70]. The most popular method for the calculation of LOD and LOQ is using the standard deviation of the blank solution (SD_{blank}), multiply it by F (factor equals to 3.3 for LOD and 10 for LOQ), and then divide it by the slope of the calibration curve (b) as seen in eq. (16) [71]:

$$(7) \quad LOD = F \times \frac{SD_{blank}}{b}$$

The last method for the calculation of LOD and LOQ is linear regression. For this method, a linear region exists within a limited range of concentrations and can be represented by eq. (17):

$$(8) \quad y = a + bx$$

In addition, an assumption of no multicollinearity among the data points must be possible. With this method the LOD and LOQ is calculated according to eq. (18) and (19):

$$(9) \quad LOD = 3 \times \frac{S_a}{b}$$

$$(10) \quad LOQ = 10 \times \frac{S_a}{b}$$

Where b is the slope of the linear regime and S_a is the standard deviation of the response and is calculated by multiplying the standard error of the y-intercept or the y-residuals of the regression line with the square root of the number of points in the linear line as seen in eq. (20):

$$(11) S_a = S_d \times \sqrt{N}$$

Where S_d is the standard error of the x-intercept and N is the number of points in the linear regime. This method is compatible with one axis being logarithmic as long as the relationship show linearity [43,72,73].

1.3.3. Recovery Rate:

The recovery rate is a parameter that compares the concentration calculated from the calibration curves to the actual concentration placed on the biosensor. It is calculated in a similar way to the % RE and indicates the biosensor's capability to predict an unknown concentration according to the obtained signal [59]. An acceptable recovery rate within the linear regime of the calibration curve is ±15 % when using a known standard.

CHAPTER 2

LAB ON A CHIP ELECTROCHEMISTRY BIOSENSORS FOR FOODBORNE PATHOGEN DETECTION: A REVIEW OF STANDARDS AND RECENT PROGRESS

This chapter contains text from the following publication:

Or Zolti, Bavithithira Suganthan, and Ramaraja P. Ramasamy. Biosensors 215, 13(2), (2023): 215.

Reprinted here with permission of the publisher.

Abstract:

Foodborne pathogens are an important diagnostic target for food, beverage and healthcare industry due to their prevalence and the adverse effects they could cause to public health, food safety and the economy. The standards that determine whether a given type of food is fit for consumption are set by governments and must be taken under account when designing a new diagnostic tool such as a biosensor platform. In order to meet these stringent detection limit, cost and reliability standards, recent research is being focused on developing lab on a chip-based approaches for detection devices that use microfluidic channels and platforms. The microfluidics-based devices are designed, developed and used in different ways to achieve the established common standards for food pathogen testing that enable high throughput, rapid detection, low sample volume, and minimal pretreatment procedures. Combing microfluidic approaches with electrochemical biosensing could offer affordable, portable and easy to use devices for food pathogen diagnostics. This review presents an analysis of established common standards and the recent progress made in electrochemical sensors towards the development of future lab-on-a-chip devices that will aid 'collection-to-detection' using a single method and platform.

1. Introduction:

Foodborne pathogens include different infectious biological agents that cause disease and are found in different food or water products. Each year, the United States federal government estimates that there are 128,000 hospitalizations and 3000 deaths due to foodborne illness annually [74]. Foodborne illness outbreak is defined as at least two illnesses caused by the same pathogen and linked to the same infective source [75]. The year 2021 saw 17 reported foodborne illness outbreaks, resulting in 1424 cases of sickness, 379 hospitalizations, and seven deaths [76]. In addition to the health effects, the last published estimated cost of foodborne pathogens was 17.6 billion USD annually [3]. There is a high interest in the early detection of foodborne pathogens that will help minimize the public health and economic burden caused by foodborne illness.

The detection of foodborne pathogens can be carried out using various methods and kits. The food industry conducts periodic testing for microbial contamination at specific control points during manufacturing and delivery as the standard procedure [11,12]. The gold standard for the detection of foodborne pathogens is culture based and includes visual, biochemical, and immunological means before or after enrichment. In this method, a sample is introduced to a nutrient filled medium, incubated, grown, and plated. It is not ideal due to the time-consuming transportation, robustness, is expensive, and requires skilled labor [13–15]. It is even more problematic for industries in remote and rural areas that cannot afford the time and monetary cost of such procedures [16,17]. Due to these restraints, alternative detection methods have been developed where the most common are polymerase chain reaction (PCR) and enzyme-linked-immunosorbent assay (ELISA), which detect the pathogen by finding either a specific DNA or RNA sequence or a specific protein. Both PCR and ELISA will detect the pathogen quickly, but in most cases, cannot distinguish between live and dead bacteria in addition to being incompatible

with field conditions [15,77]. Another approach is to develop biosensors; these devices combine a biological recognition element (i.e., bacteriophage, antibody, enzyme, protein, etc.) with a transducer that transforms the interaction between the target pathogen and the biorecognition element to an electrical signal [78].

Electrochemical biosensors (ECBS) have an advantage with respect to other bio-sensors due to their selectivity, sensitivity, and relative simplicity of use. ECBS have several techniques, differentiated according to the electrical signal that is measured. The most common technique for foodborne pathogens is electrochemical impedance spectroscopy (EIS) due to its very high sensitivity but is limited by the alternating cur-rent (AC) potentiostat required for signal generation, which reduces its portability and increases the cost with respect to direct current (DC) methods [79–85]. In contrast, amperometric methods (i.e., cyclic voltammetry, chronoamperometry, linear sweep, etc.) have an advantage with low cost and an equivalent sensitivity to EIS. Their main disadvantages are the need to continuously correct their calibration due to Faraday's processes, higher sensitivity to mass transfer limitations in the solution, and relative high applied potential [80,86–89].

Microfluidics is a term describing the movement of fluids in geometrically restricted dimensions in orders of magnitude of 10−4 m or smaller and manipulate them at a µL-nL volume. In the field sensors, the initial use of microfluidics was to improve the sensor's performance and reduce the consumption of reagents. In addition, micro-fluidic channels enable the integration of separation, mixing, and monitoring within a single device. Advances in micro and nano fabrication techniques have proven to im-prove the synergy of new electrochemical biosensors and microfluidic designs to achieve better portability, reduce energy consumption, need of sample pretreatment, and better integrability of the systems into existing production lines. The

combination of microfluidics and biosensors have been a major vector in the development of new lab-on-a-chip (LOC) or miniaturized total analysis system (μTAS) platforms [86,90–92]. The major reasons for the focus on point of care LOC platforms is their ability to minimize the required pretreatment, automate all fluid handling, and the integration of sample preparation to detection on one easy to use device that is portable and does not require any specially trained personal or additional cost due to expensive equipment [93,94].

Foodborne pathogens ECBS have been the subject of many reviews in recent years. Mei et al. [95] focused mostly on carbon nano-materials on the surface of the electrochemical bio-sensor and their advantages in detecting foodborne pathogens. Villalonga et al. [96] focused on ECBS for food bioprocess monitoring, and Curulli et al. [97] focused on ECBS for food toxins and contaminants. All three reviews mentioned microfluidic channels, but the focus of those review articles was not specific toward ECBS platforms. Other recent reviews have focused more on the integration of microfluidics to ECBS and other biosensors, but have not placed an emphasis on foodborne pathogens [98,99]. Additionally, none of the foodborne pathogen biosensor reviews discussed and analyzed the established diagnostic standards accepted in the food industry or the health impact of foodborne diseases. Hence, it is clear that the need for a review that com-bines all three subjects is needed. This review starts with an overview of the established standards regarding foodborne pathogens that set the requirements for current and future detection methods. In addition, recent advances in LOC platforms for the detection of different pathogens will be analyzed, and the design and capabilities of both the microfluidic channels and biosensors will be discussed.

2. Foodborne Pathogens Statistics and Standards:

The standard that governs the standard for the allowed concentration of food-borne pathogens is set by governmental organizations. The standard of whether or not a product is fit for human consumption is set for each specific type of food products separately such as dairy, shellfish, ready to eat foods, etc. While some countries like Great Britain set quantitative limits that correspond to consuming population susceptibility and the infective dose, other countries like the United States of America have mostly set the standard on any detectable trace of these pathogens in the products tested [100–104]. These standards are affected by the minimum infective dose (MID) of each foodborne pathogen, and describe the detectable amount in a specific food or drink. Both the standards, MID, products that contain the pathogen, and the fitness of the tested sample for human consumption for the detected concentration are shown in Table 1. As seen in table 1, not all pathogens appear in both standards, which is due to its prevalence in that country. These standards will be mostly used during testing prior to the product reaching the consumer or during specific steps in the production and distribution chain [43,100–104]. It is important to also analyze the effect of the most common pathogens on the infected individuals. The biggest issue with such analysis is generated from the nature of the illness, which in most cases will be very mild and will not be diagnosed. The analysis shown in Figure 4 displays the percentage of hospitalization and mortality from the total number of con-firmed illnesses in the U.S. between 1996 and 2020. With the exception of Listeria monocytogenes, the mortality rate is low, but the hospitalization rate is over 20% for most of the common pathogens. The hospitalization rates can explain the high annual cost of foodborne pathogens and why they have received the focus as targets for different biosensors [3].

Table 1: Common foodborne pathogens, infection sources, epidemiological data, and standards.

Foodborne Pathogen	Food Products [100,105,106]	USDA minimum infective dose (MID) levels [Cells] [101,105,107–110]	British Standard [CFU/g] [100,101]	FDA Standard [CFU/g] [102–104]	Meaning [100–104]
Campylobacter spp.	Poultry, beef, dairy products, and untreated drinking water.	[a]400-500	>0.04	Any detectable presence [c]	Potential health hazard and unfit for human consumption
			<0.04	No detectable presence [c]	Fit for human consumption
Shiga toxin-producing *Escherichia coli*	Under cooked beef, dairy products made with unpasteurized milk or post pasteurization	10-100	>100	Any detectable presence [c]	Not fit for human consumption
			20-100	No detectable presence [c]	Farther testing is needed mostly still fit for human consumption
			<20		Fit for human consumption

	contaminated milk, vegetables, and untreated drinking water.				
Salmonella typhimurium	Eggs, poultry, pork, beef, dairy products, seeds, herbs, vegetables, chocolate.	15-20	>0.04	Any detectable presence [c]	Potential health hazard and unfit for human consumption
			<0.04	No detectable presence [c]	Fit for human consumption
Listeria monocytogenes	Poultry, pork, beef, dairy products, bread, fish	Unknown. May vary with the strain and susceptibility of the individual.	>100	>100 [d]	Not fit for human consumption
			10-100		Not fit for vulnerable groups consumption (e.g., hospital food)
			<10	<100 [d]	Fit for human consumption
Shigella spp.	Foods that are consumed raw, fruits, vegetables, recreational water, water	[a] 10	[a] *S. sonnei* <500 CFU	NA	Potentially injurious to health and/ or unfit for human consumption
			[a] *S. dysenteriae* <200 CFU		

	contaminated with stool.		[a] *S. flexneri* <140 CFU [a] virulent strain <10 CFU		
Mycobacterium bovis	Contaminated, unpasteurized dairy products, cattle, bison, elk, and deer. Can be acquired through air or wounds of contaminated animal.	[b] 1 CFU	NA	NA	Potentially injurious to health and/ or unfit for human consumption
Vibrio vulnificus	Raw or undercooked oysters and other seafood	10^6 (10^2 in predisposed persons)	NA	>30 [MPN/g] [e]	Not fit for human consumption

Yersinia enterocolitica	Raw or undercooked pork	10^9	NA	Any detectable presence [c]	Not fit for human consumption
Norovirus	Contaminated food, drinks, surfaces, or people	10-100 viral particles	NA	NA	Potentially injurious to health and/ or unfit for human consumption
Rotavirus	Stool particles in food and drinks due to bad hygiene.	10-100 viral particles	NA	NA	Potentially injurious to health and/ or unfit for human consumption
Cyclospora	Water, fresh produce, food or water contaminated with stool.	Unknown, predicted to be as low as 200 oocysts.	NA	NA	Potentially injurious to health and/ or unfit for human consumption

[a] Infective dose (ID_{50}), i.e., the oral dose required to cause disease in 50% of healthy adult volunteers challenged with a virulent strain of the pathogen. [b] Minimum infective doses in Cattle [c] In dairy products according to section 402(a)(1) of the Act (21 U.S.C. 342(a)(1)) [d] In ready to eat foods according to section 402(a)(1) of the Act (21 U.S.C. 342(a)(1)) [e] In Shellfish according to 2009 NSSP Guide for the Control of Molluscan Shellfish, FDA.

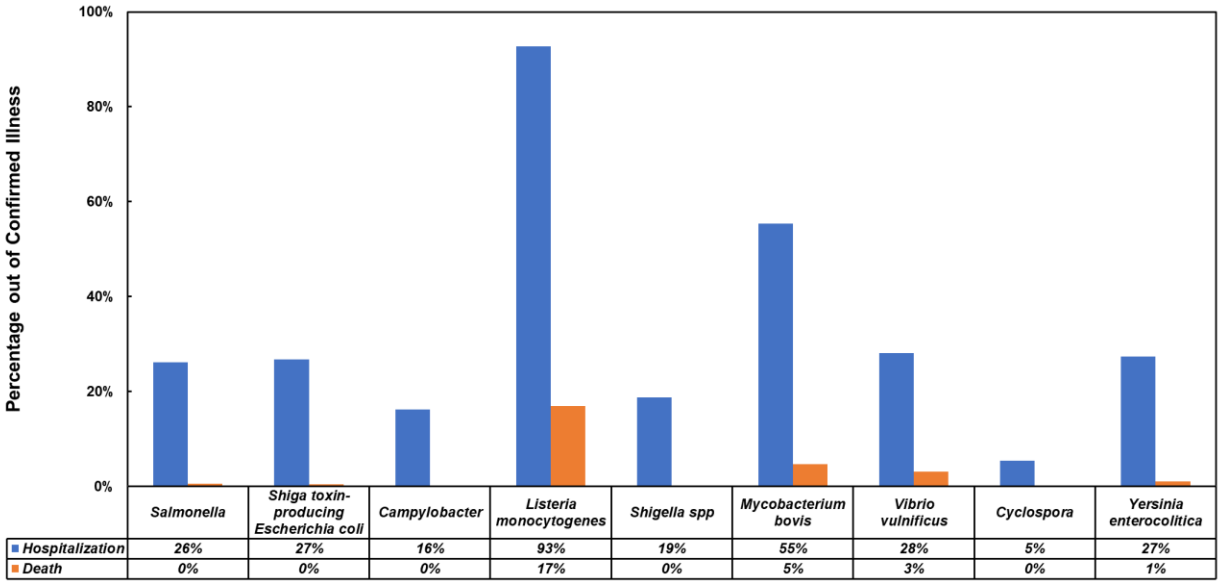

	Salmonella	Shiga toxin-producing Escherichia coli	Campylobacter	Listeria monocytogenes	Shigella spp	Mycobacterium bovis	Vibrio vulnificus	Cyclospora	Yersinia enterocolitica
Hospitalization	26%	27%	16%	93%	19%	55%	28%	5%	27%
Death	0%	0%	0%	17%	0%	5%	3%	0%	1%

Figure 4: Hospitalization and death rates from confirmed infections with common foodborne pathogens [111–114]

3. Microfluidic Channel Material Choice:

The characteristics of a microfluidic channel are derived from the material used to fabricate them. The channel's biocompatibility, reusability, fabrication simplicity, and cost are among the first characteristics that come to mind when considering a micro-fluidic channel for electrochemical biosensor use. In addition to the qualities that are important, their ability to be used in the field, the use of low sample volume, and compatibility to be used with multiple different pathogens (multiplexability) will make a huge impact when they are considered as a viable solution for detection in industrial settings [115–118]. Focus on microfluidics for foodborne pathogen electrochemical detection since 2017 has shown that the main materials used are glass [119], polydimethylsiloxane (PDMS) [81,82,84,85,120], thermosets [83], paper [121], and thread based [122]. In addition, there are also other materials that should be considered as microfluidic channel

fabrication materials, although not as common such as polymethylmethacrylate (PMMA), cycloolefin polymer (COP), cyclic olefin copolymer (COC), and silicon. These characteristics were evaluated on a scale of 1–5 and are presented in Figure 5 as per channel material, while the details leading to the evaluation are presented be-low. Some microfluidic channels can be made by the combination of two or more materials and their characteristics will change accordingly. More about the fabrication of microfluidic channels can be found in appendix G. Figure 5 further explains the popularity of glass and PDMS since both display preferable traits in most categories.

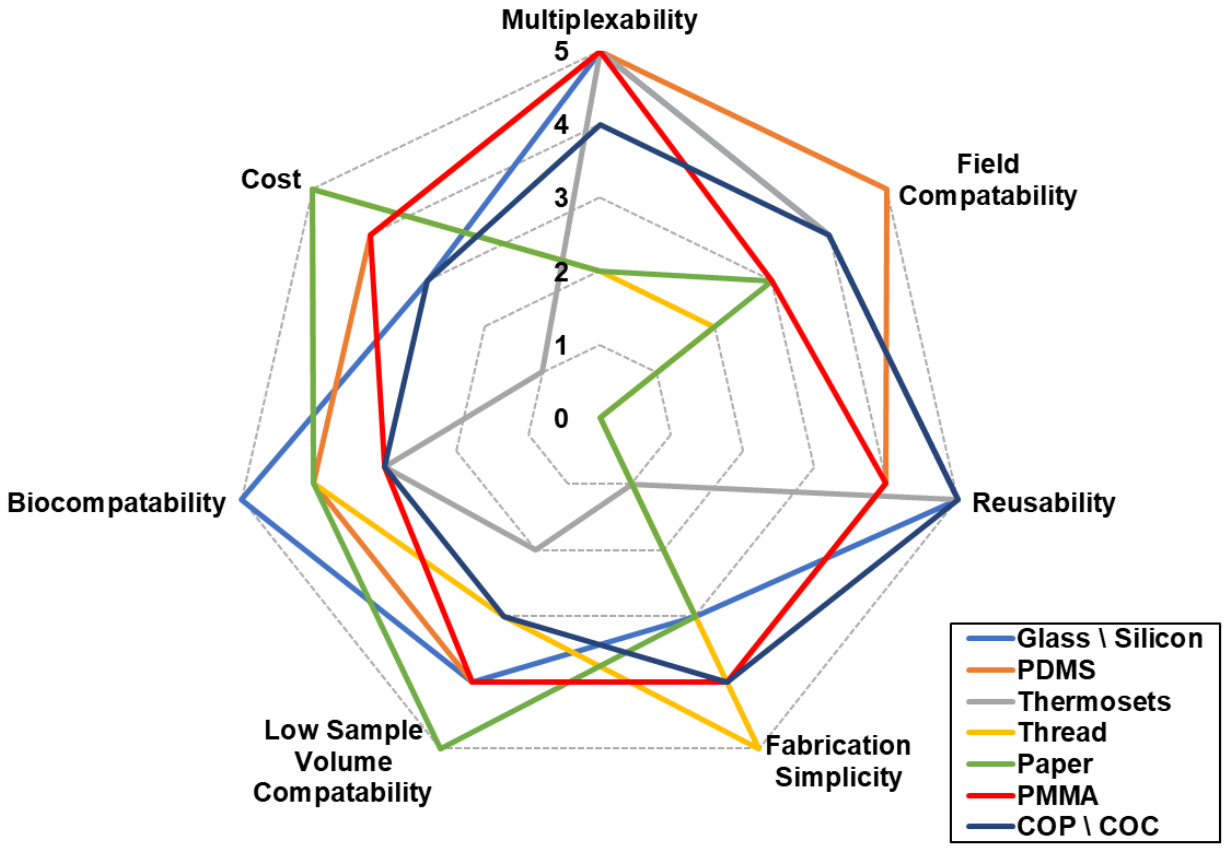

Figure 5: Microfluidic channel material choice according to main characteristics.

3.1. Glass:

The word glass is used to describe various materials among them: Borosilicate [115,123,124], Pyrex [125], Soda lime [126], Quartz [127], and others [128,129]. Glass

microfluidic channels are usually fabricated by using photolithography to print complex patterns on them and etch specific areas to form channels of specific height and width. Due to its amorphic structure, glass etching usually results in a round cross-sectional profile, which can help create a more homogenous flow pattern but forms a challenge when a high aspect-ratio is required [115,123,125]. Other fabrication methods include micromachining, where material is removed from the substrate and bonding or adhering it to another substrate [124] or laser patterning, where a beam of high-energy laser is used to pattern the channel [126,127]. These fabrication methods are highly accurate, where their resolution is determined by the etching chemicals or the resolution of the lithography and laser machines. The machinery usually comes with a very high-price tag and the use of harsh chemicals increases the complexity of the fabrication process. Glass is also thermoconductive, which means that the temperature of the work environment will be limited to a range that will not affect either the sample or the sensor. Another limitation comes from the hardness of glass and its brittle nature, which makes it harder to use in field conditions and makes the addition of valves or bonding very challenging. Although glass is very biocompatible, it is not permeable to gases, which limits the time a live pathogenic sample can survive in it. Additionally, glass has some very attractive qualities. Its resistance to most organic solvents significantly improves its ability to be washed and reused for multiple experiments, and it is very compatible with metal deposition, high surface stability, and as a substrate, it is commonly found, which reduces the overall cost of the devices. Another quality of glass is its electro isolation property, which allows for the incorporation of electrophoresis within it [115–119,130].

3.2. Silicon:

Silicon microfluidic channels fabrication is very similar to glass. Si microfluidic channels are fabricated by means of micromachining and photolithography and wet etch similarly to the

fabrication of glass microfluidics. Another technique that is mostly used in Si is the buried channel technique, where a deep vertical trench is etched into the Si by deep reactive ion etching (DRIE) followed isotropic etching of the bottom [131]. Another advantage of Si lays in its ability to fabricate thin membranes that can be used to form integrated micropumps [132], and microvalves [133] in the channel. Silicon and glass have very similar characteristics, but one major difference is due to the crystalline structure of silicon that causes a rectangular cross-sectional shape while glass has round one. Another difference between the two, is the fact that Si is opaque and will not let light pass through it [115].

3.3. PDMS:

PDMS is the most popular material used for microfluidic fabrication in general and as a microfluidic channel for foodborne pathogen microfluidic electrochemical detection specifically [81,82,84,85,120]. PDMS microfluidic channels are fabricated using a mold, also known as soft lithography, along with low temperature curing which makes it very repeatable and highly cost efficient. More details about lithography can be found in appendix F. The advantages of PDMS includes ease to bond with other PDMS components to form complexed multi-level channels, and hard substrates like glass or Si to provide mechanical stability. It is very compatible with high concentration of valves, it's biocompatible, possesses very low toxicity, high permeability to gasses which allows long time biostability of living pathogens in the channel, and support a very low resolution and any cross-sectional profile which depends on the mold used. While these advantages make it a very popular material to be used, it also possesses some significant disadvantages. PDMS is hydrophobic and tends to adsorb or absorb small hydrophobic molecules into its walls and cause swelling. It is very sensitive to most organic solvents which restricts it to aqueous samples only and reduces its reusability. PDMS's rigid surface can cause pathogens to be

trapped in its surface, and its high permeability to gasses can change the concentration of a sample due to water evaporation through its walls [115–118,130].

3.4. PMMA:

PMMA is a transparent and rigid thermoplastic polymer, which makes it ideal for sustainable applications. It also possesses glass-like quality with its clarity, UV resistance, low-toxicity, and transparency with half the density and an order of magnitude better impact resistance. PMMA is chemical resistant and is not affected by aqueous solutions, detergents, inorganic acids, alkalies, and aliphatic hydrocarbons. Among its disadvantages are low impact resistance with respect to other polymers, very limited heat resistance, sensitive to some organic solvents, poor wearing resistance, and tends to crack under medium to high load [134,135]. One of the common fabrication methods is hot embossing, where a piece of PMMA is placed on a Si or metal negative master pattern. The system is then heated under continuous pressure [136]. Another technique is room-temperature imprinting, where the PMMA is placed on a silicon template and then pressed together under high pressure [137]. As most polymers, PMMA microfluidic channels can also be made with injection molding, where PMMA pallets are melted and injected on a master template under high pressure and then cooled down to room temperature [138]. Finally, as in glass and silicon, PMMA can be molded into microfluidic channel by laser ablation or wet etching [139].

3.5. COP \ COC:

COP and COC are promising materials for microfluidic channels due to their chemical resistance for polar solvents, low water absorption, transparency, ease of fabrication, and bio-inertness [140,141]. COP and COC fabrication methods are laser ablation, injection molding, hot embossing and nanoimprint lithography. They are also thermoplastic polymers like PMMA and

possess a very high electric insulating capability. Their major disadvantage is their low chemical resistance to organic solvents [142,143].

3.6. Thermosets:

Thermosets, such as VisiJet® M2R-CL [83], are very limited in their microfluidic applications mostly due to their high cost and high stiffness. Their advantages lay with their high chemical and thermal stability which improve their field compatibility and reusability. Farther more, their compatibility with 3D printing allows them to be shaped into highly complexed channels but reduces their ability to work with low sample volume. Thermosets can also support very high aspect ratio due to their high strength [115,116].

3.7. Paper:

The fabrication of paper-based microfluidics is done by creating hydrophobic barriers on selected areas on the paper substrate to force the sample to flow in a specific path. Paper-based microfluidics are very cost effective. Paper based microfluidics are also very simple to make, high porosity and physical absorption makes them more compatible with the field. They are easily sterilized and modified which assist in letting only specific biocomponents through, biocompatible, and it doesn't require a pump or any other supporting equipment. Alternatively, paper based systems have very low mechanical properties, and in more complex design the sample flow might experience some challenges [118,144].

3.8. Thread based:

Thread based materials for microfluidics have some great advantages with respect to paper-based ones. Thread based microfluidic are very cost efficient since they don't require a cleanroom, complex fabrication methods, or expensive machinery. They are therefore also very simple to fabricate, while their hydrophilic nature and capillary nature make pumps and hydrophobic barriers

redundant. Most threads used for bio detection are very biocompatible, easily modified with different biorecognition elements, and can be easily shaped to almost any planar or 3D structure. Their low weight and handling simplicity make them relatively suitable for field work. Also, threads cannot be reused, they do have high strength compared to paper but overall are very sensitive to mechanical strain. Thread based microfluidics are still only available in laboratory settings and have not yet been used for any commercial application [122,145,146].

4. Microfluidics for Sample Preparation in Electrochemical Biosensors:

Microfluidics for the use of electrochemical pathogenic biosensors can be divided according to their goal in the system [92,124,147]. The goals from recent publications were mapped and found to be separation, concentration, detection, and mixing of reagents before detection as seen in Figure 6. Examples for each category since 2018 are shown in Table 2, each example includes a summary of the method of which the goal is achieved along with the target pathogen, flow characteristics, channel material, and the electrochemical detection technique. A few trends that are emerging from the data are that the majority of microfluidic channels are fabricated with traditional photolithography methods to create a mold out of SU-8 photoresist and use it to create an inversed PDMS channel [81,82,84,85,120,148], another fabrication methods were micromachining glass [119], cotton thread [122], and 3D printing of polyacrylate [83]. PDMS channels are used since the technology is very established and allows to form complex 2D designs quickly and accurately when the smallest segment's dimension is determined by the resolution of the photolithography mask aligner and the type of photoresist used to form the mold. The advantage of 3D printed channels is the ability to create complex 3D shapes without the need of alignment process. It is also very clear that the majority of microfluidic integrated electrochemical biosensors for foodborne bacteria are using EIS as their electrochemical technique

[81–85], Differential Pulse Voltammetry (DPV) was used for the detection of *Norovirus* [120], potentiometric electromotive force (EMF) was used to detect *Salmonella typhimurium* [121], and amperometric techniques were used to detect *Vibrio parahaemolyticus* [122]. It should be noted that most microfluidic channels reported in the literature, are meant for multifunctional use, that include two or more of the following functions: separation or isolation, concentration, enrichment, mixing, detection, etc. [147,149].

Table 2. The different uses of microfluidic channels for electrochemical biosensors.

Goal	Methodology	Foodborne Pathogen	Flow Rate [µL/min]	Sample volume [µL]	Concentration range	Channel Material	Detection Technique	Ref.
Separation	Gradient magnetic field.	*Listeria monocytogenes*	1000	3500	10^2-10^5 [CFU/mL]	PDMS	Impedimetric Phase shift analysis	[81]
	SiO2 microbeads separation.	*Norovirus*	NA	NA	100 [pM]-3.5 [nM]	PDMS	Differential Pulse Voltammetry	[120]
Concentration	Dielectrophoresis	*Escherichia coli* O157:H7	2 [µL/min] - sample flow 4 [µL/min] - wash flow 4 [µL/min] - Ag enhancement	20 [µL] - sample 8 [µL] - wash 8 [µL] - Ag enhancement	10^3-10^5 [CFU/mL]	PDMS	Impedimetric	[82]
	Positive dielectrophoresis	*Escherichia coli* O157:H7	1-2 [µL/min]	1000	10-120 [Cells/mL] -	Glass	Impedimetric	[119]

		Salmonella typhimurium			*Salmonella typhimurium* 13-1000 [Cells/mL] - *Escherichia coli* O157:H7			
Detection	Transporting the solutions to the sensor	*Escherichia coli* Crooks Strain	180	100	10^5-10^8 [Cells/mL]	Polyacrylate	Impedimetric	[83]
	Transporting the solutions to the sensor	*Listeria monocytogenes*	sample was dripped into specifically made wells on the microfluidic chip.	80	10^2-10^3 [CFU/mL]	PDMS	Impedimetric	[84]

	Transporting the solutions to the sensor	*Salmonella (B and D)*	2	NA	290-1000 [Cells/mL]	PDMS	Impedimetric	[85]
	Polymer coated paper modified with PAMAM(NH2)64-Ab	*Salmonella typhimurium*	NA	5000	10^1-10^8 [Cells/mL]	Paper	Potentiometric	[121]
	Cotton thread carried the sample to an aptamer functionalized MoS_2 nanosheets.	*Vibrio parahaemolyticus*	NA		10^1-10^6 [CFU/mL]	Cotton thread	CV and DPV	[122]
Mixing	Tesla mixing structure.	*Escherichia coli* O157:H7	2	20	10^3-10^5 [CFU/mL]	PDMS	Impedimetric	[82]
	Magnetic stirring.	*Listeria monocytogenes*	2000	205	10^2-10^5 [CFU/mL]	PDMS	Impedimetric Phase shift analysis	[81]

4.1. Microfluidic Separation Channel:

Microfluidic separation can be achieved with different methods. The most common approach is the use of microbeads. These microbeads can act as a filter according to their size and concentration within a specific area in the channel [120]. Another use of microbeads is by creating complexes of the target pathogen and magnetic microbeads and separate them by exposing it to a magnetic field [81,150,151]. Except for nanostructures another separation approach is utilizing mechanical forces, such as centrifugal forces to separate the pathogen from the sample. The channels are designed to separate the target pathogen from the sample according to their size or mass [152–154]. In addition, another approach for separation is using external forces like acoustophoretic separation that can separate large particles (>10 μm) from the target pathogens (≤4 μm) by applying ultrasonic acoustic waves [155]. Electrokinetic separation (electrophoretic and dielectrophoretic), which is quite popular for bacterial separation has not been reported extensively for foodborne pathogens in recent years [156,157]. A Microfluidic channel for the filtration of food particles that was fabricated as part of the work in this dissertation is presented in appendix G.

4.2. Microfluidic Concentration Channel:

The use of microfluidic channels for concentration and enrichment has been in recent interest due to the small volume most sequencing techniques require (~100 μL for PCR) and the low MID of most foodborne pathogens. Using a concentration microfluidic channel reduces the need of pretreatment processes for the tested sample and lowers the required time from sample collection to detection. One approach to increase the concentration of the pathogens, specifically viruses and bacteria, is the use homobifunctional imidoesters (HIs) that includes positively charged chemical solutions followed by isothermal solid-phase nucleic acid amplification to detect the pathogens according to their nucleic acids [158], although this method will allow significant amplification of the nucleic acids in the sample it is still

required about an hour of pretreatment and laboratory settings for it to work. Another approach is the use of auxiliary forces such as acoustic waves, magnetic fields, or electric fields. Similar to microfluidic separation the auxiliary forces are used to remove the target pathogen from the main sample volume and force it into a specific area where the same amount of cells are now in a smaller volume of carrier fluid which in turn effectively increase the concentration of the tested sample [82,153,154]. In a similar fashion, the use of mechanical forces as described for separation channels to again force the pathogens into smaller volume and hence increase their concentration [152–154]. The major advantages of using auxiliary forces or internal forces are in time saving and compatibility with field conditions. It is very clear that when using auxiliary or internal mechanical forces the channel is separating the pathogen and increasing its concentration all at once.

4.3. Microfluidic Detection Channel:

Microfluidic detection channels show the simplest design and are used mostly as a way to bring the sample to the biosensor with the correct flow characteristics that will allow the successful detection of the target pathogen. The detection channel will mostly use very low flow rates to avoid kinetic interference from the movement of the particles. They will also be combined with a screen printed electrode (SPE) platform or a fabricated integrated circuit (IC) to carry out the electrochemical detection [83–85,119,148]. A big advantage of these platforms is in their simplicity which makes their fabrication easily repeatable. Detection channels also will only require a pump of sort to inject the sample which will significantly reduce cost and increase their field compatibility [148].

4.4. Microfluidic Mixing Channel:

Microfluidic channels pose the biggest design challenge due to the laminar nature of microfluidic flow and its typically very low Reynolds number that does not allow the formation of turbulences. Microfluidic mixing channels in the field of biosensing is used mostly to form complexes of the target

pathogens with other micro-particles. These complexes will in turn help the specificity and sensitivity of the detection [81,82]. One approach to allow the mixing within a microfluidic channel is a mechanical one and called Tesla mixing structure. This design has 2 inlets that are opposite to one another (top of a "T") and a single outlet that is perpendicular to both (Tail of a "T") to form a "T" like shape. To farther improve the mixing the tail is designed so that the flowlines will overlaps by creating a back flow at different regions of the [82,159,160]. Another approach is a diffusive one, by adding a perpendicular channel with a very low flow rate to the main channel will cause the main flow to carry the secondary flow and mix the reagents or assisted diffusion by placing a magnetic stirrer to a specific area in the channel. In addition, a passive approach for mixing can be achieved by adding different barriers and holes at strategic locations in the channel will also change the flow profile and force mixing of the different reagents, or storing dry and wet reagents at different locations in the channel to be carried by the main flow when the sample is injected [159]. There are also many other microfluidic mixing techniques, including electric or magnetic field-based mixing [161,162], ultrasonic or acoustic mixing [163,164] that could be used, but have not been reported in the literature in recent years.

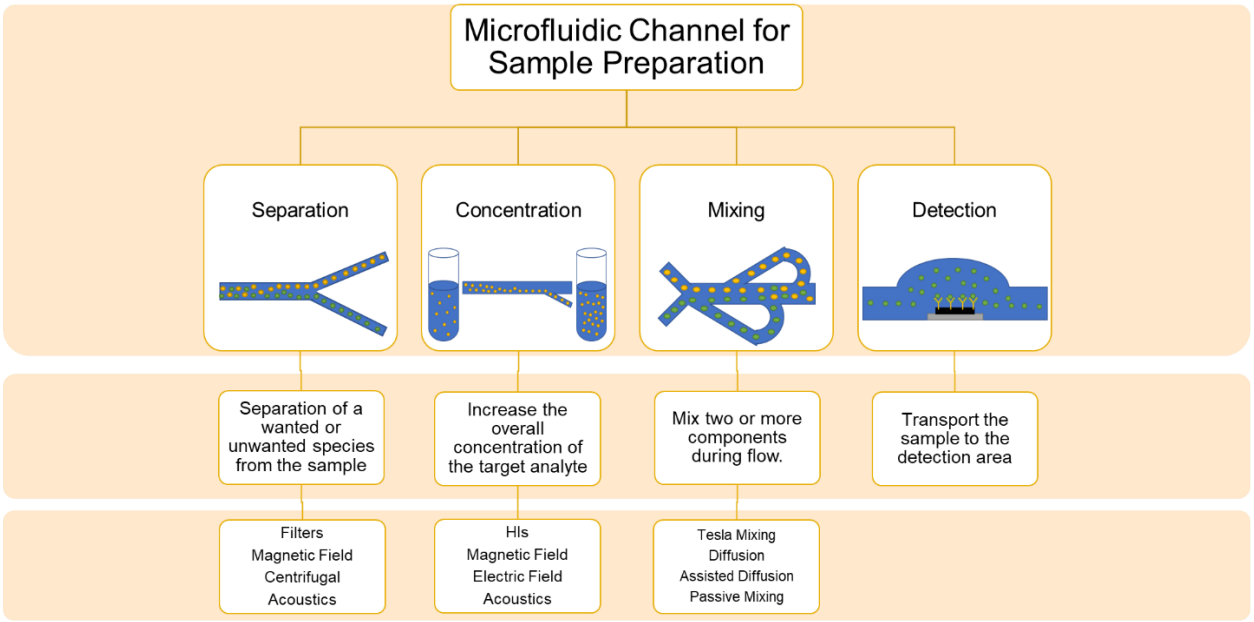

Figure 6: A schematic of different microfluidic approaches for sample preparation.

5. Lab on a Chip Electrochemical Biosensors:

Although most LOC devices are based on FET-biosensors as described in appendix H, the combination of microfluidics and electrochemical detection on one LOC platform offers the benefits of both worlds. The small fluid volume and quick processing of microfluidics along with the sensitivity and specificity of electrochemical biosensors. Electrochemical biosensors can be easily implemented into a microfluidic chip by utilizing modern integrated circuits fabrication techniques [119], microfluidic paper-based technology [121], and 3D printing techniques [83] as seen in Table 2. It is also clear that LOC devices present relative quick and accurate detection as portrayed by the quick detection time of a few minutes [165–168] and up to no more than 3 hours and the LOD of down to 4 CFU/mL for whole bacteria or 60 copies when the biorecognition element is genome-based [169,170] even when the detection is done in complex food matrices as seen in Table 3. LOC devices also have the ability to combine multiple sensors on one platform to detect multiple pathogens at the same time. This technique known as multiplexing and utilizes more than one biorecognition element on different detection regions of the device, it reduces the consumption of resources and reduces farther the sample pretreatment [119].

LOC portability and field compatibility is an important factor when assessing a device. In addition to the material the microfluidic channel is made from, as shown in Figure 5, auxiliary equipment like pumps, readers, or a potentiostat, and biorecognition element stability. In most cases the required auxiliary devices are larger than the LOC device and take significant space [171], and therefore limits the application for on-field use. Miniaturization of pumps [132,133,172,173] and the use of microcapillaries [174,175] enabled their integration into the device. In some instances, hand held potentiostats [176,177] integrated with a smart phone reader have been shown to provide better field compatibility [172,174], upon significantly reducing the need for auxiliary equipment. The stability of the biomolecules of the biosensors presents the biggest challenge for wide used LOC biosensors in the field. Most natural

biorecognition elements such as peptides, antibodies, bacteriophage, etc. are very sensitive to environmental conditions. To overcome their stability, molecularly imprinted polymers (MIPs) have been rising as an alternative. MIPs are artificially prepared materials the show advantages with respect to natural biorecognition elements like, reversable adsorption/release of the target pathogen. MIPs can be also imprinted with different nanomaterials to improve their magnetic, optic, or electric characteristics [178–180].

Table 3: Different examples for electrochemical platform for foodborne pathogen detection.

Food borne Pathogen	Detection technique	Bio-recognition event	Sample type	Analysis time	Detection range/ Detection limit	Ref.
Listeria monocytogenes	Amperometric	Antigen-antibody	Milk	NR	10^2 to 10^6 [CFU/mL]	[181]
	Impedimetric	Antigen-antibody	Filtered tomato extract	NR	4 [CFU/mL]	[182]
	Impedimetric	Magnetic nanoparticles-antibody-urease	Spiked lettuce	NR	3 x 10^2 [cells]	[183]
	Impedimetric	Modified magnetic nanoparticles-antibody-urease	Spiked lettuce	1 h	1.6 x 10^2 [CFU/mL]	[184]

	Impedimetric	Micro-electrodes functionalized with antibodies – miniaturized, portable EIS biochip	Milk	NR	55 [CFU/mL]	[84]
	Impedimetric	Immunomagnetic nanoparticles-urease -screen-printed electrode	Spiked lettuce	<3 h	1.6 x 10^3 [CFU/mL]	[185]
Campylobacter jejuni	Amperometric	Antibody, phosphatase	Turkey carcass wash,	2.5 h	10^2 -10^7 [CFU/mL] LOD=2 x 10^4 [CFU/mL]	[186]
	Amperometric	Antibody	Milk	<1.5 h	1*10^3 - 5*10^5 [CFU/ mL] LOD = 4*10^2 [CFU/mL]	[187]
E. coli O157:H7	Impedimetric	Antibody	Ground beef	NR	2.05 × 10^3 [CFU/gr]	[188]

Salmonella typhimurium	Amperometric	Antibody	Milk	125 minutes	10 [CFU/mL]	[165]
	Impedimetric	Aptamer	Apple juice	45 minutes	NR	[166]
	Impedimetric	Aptamer - Diazonium base	Apple juice	30 minutes	NR	[167]
	Impedimetric	Interdigitated electrode array coated with Salmonella antibody	Ready to eat turkey	1 h	300 cells/mL	[85]
Staphylococcus aureus	Impedimetric	Antibody	Spiked milk	~30 minutes	13 [CFU/mL]	[168]
	Potentiometric	Aptamers	Pig skin	NR	2.4×10^3 - 2.0×10^4 [CFU/mL]	[189]
Norovirus	Cyclic Voltammetry	Selective capture agent concanavalin A	Lettuce extract		60 copies/mL	[169]
	Immuno-based Electrochemical biosensor	Monoclonal antibody	Clinical fecal sample	1 hour	10^4 copies/ mL	[170]

LOC offer not only the combination of microfluidics and detection, but also the automation of the whole process. For example, a device using microfluidics to bring the sample to the electrochemical

biosensor that utilizes amperometric tests to detect *Escherichia coli* O157:H7 by using horse radish labeled antibody as the biorecognition element and forms an immobilized Ab/bacteria/anti-E.coli antibody structure following exposure to the bacteria [190]. Another interesting approach is the use of paper science to fabricate LOC devices. Paper offers an easier way to transport the fluid and allows complex 2D structures to be utilized with the use of a printer and specialized ink. They are very portable and can not only deliver the sample to the sensing area but also to merge multiple reagents, split sample, and delay the delivery by creating hydrophilic or hydrophobic areas on the paper [168,191]. This technology was shown to create a disposable impedimetric biosensor with immobilized antibodies as its biorecognition element. The paper itself acted as the microfluidic channel and carried the sample to the desired location [121]. On the other hand, paper based LOC platforms tend to lack in sensitivity and their reproducibility is also a big issue that was yet to be solved [192]. LOC platforms can utilizes also auxiliary forces, such as dielectrophoresis [82,119,160] or magnetic field [81] to manipulate, focus, and concentrate the sample. They are doing that by adding focusing electrodes to form the electric field for dielectrophoresis while an electric coil or a strong magnet can form the magnetic field. Applying such forces have reported to enhance signal response by up to 18 fold when compared to the reaction without them [119]. Although these methods are offering significant advantages and their fabrication is relatively established and well common, they also add significant cost and energy requirements to the device.

Conclusions:

This article begins with the review of the impact of foodborne illnesses on public health and the economy. Further in this review, the established standards for foodborne pathogen diagnosis for a range of food matrices and pathogen types have been elaborately discussed. The types of different foodborne pathogens along with their minimal infective doses and recommended standards for human consumption have been discussed. The review comprehensively discusses the various types of microfluidic platforms

that have been developed and reported for biosensing applications with emphasis on electrochemical based platforms for foodborne pathogens. The review also discusses, the distinction between platforms that solely focus on detection versus the platforms that combine sample preparation and detection on a single device. The importance of material choices for microfluidic platforms based on desired sensitivity, selectivity, reusability, portability, and field suitability for end application, is critically reviewed in this article. The use of MIPs instead of the commonly used natural biorecognition elements could significantly improve the shelf life and stability of ECBS platforms. Moreover, the use of hand held potentiostats, integrated capillaries, micropumps, and valves as part of LOC instead of using syringes and other large auxiliary equipment will aid in simplification of these platforms for field use.

Future Directions: The research in the field of microfluidic electrochemical biosensors points to the development of devices that will combine all steps from sample preparation to detection including separation, isolation, enrichment, concentration, mixing, etc. Another trend, is developing LOC with multiplexing capabilities to process large volume samples and to screen multiple pathogens simultaneously. Finally, the integration of LOCs with smart phones-based user interface could enable easier adoption of these devices by the food industry for in house testing.

CHAPTER 3

ELECTROCHEMICAL BIOSENSOR FOR RAPID DETECTION OF LISTERIA MONOCYTOGENES

This chapter contains text from the following publication:

Or Zolti, Bavithithira Suganthan, Ryan Maynard, Hamid Asadi, Jason Locklin, and Ramaraja P Ramasamy. Journal of The Electrochemical Society, 169 (6), (2022): 67510.

Reprinted here with permission of the publisher.

Abstract:

Listeria monocytogenes (*L. monocytogenes*) is a common foodborne pathogen that has been responsible for many foodborne illness outbreaks in recent years. Currently, *Listeria* contamination in food products is identified only through molecular tests conducted in diagnostic laboratories. No established phage based diagnostic methods for *L. monocytogenes* during food production or processing are used. Here we report a potentially disruptive rapid diagnostic method based on electrochemical biosensing principles that use bacteriophages as bioreceptors for selective identification and quantification of *L. monocytogenes*. Electrochemical biosensors are good alternatives to molecular detection methods due to their ease of use, high specificity, sensitivity, and low cost. Bacteriophages can serve as excellent biorecognition elements in biosensors due to their robust stability in a range of environmental conditions and their ability to distinguish between live and dead bacterial cells. The impedimetric biosensing platform for *L. monocytogenes* detection was developed by immobilizing P100 bacteriophage onto quarternized polyethylenimine modified carbon nanotubes using an in-house developed molecular tethering method. The resulting sensor showed high selectivity and sensitivity toward *L. monocytogenes* with a limit of detection of 8.4 CFU/mL. Initial results demonstrate that the biosensing platform is highly reliable in its selectivity towards its target analyte, *L. monocytogenes*.

1. Introduction

Foodborne pathogens are becoming increasingly problematic worldwide due to increased hospitalization, mortality, and food-related financial cost. Among foodborne pathogens, *Salmonella* spp., *Escherichia coli* O157:H7, and *L. monocytogenes* are very commonly found in fresh produce, eggs, deli meats, ready to eat food products, soil, foliage, water, mud, and silage [193–195]. The FoodNet surveillance reports show that *L. monocytogenes* is the highest cause of hospitalization, at 93 % of confirmed infection cases, and death at 17 % of these cases, according to studies conducted over ten years between 2006 to 2015 [114]. *L. monocytogenes* can multiply at temperatures as low as 4 ^{o}C and survive in freezing temperatures as low as -18 ^{o}C. *L. monocytogenes* causes a severe illness called listeriosis that is life-threatening, especially for pregnant women, newborns, babies, the elderly, and immunocompromised patients. Listeriosis, in most cases, infects the central nervous and circulatory systems. It is hazardous to pregnant women because it affects the placenta and can infect the fetus in the uterus. Like other foodborne pathogens, symptoms of *Listeria*-related infections include diarrhea and fever, but if those are the only symptoms, most cases will not be diagnosed as Listeriosis. When the pathogen spreads out of the stomach and into different areas of the body, symptoms include headache, confusion, loss of balance, convulsions, fever, and muscle aches. Therefore, it is essential to develop accurate and robust detection methods for the bacteria present in the food samples as early as possible in food production and supply [196].

The prevailing gold standard for foodborne pathogens detection is culture-based methods. Samples are taken at specific control points during the manufacturing and distribution process, cultivated on a nutrient-filled medium, plated, and tested with visual, biochemical, and immunological means before and after enrichment. Although very accurate, this method is not ideal due to the long processing time, sample transportation, robustness, and expensive skilled labor and equipment [11–15]. To overcome these

shortcomings, the industry needs a faster and cost-efficient detection method with similar or even better sensitivity to comply with modern food and safety standards [16–18]. These concerns have encouraged researchers to improve current methods and develop new analytical methods. The target sensitivity standard is currently coming from PCR testing, with an average limit of detection (LOD) of 100 CFU/mL depending on the buffer and the gene used for amplification [197,198]. Electrochemical biosensing has emerged as a viable method for this application with its simple signal generation instrument, fast detection time, and very high sensitivity. Its simplicity allows anyone with basic training to operate such a sensor and still obtain reliable results. Their quick detection time makes electrochemical biosensors compatible with food industry demands, and high sensitivity enables the user to adhere to regulatory agency guidelines without risking mass recalls [199]. An electrochemical biosensor consists of an electrochemical transducer (electrode) with a bio-recognition element immobilized on its surface. Commonly used biorecognition elements are DNA/RNA, oligonucleotides, aptamers, enzymes, antibodies, or bacteriophages. Bacteriophages possess certain advantages over other types of bio-recognition elements due to their robust stability in non-ideal environmental conditions such as temperature, pH, and humidity and their ability to distinguish between live and dead bacterial cells. Bacteriophages are relatively inexpensive, easy to handle, ubiquitous in nature, and can be prepared and maintained using simple procedures [200]. literature reported the use of phage peptides, enzymes, and proteins to detect *L. monocytogenes*. Still, the whole phage was not used to detect *L. monocytogenes* electrochemically [201–205]. The low number of publications involving the use of bacteriophage as a biorecognition element suggests they have not yet been fully explored, increasing the interest in exploring it further.

The orientation of phage upon immobilization on the transducer's surface significantly increases its effectivity in capturing its target bacteria [206]. Bacteriophage P100 belongs to the *Caudovirales* order and the *Herelleviridae* family with a negatively-charged capsid and a positively-charged contractile tail

that consists of the capturing protein [207,208]. Due to this structured dipole, by creating a positively charged surface, it is possible to control the orientation of the P100 phage and ensure that its capsid proteins are positioned to capture the target bacteria. This orientated immobilization method has already been demonstrated in our previous work using the myoviridae family of bacteriophages on polyethylenimine functionalized carbon nanotubes (PEI-CNT) electrodes for the capture of *E. coli* and *Staphylococcus aureus* cells [206,209–211]. To increase the transducer's surface positive charge for the orientation of phage during immobilization, a quarternization of the amine groups in the PEI molecules could be used, as it has been reported to possess a good yield [212,213]. The quarternized amines possess a high positive charge and can improve phage orientation on the carbon nanotube electrode for bacterial cell capture.

This paper presents our work on developing an electrochemical biosensor to detect *L. monocytogenes* using P100 phage as the biorecognition molecule. The biosensor platform was made of a nanostructured carbon nanotube-based electrode, on which P100 phages were immobilized as recognition molecules (bioreceptors). The carbon nanotubes were functionalized with quarternized polyethylenimine-modified CNT (q-CNT) to aid in a charge-directed oriented immobilization of phages on the electrode to enable selection detection of *L. monocytogenes*.

2. Experimental

Materials

Acid treated multiwalled carbon nanotubes (COOH-functionalized multiwalled CNTs) with an outer diameter of 30-50 nm and length of 10-20 μm (Cheap Tubes Inc.), 0.05 micron type N gamma silica powder (silica polishing powder) (Electron Microscopy Sciences), polyethylenimine, potassium bromide (KBr), 1-pyrenebutanoic acid succinimidyl ester (PBSE), bovine serum albumin (BSA), glutaraldehyde (all four from Sigma-Aldrich), disodium phosphate (Na_2HPO_4) (Research Products International Corp),

sodium chloride (NaCl) (EMD chemicals), magnesium sulfate heptahydrate ($MgSO_4.7H_2O$ (J.T. Baker), agar powder, thionyl chloride ($SOCl_2$) and iodomethane (CH_3I) (all three from Alfa Aesar), potassium phosphate dibasic (KH_2PO_4) and potassium chloride (both from BDH), tris base, typtone, ethanol (all four from Fisher scientific), yeast extract (Becton Dickinson and Company), methylene chloride (DCM) (VWR) were purchased and used as received.

Phosphate-buffered saline (PBS, 10X) (100 mL) was prepared by mixing 0.2 g of KCl, 8 g of NaCl, 0.245 g of KH_2PO_4, 1.4 g of Na_2HPO_4. PBS (1X) (pH 7.4) was prepared by diluting the 10X PBS buffer. Luria Bertani (LB) (100 mL) (pH 7.0) was prepared by mixing 1 g of typtone, 0.5 g of yeast extract, 1 g of NaCl. SM buffer (pH 7.5) was prepared by mixing 100 mM NaCl, 8 mM $MgSO_4$. $7H_2O$, 50 mM Tris base, and 0.01 % Gelatin. Standard Brain Heart Infusion (BHI) media was prepared according to the instructions on the bottle. Milli-Q water (resistivity =18 MΩ.cm) was used to prepare all the media and chemicals. All buffers and media are sterilized before use. Electrodes were purchased from CH Instruments, Inc. Glassy carbon (part number CHI104), screen printed electrode (Zensor), platinum wire (part number CHI115), and Ag/AgCl (part number CHI111) were used as working, counter, and reference electrodes

Methods

Microbiological Methods

Listeria monocytogenes Scott A, a pathogenic strain, was used as the target analyte, whereas *Salmonella enterica* subsp. *Enterica* serovar Typhimurium 291RH (ser. Typhimurium-291RH) and *Escherichia coli* O157:H7 (*E. coli* O157:H7) were used as the non-target analytes. Listex P100 bacteriophage (P100 Phage) was purchased from Micreos Food Safety B.V. *L. monocytogenes* Scott A was grown by inoculating a single colony in 3 mL of BHI media and incubated at 37 ^oC for 24 hours at 200 rpm. A 500 µL aliquot of the overnight culture was inoculated in 50 mL of fresh BHI medium and

incubated at 37 °C for about 5 hours in an incubator shaker until it reached the mid-log phase. In this study, ser. Typhimurium-291RH and *E. coli* O157:H7 are used as the non-target analyte and grown by the same method with the use of LB media for *E. coli* O157:H7 strain as the only difference made. One milliliter of the mid-log phase bacterial culture was centrifuged at 5000 rpm for 8 min. The supernatant was removed and washed twice with 1X PBS buffer to remove any media residue, and finally, the pellet was resuspended in 1X PBS buffer. Then, dilution series was prepared. Enumeration of bacteria was performed by plate-count techniques and expressed in CFU/mL. Plaque assay was carried out with P100 phage and *L. monocytogenes* to measure the phage titer and was expressed in PFU/mL. A soft agar overlay technique was carried out to evaluate the specificity of the P100 phage. The soft agar overlay technique was carried out with the target (*L. monocytogenes*) and non-target bacteria (ser. Typhimurium-291RH and *E. coli* O157:H7) with the presence and absence of P100 phage.

Quaternization of PEI-f-CNT

The first step was to convert the commercially available COOH-functionalized multiwalled CNTs into PEI-CNT using the procedure described in our previous work [206]. For this, 2 mg of COOH-functionalized CNTs were dispersed in 1 mL of dimethylformamide and sonicated for 5 minutes. 6 mL of $SOCl_2$ was added to the suspension to acylate the carboxylic acid, and the $SOCl_2$ acylated the carboxylic group. The suspension was refluxed for 24 hours with constant stirring under 120 °C. The suspension was centrifuged at 10000 rpm for 8 minutes following the reflux to form a pellet. The pellet was washed with anhydrous tetrahydrofuran (THF) and dried at room temperature under a vacuum for 2 hours. 5 mL dimethylformamide (DMF) was used to resuspend the pellet and then stirred in an N_2 environment at 90 °C. 100 mg of PEI was then added and reacted for three days. It was then centrifuged at 10000 rpm for 8 minutes, washed with methanol, and dried at a temperature of 70 °C. The second step was to quarternize the amine groups in the PEI functional group. Iodomethane was used to quarternize the PEI functional

group, as schematically shown in Figure 7 (a). For this purpose, 8 mg of PEI-CNT powder was added to a 5 mL round bottom flask. 2 mL of methylene chloride was added to the flask using a micropipette. 20 wt% of iodomethane was pipetted into the flask sealed by a septum and vented using a 23G needle. The heterogeneous mixture was then stirred at room temperature for three days before the solvent and excess reactant was evaporated with gentle heating over one hour. The quarternized product (q-CNT) was analyzed using a Nicolet 6700 FT-IR spectrometer to verify the quarternization of the amine groups and the surface potential of the different modification steps (e.g., COOH-CNT, PEI-CNT, q-CNT, and the P100 phage), all samples were suspended in deionized water and were measured using by ZetaSizer (Malvern) to confirm the increase in positive charge. The q-CNT dispersion was made by suspending the product in deionized water at a 1 mg/mL ratio and sonicated for an hour using an ultrasonic homogenizer (Omni International, SONICRAPTOR 250). Farther details about the preparation of the q-CNT can be found in Appendix C.

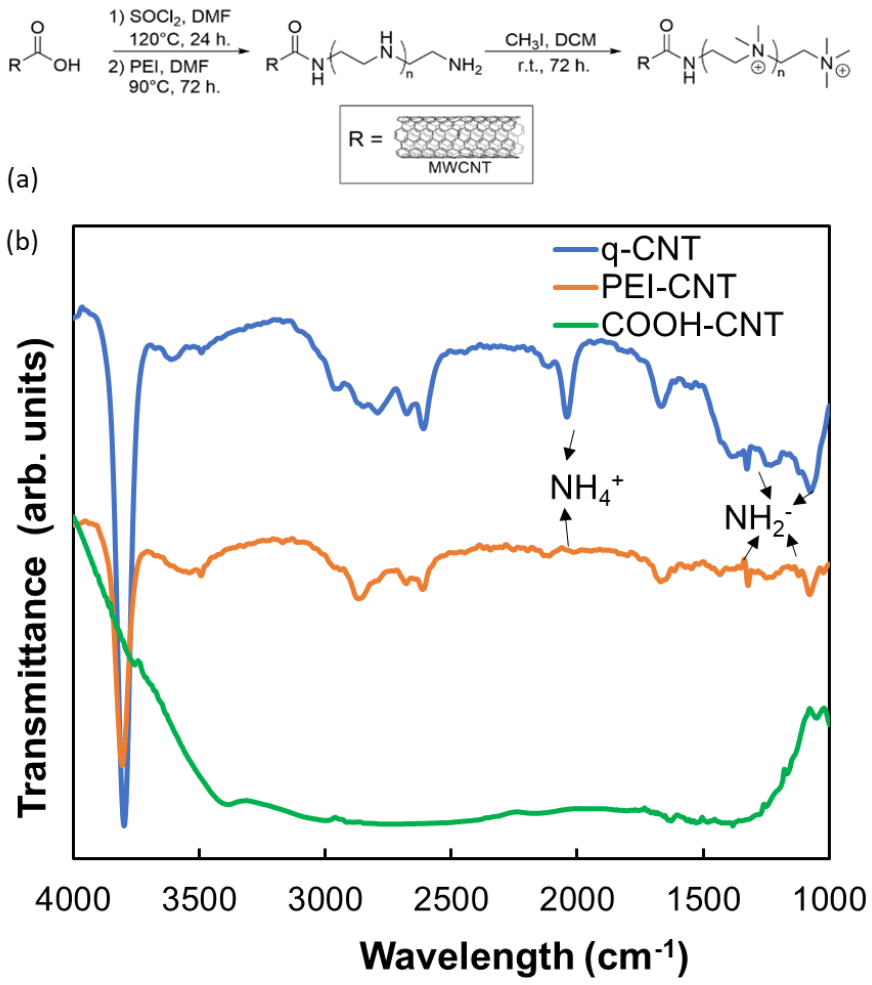

Figure 7. (a) Quaternization of CNT for phage immobilization and (b) FTIR spectrum of CNT after different steps during modification.

Electrode Preparation

A glassy carbon electrode was polished with alumina polishing powder on a polishing pad, followed by sonication in deionized water in a sonication bath for 5 minutes, and dried in an oven for 1 hour at 70 ^{o}C. Once the electrode dried, 16 µL of the q-CNT solution was drop cast onto a glassy carbon electrode and then dried in an oven at 70 ^{o}C, as shown in Figure 8 (a).

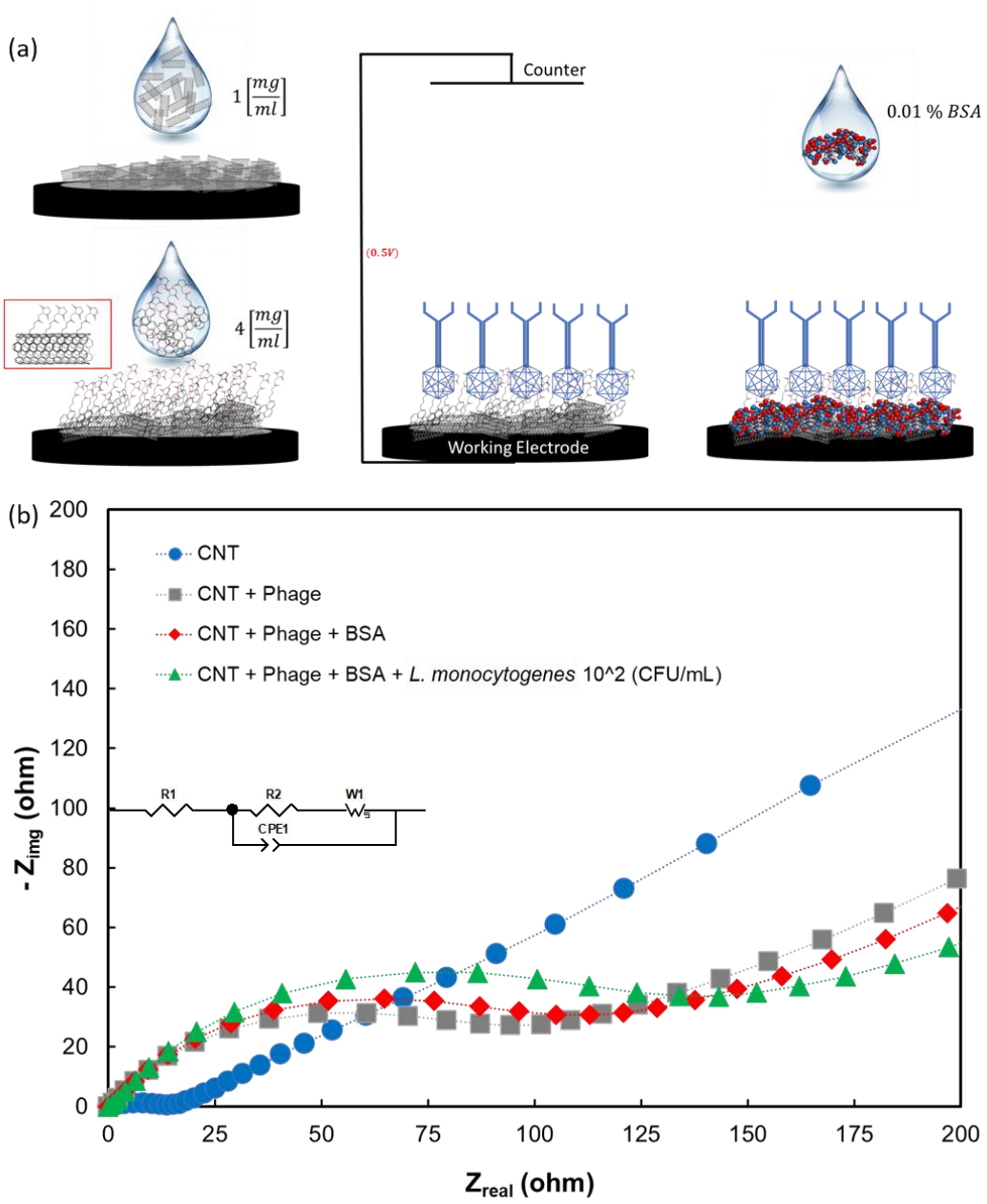

Figure 8. (a) Electrode preparation steps including drop-cast deposition of q-CNT on the electrode followed by PBSE crosslinker deposition and electric-field induced P100 phage immobilization and finally deposition of 0.01 % BSA as a surface blocking agent and (b) Nyquist plot of the electrode after each step of the electrode preparation process.

Before phage attachment, the q-CNT modified electrode was activated using 1-pyrenebutanoic acid succinimidyl ester (PBSE) as a molecular tethering agent, chemical structure is shown in Figure 9. The modified GCE was placed in an ice container, four microliters of 10 mM PBSE solution (in DMF) were drop cast onto it and reacted for 15 minutes. Excess PBSE was rinsed using DMF, and finally, the electrode was washed twice with 1X PBS prior to phage attachment.

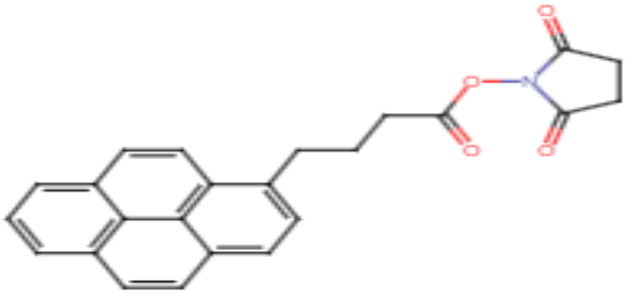

Figure 9. The chemical structure of the PBSE crosslinker molecule

An electric field-induced phage immobilization method [209–211] was developed and demonstrated previously in our group to attach phages to the modified GCE electrode. P100 phages contain negatively charged capsids and positively charged tail fibers. The strong positive charge on the q-CNT and electric field-induced immobilization created an oriented phage layer chemically anchored to the surface by applying a potential 0.5 V between the working and counter electrodes for 2 hours [206]. After immobilization, the electrode was rinsed twice with SM buffer and washed with 1X PBS buffer. Following the wash, 6 µL of 0.01 % BSA solution was deposited on the electrode to block areas that might not have been completely modified for 30 minutes. Finally, the electrode was incubated in 1X PBS for 15 minutes before using in electrochemical experiments. Farther immobilization details are shown in appendix D.

To verify the activity of the phage, propagation experiment was conducted. L. monocytogenes was grown in 3 mL BHI liquid media in a shaker overnight at a temperature of 37 ^{o}C and 200 RPM, as described in appendix B. 1 mL of the culture was centrifuged at 8000 RPM for 8 minutes. The media was

removed and the pallet was resuspended in 1mL of 1X PBS, the same process was repeated one more time. P100 phage was serial diluted in 1X PBS to a concentration of 10^{10} PFU/mL. To each 100 µL phage solution, 250 µL of bacteria culture were added and mixed. The mixture was added to 3mL liquid soft agar, preparation of soft agar is described in appendix A, and was poured into BHI hard agar plates. The plates were incubated overnight at a temperature of 37 ^{o}C, and the results are shown in Figure 10.

Figure 10: Plaque assay, P100 phage plaques are visible on the plate.

Electrochemical Impedance Measurements

The bacterial solution (50µL) was drop casted on the working electrode and incubated for 8 minutes before the measurement, the impedimetric characterization was carried out using CHI-920C model potentiostat (CH Instruments Inc., Austin, TX). The electrochemical system was a standard 3-electrode cell using a glassy carbon working electrode (GCE) (CH Instruments Inc., Austin, TX), Ag/AgCl reference electrode. The counter electrode was a Pt wire. Electrochemical impedance spectroscopy (EIS) measurements were done in 5 mM $[Fe(CN)_6]^{4-}/[Fe(CN)_6]^{3-}$ as redox couple, with a frequency range of 1 Hz to 100 kHz and an AC amplitude of 5 mV. The resulting measurement is presented as ΔR_{CT} (ohm) or ΔR_{CT} (%) where:

$$(12)\,\Delta R_{CT}\ (\%) = \frac{R_{CT,measured} - R_{CT,baseline}}{R_{CT,baseline}} \times 100\ \%$$

$$(13)\,\Delta R_{CT}\ (ohm)\ =\ (R_{CT,measured} - R_{CT,baseline})$$

All measurements were done at room temperature under standard conditions.

Electrode Preparation for Scanning Electron Microscope (SEM) Images

Morphological characterization of the prepared electrode after exposure to target and non-target bacterial cells was done with a SEM scanning electron microscope (SEM, FEI Teneo, FEI Co.). A screen-printed electrode was modified with P100 phage as described before. Target and non-target bacteria were incubated for 8 minutes on the electrode, followed by fixing them to the electrode with 3 % glutaraldehyde solution overnight. Once fixed, the electrodes were dehydrated using increasing concentrations of ethanol for 10-20 min each (50, 60, 70, 80, 90, and 100 %). The electrodes were then sputter coated (Leica sputter coater) in 10 nm thickness of Au-Pd for SEM imaging.

3. Results and Discussion

Quaternization of PEI-CNT

An FTIR absorption spectra were obtained and analyzed for the peaks corresponding to the desired functional groups after each step of the CNT modification process shown in Figure 7 (a). The spectra for COOH modified, PEI modified, and quarternized CNT is shown in Figure 7 (b). The peaks pointing to the successful PEI modification on the CNT were confirmed by the formation of C-N stretching band at wavelengths: 1020 cm^{-1}, 1170 cm^{-1}, and 1620 cm^{-1}. A second confirmation was obtained from the C=O stretching band at 1700 cm^{-1} that became more pronounced as the modification process advanced. The quaternization of CNT following the second step of the modification was confirmed by the band that appeared at 2040 cm^{-1}, as shown in Figure 7 (b), which points to the formation of quaternary ammonium ion [214].

The modified q-CNT were analyzed for their surface charges using zeta potential measurements for a secondary confirmation of the quaternization process, resulting in a high positive charge. As shown in Table 4 the zeta potential in 1X PBS (pH 7.4) results show a positive charge after PEI modification due to the oxygen electronegativity that created a localized positive charge at the succinimidyl functional group. After quarternization, the zeta potential of the CNT went up additional 46 %, which corresponds to the transformation of the amine groups on the PEI-CNT, confirming the successful quarternization step of PEI-CNT and the formation of quaternary amines. The negative zeta potential from the P100 phage suggests that a positive electric potential should be used for charge-directed immobilization on the q-CNTs, as demonstrated by us in previous work [209–211].

Table 4. Surface charge measurements of the phage and the different stages of CNT modification

	Zeta potential
COOH-CNT	$-31.25 \pm 0.35\ [mV]$
PEI-CNT	$31.65 \pm 0.8\ [mV]$
q-CNT	$46.3 \pm 0.8\ [mV]$
P100 Phage	$-9.7 \pm 0.7\ [mV]$

Impedimetric Response of Biosensor

The phage-modified electrode platform was optimized for its phage and carbon nanotube loading. Immobilization procedures were also optimized to allow the biosensor to accurately detect *L. monocytogenes.* The biosensor was tested using electrochemical impedance spectroscopy using 5 mM $[Fe(CN)_6]^{4-}/[Fe(CN)_6]^{3-}$ as a redox couple. The Nyquist plots in Figure 8 (b) show the electrochemical impedance responses of the modified electrode biosensor before and after phage immobilization on the CNT modified electrode. A significant increase in the charge transfer resistance (R_{CT}), as observed by the

magnitude of the semicircle can be observed upon immobilization of the phage. This is expected as an insulating layer of phage covers the conductive forest of the CNT interface on the electrode, which significantly decreases the charge transfer kinetics. The addition of BSA molecules as surface blockers (using 0.01 % BSA solution) further increased the R_{CT}. The BSA surface blockers aid in minimizing the non-specific binding of components other than the P100 phage on the electrode to reduce the the R_{CT} value from non-target pathogens. The R_{CT} also noticeably increased upon introducing the target pathogen *L. monocytogenes* on the surface, even at low concentrations (10^2 CFU/mL).

Detection of L. monocytogenes

The impedimetric biosensing response of the phage modified electrode was tested at different concentrations of the *L. monocytogenes* in the sample ranging from 1 CFU/mL to 10^8 CFU/mL, the results shown in Figure 11 (a). For comparison, the R_{CT} response of the biosensor in the absence of *L. monocytogenes* was also obtained. The responses originated from the same starting point in the high-frequency region; however, at increasing concentrations of bacteria, the magnitude of the semicircle increased with the bacteria (analyte) concentration. The Nyquist response was fitted with a Randles equivalent circuit (shown as an inset in Figure 11 (a)) as reported before to determine the values of the constant phase element (CPE1), the diffusional resistance element (the Warburg impedance, W1), the ionic solution's ohmic (R_{ohm}) resistance, and the electrode's charge transfer (R_{CT}) resistance. A calibration curve between charge transfer resistance and the analyte concentration was generated from the R_{CT} data and plotted in Figure 11 (b). The calibration curve shows a linearity to a confidence of 95 % at a reliable range of detection between 10^1 and 10^5 CFU/mL, beyond which the signal reaches a plateau as seen in the inset. Based on triplicates measurements, the limit of detection and limit of quantification were estimated using the following expressions [73]:

$$SD = SE \times \sqrt{n} \quad (14)$$

$$(15)\, LOD \;=\; 3.3 \times \left(\frac{SD}{s}\right)$$

Where *SD* is the standard deviation of the intercept, *SE* is the standard error of the intercept, *n* is the number of points used for the linear fit, and s is the slope of the linear fit. The LOD of the phage-modified biosensor for *L*. *monocytogenes* was calculated to be ~ 8 CFU/mL. It is about two orders of magnitude lower than molecular-based methods and exceeds the commonly used standards of detection limits. To verify this limit of detection the six-sigma approach was also used by looking at the value of three standard deviations from the baseline as described in eq. (25) and was found to be LOD = 10 CFU/mL. Any signal value above the three standard deviation is a legitimate signal with confidence interval of 99 % [100].

$$(16)\, LOD \;=\; 3 \times \sigma = 3 \times \sqrt{\frac{1}{n}\sum_{i=1}^{n}(y_i - \bar{y})^2}$$

Where σ is the standard deviation of the R_{CT} values from the baseline, n is the number of observations, y_i is a specific observation, and $\bar{y}$ is the average R_{CT} value for the baseline. The recovery rate is a parameter that compares the concentration calculated from the calibration curves to the actual concentration placed on the biosensor and points to the ability of the biosensor to predict a concentration of an unknown sample withing the linear range as seen in Table 5 [59].

Table 5. Recovery Rate of the Biosensor

Actual Concentration Log_{10}(CFU/mL)	Calculated Concentration Log_{10}(CFU/mL)	Recovery Rate
1	0.73	84.1%
2	1.91	98.8%
3	3.26	109.2%
4	4.18	103.9%
5	4.79	95.0%

It is clear to see that the recovery rate of the biosensor has a very high predictability for solution with concentrations between 10^2 to 10^5 CFU/mL where the recovery rate is within 15 % of the actual

concentration. These values also correspond to the limit of quantification which is 24 CFU/mL according the linear regression method and 30 CFU/mL from the six-sigma methodology.

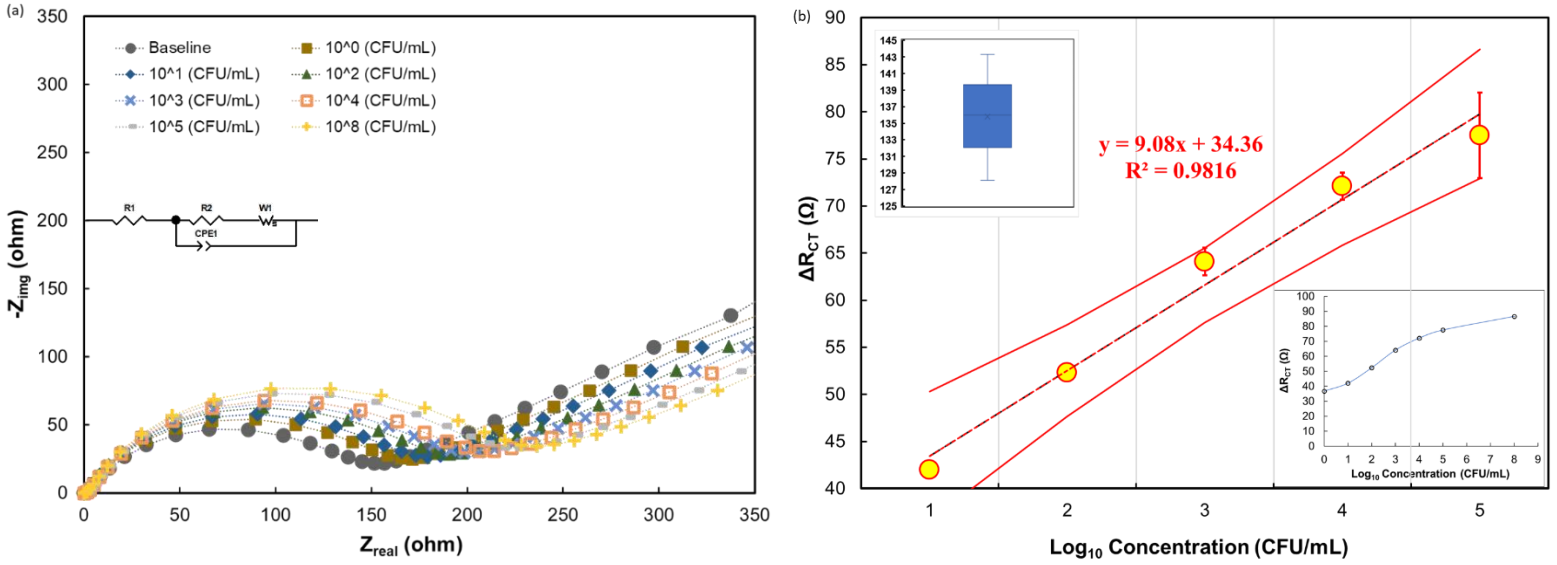

Figure 11. (a) Nyquist plots show biosensor's impedance response to varying concentrations of the target analyte, L. monocytogenes. The equivalent electrical circuit used for fitting the Nyquist data is given in the inset. (b) Calibration curve showing a linear relationship between the differential charge transfer resistance ΔR_{CT} (ohm) and the logarithmic of bacterial concentration with the linearity confidence limits at confidence level of 95 %. The baseline boxplot is presented in the upper inset and the full concentration range of the calibration curve is given in the lower inset.

Role of Phage as Biorecognition Element:

The role of the P100 phage as the biorecognition element for detecting the target *L. monocytogenes* is evident from the differences in the impedimetric signals arising from the phage-immobilized electrode when compared to an electrode that does not contain phage as seen in Figure 12 (a). The R_{CT} measured by the biosensor is significantly higher when phage is present on the surface. The numerical values as distance from the measured baseline are shown in Figure 12 (b) with the absolute measured R_{CT} values displayed in the bars. This is expected as the phage plays a key role in capturing and attaching *L. monocytogenes* cells onto the electrode, which increases the interfacial impedance, resulting in higher charge transfer resistance value. In comparison, the electrodes with no phage have a far less selective attachment of *L. monocytogenes* cells onto the electrode resulting in lower interfacial impedance value. It can also be noticed that the difference is more pronounced at higher concentrations of bacteria. The results indicate that the phage plays a key role in aiding selective attachment of *L. monocytogenes* to the electrode and as a signal enhancer for quantitative detection.

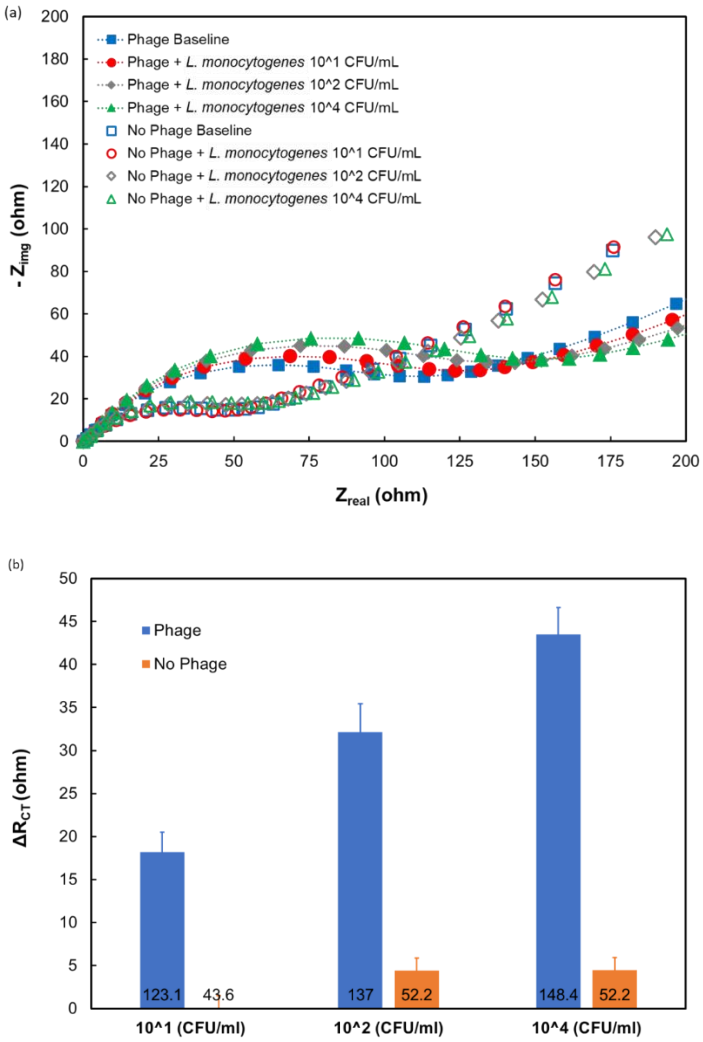

Figure 12. Impedance response of the biosensor to target *L. monocytogenes*: (a) Nyquist plot of the impedimetric response to *L. monocytogenes* with (full shapes) and without (hollow shapes) P100 phage and (b) ΔR_{CT} (ohm) values with and without phage expressed as the difference from baseline impedance values with no bacteria.

Specificity of the Biosensor:

The specificity of the P100 phage was evaluated using non-target bacterial analytes. SEM images of a modified electrode after exposure to *L. monocytogenes*, ser. Typhimurium-291RH, or *E. coli* O157:H7 were taken. In addition, a soft agar overlay technique was used with the same bacteria in the presence of

the P100 phage. An SEM image of the electrode after exposure to *L. monocytogenes* is shown in Figure 13 (a), the yellow arrow points to one of the bacterial cells that were captured by the P100 phage attached to the surface. Figure 13 (b) shows a plate clear of bacterial colonies after their exposure to the phage. The yellow arrow shows that the other side of the petri dish is visible through the semi transparent media. Figure 13 (c) and Figure 13 (e) show the electrode surface after exposure to ser. Typhimurium-291RH and *E. coli* O157:H7 respectively. As expected no bacterial cells were visible on the electrode surface. The specificity was confirmed by the soft agar overlay with either bacteria as seen in Figure 13 (d) and Figure 13 (f) where both plates were completely covered with colonies and formed non-transperant layer and no plaques appeared. The spherical structures in Figure 13 (a), Figure 13 (c), and Figure 13 (e) show the BSA molecules on the electrode surface.

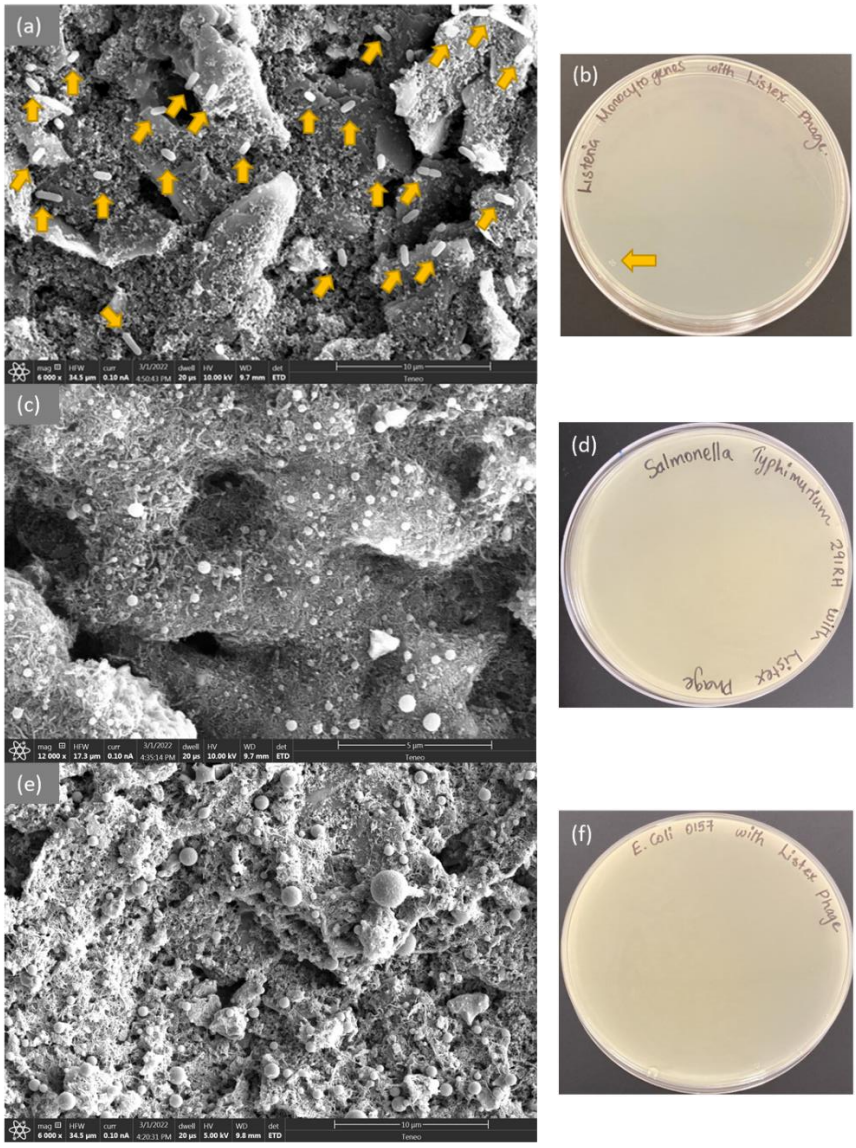

Figure 13. P100 phage selectivity in SEM and phage assay studies with target and non-target bacteria. (a) SEM image of a modified electrode after exposure to *L. monocytogenes*. The arrows mark the bacterial cells; (b) phage assay on a plate with *L. monocytogenes*, arrow marks the visible mark on the other side of the media; (c) SEM image of a modified electrode after exposure to E. coli O157:H7; (d) phage assay on a plate with E. coli O157:H7 with P100 phage; (e) SEM image of a modified electrode after exposure to ser. Typhimurium-291RH; and (f) phage assay on a plate with ser. Typhimurium-291RH with P100 phage.

The EIS measurements revealed similar results with respect to the specificity of the P100 phage towards *L. monocytogenes* detection, as shown in Figure 14 (a). For phage-modified electrodes, the Nyquist plots show only a small variation in the ΔR_{CT} from their baseline value for the non-target pathogens (ser. Typhimurium-291RH, *E. coli* O157:H7). In contrast, a significant variation in ΔR_{CT} was observed for *L. monocytogenes*. Moreover, in the absence of phage, the electrode exhibited the lowest R_{CT} change from the baseline for *L. monocytogenes* compared to non-target pathogens as seen in Figure 14 (b), which contributes to the non-target R_{CT} signal. The results demonstrate that phage provides the specificity needed for *L. monocytogenes* detection. In addition, the effect of the surface blocking agent BSA was studied and presented as well in Figure 14 (c) and the R_{CT} values presented in Figure 14 (d). BSA had reduced the effect of quasi-analytes however, the specificity could further be improved by minimizing the non-specific attachment of non-target pathogens on the electrode surface by exploring other surface blocking molecules that were not in the scope of this work.

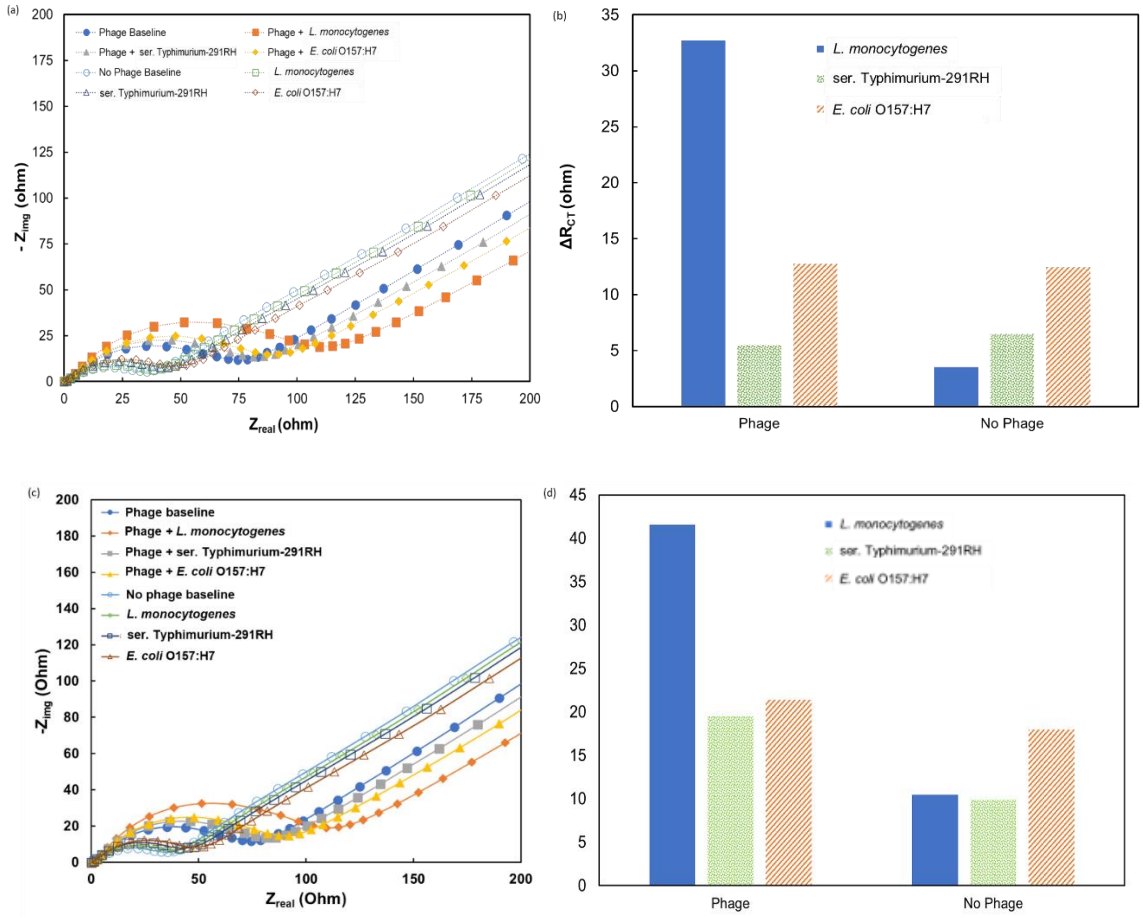

Figure 14. Response to target and non-target pathogens with and without phage. (a) Nyquist plot of the impedimetric response to target and non-target bacteria with (full shapes) and without (hollow shapes) P100 phage; (b) ΔR_{CT} (ohm) values of the response as the difference from baseline values with and without P100 phage; (c) Nyquist plot of the response without BSA; and (d) ΔR_{CT} (ohm) values of the response as the difference from baseline values without BSA.

Stability Studies

The electrochemical stability of the biosensor was evaluated after electrode preparation. Phage immobilized electrodes were stored at 4 ^{o}C in 1X PBS solution for one hour, one day, one week, and two weeks. After each period, a detection experiment with 100 CFU/mL of *L. monocytogenes* was performed. Each period was tested in duplicates, and the measurement error was calculated for each one. The R_{CT} value was measured, and the ΔR_{CT} (%) was calculated with respect to the response after one hour. Figure 15 shows that the biosensor's responses were stable after 24 hours with only 10 % drop in signal and a very low error margin of ± 2 %. After a week, the reduction in the signal was 30 % with respect to the response obtained an hour after preparation, but the response was stable with an error of ±1 %. The low error value suggests that the sensor performance is repeatable after one week. After two weeks, the reduction in the signal was 70 %, and the error went up to ±7 %. It is clear that after two weeks, there is a degradation of the phage's activity and that the signals are very low; the high error suggests that they are also less accurate beyond two weeks.

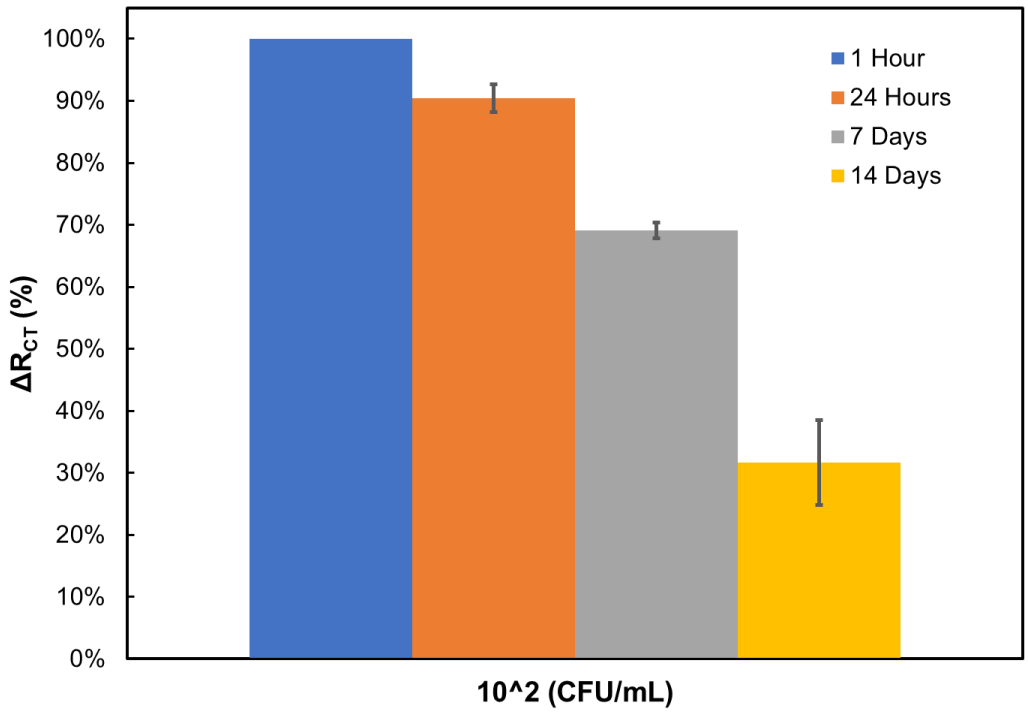

Figure 15. ΔR_{CT} (%) values as difference from baseline value taken within the first hour of making the electrode.

4. Conclusions

An ultra-sensitive and selective sensor for *L. monocytogenes* was developed and tested in this work. It was shown that the sensor could selectively detect the target bacteria with a LOD of 8.4 CFU/mL. This value is below the current commonly used PCR standards, although demonstrated only in laboratory buffer samples. The biorecognition element, P100 phage, exhibits desirable selectivity towards *L. monocytogenes*, although more work should be done to non-selective binding between the electrode and other non-target analytes. This is the scope of future work where suitable surface blocking agents will be employed to minimize non-specific binding and the accuracy of *L. monocytogenes* detection by the sensor platform. The novel quaternization of the PEI-CNT has made their surface much more suitable for oriented phage deposition, which was critical in achieving high selectivity and sensitivity. The biosensor was

shown to be stable for up to a week after phage attachment with a signal that is 70 % of the one achieved one hour after preparation. The biosensor, under optimal conditions, gave a linear response from 10 to 10^4 CFU/mL, with good reproducibility and stability. These characteristics make it a promising method for industrial and private food monitoring detection of foodborne pathogens. Our future work would involve testing the biosensor with food samples to investigate and quantify the performance of the sensing platform in practically relevant food samples.

CHAPTER 4

PORTABLE ELECTROCHEMICAL FOODBORNE PATHOGEN BIOSENSOR IN BROTH SAMPLES

Or Zolti, Bavithithira Suganthan, Sanket Naresh Nagdeve, Ryan Maynard, Jason Locklin, and Ramaraja P Ramasamy, to be submitted to Journal of The Electrochemical Society.

Abstract:

Foodborne pathogens can be found in any food product around the globe and can cause serious illness when contaminated products are consumed. Among these pathogens, *Listeria monocytogenes* has the highest rates of hospitalization and death from confirmed cases, which in turn makes it a very important detection target. The current detection techniques of *Listeria monocytogenes* are done by utilizing colony counting or molecular approaches that require specialized laboratory. An electrochemical biosensor combined with a microfluidic flow chamber was developed for the detection of *Listeria monocytogenes* in phosphate saline buffer and chicken broth. The selective, sensitive, and quick detection was achieved by depositing P100 bacteriophage on the surface of a screen-printed electrode and conducting impedimetric measurements in stationary conditions and underflow in ferri/ferro-cyanide redox couple. The biosensing platform was able to reach a limit of detection of 55 CFU/mL in 1X PBS buffer and 10 CFU/mL in 1 % diluted chicken broth. The biosensor demonstrated recovery rates of 83%-98% in buffer and 87%-96% in chicken broth. These results show high sensitivity, selectivity, and accuracy.

1. Introduction:

There are 17 different species of the Listeria genus. Among them only two species are pathogenic, *Listeria ivanovii* that is found almost exclusively in ruminants and *Listeria monocytogenes* (*L. monocytogenes*) that can infect and cause illness in humans [215,216]. *L. monocytogenes* is a facultative anaerobic graham positive rod-shaped bacterium that have been detected in humans since 1924, it is a psychrophile pathogen capable of multiplying in as low temperatures as 4 ^{o}C and to survive temperatures of down to -17 ^{o}C with an optimum growing temperature range of 30 to 37 ^{o}C [43,196]. Upon *L. monocytogenes* infection, illnesses such as listeriosis, sepsis, myocarditis, meningitis, encephalitis, bacteremia, and intrauterine or cervical infections in pregnant women can occur that can cause miscarriages or stillbirth [217].

The most common path of *L. monocytogenes* infection is through the gastrointestinal tract, similar to other foodborne pathogens. It can be found in various food products like poultry, pork, beef, dairy products, bread, fish, ready to eat foods, and fresh produce [42]. Its ability to form biofilms facilitates infection from surfaces, transport vehicles, and stainless steel appliances [216,218]. Recent *L. monocytogenes* outbreaks in the US have been from deli meats, cheeses, mushrooms, and chicken products [218–222]. The most common technique to reduce pathogenic bacteria infection in the food industry is pasteurization. In this process the food is heated to a temperature lower than 100 ^{o}C and then cool down at rates and duration depended on the acidity and likely bacterial risks. *L. monocytogenes* has been reported to increase its heat resistance in specific food components [223]. There is hence an important need to detect *L. monocytogenes* in a quick and accurate manner.

The most commonly used current method of detection for *L. monocytogenes*, is microbiological culturing. The advantages of this method are accuracy, it is well established, sensitivity, and assistance to differential diagnosis. Its major shortcomings lay in its 2-5 days duration from sample collection until

obtained results, the need for highly trained personal, and expensive equipment [42,43]. Other common tools for detection are polymerase chain reaction (PCR) and enzyme-linked-immunosorbent assay (ELISA). These methods search for sequences of DNA, RNA, or specific proteins for a positive detection of the target pathogen. Their advantages include sensitivity, selectivity, and detection time. Their shortcomings are the need for highly trained personal, operation in a clean lab environment, and inability to distinguish between live and dead pathogen [42,224]. To overcome the shortcomings various methods have been developed like chromatographic based sensors, that in the case of *L. monocytogene*s utilizing gas chromatography to characterize metabolites, fatty acids, and other volatile organic compounds (VOC) affiliated with different strains of *Listeria*. These methods are fast, sensitive, and selective but cannot distinguish between pathogens with similar characteristics to their target [225–227]. To overcome all these limitations, the use of biosensors has gained attention. Biosensors uses biorecognition molecules like enzymes, proteins, antibodies, bacteriophage, and more to detect different biological or chemical species. In addition to these recognition elements, they utilize a transducer to transform the biological interaction into a measurable signal that can be collected and analyzed [42,43,78,224,227,228]. The detection of *L. monocytogenes* has been done with various types of biosensors. Optical biosensors as their name suggests, provide an optical signal through luminescence, fluorescence, or color. The optical approach is very sensitive, and selective but require expensive optical equipment and very sensitive to environmental interference [229]. Thermal biosensors measure the heat change as a result of bioreaction between the biorecognition molecule and specific analytes that corresponds with the target pathogen. The method is fast and sensitive but its selectivity is low due to non-target responses [30]. Electrochemical biosensors (ECBS) measure the change in electric parameters like current, potential, or impedance of a system as a result of biological interaction between the target analyte and the biorecognition molecule on the working electrode. ECBS are sensitive, selective, fast, low cost, and do not require trained personal to

work. They require small sample volume and can be portable which makes them great for home or field detection in buffer or food samples [42,228–230].

In our previous work, we developed different phage-based approaches for separation and detection of different pathogens [150,151,206,209,231]. A biosensor utilizing quarternized carbon nanotubes (q-CNTs) to form a charge directed oriented immobilization of the P100 phage for the detection of *L. monocytogenes* in 1X phosphate-buffered saline (PBS) with a limit of detection of 8.4 CFU/mL was also presented [43]. In this work, an adaptation of our biosensor to a portable screen-printed electrode platform for the detection of *L. monocytogenes* in chicken broth samples is presented.

2. Experimental:

Materials

Carboxyl functionalized multiwalled carbon nanotubes (COOH-CNT) with 30-50 nm outer diameter, and 10-20 μm length (from Cheap Tubes Inc.), 1-pyrenebutanoic acid succinimidyl ester (PBSE), bovine serum albumin (BSA), Tween® 20, and chlorodimethylsilane (all four from Sigma-Aldrich), dimethyl sulfoxide (DMSO) (Thermo-scientific), disodium phosphate (Na_2HPO_4) (Research Products International Corp), sodium chloride (NaCl) (EMD chemicals), magnesium sulfate heptahydrate ($MgSO_4.7H_2O$ (J.T. Baker), thionyl chloride ($SOCl_2$) and iodomethane (CH_3I) (both from Alfa Aesar), potassium phosphate dibasic (KH_2PO_4) and potassium chloride (both from BDH), tris base, typtone, and ethanol (all three from Fisher Scientific), yeast extract and agar powder (both from Becton Dickinson and Company), Dichloromethane (DCM) (VWR), and Chicken broth (GreenWise ®) were purchased from respective commercial vendors and used as received.

Phosphate-buffered saline 10X (100 mL) was prepared by mixing 0.2 g of KCl, 8 g of NaCl, 0.245 g of KH_2PO_4, 1.4 g of Na_2HPO_4. PBS (1X) (pH 7.4) was prepared by diluting the PBS 10X buffer. 0.01% tween 20 solution was prepared by mixing 10 mL of PBS (1X), 85 mL deionized water (DIW), and 20 μL

of Tween® 20. Luria Bertani (LB) (100 mL) (pH 7.0) was prepared by mixing 1 g of tryptone, 0.5 g of yeast extract, 1 g of NaCl. SM buffer (pH 7.5) was prepared by mixing 100 mM NaCl, 8 mM $MgSO_4$. $7H_2O$, 50 mM Tris base, and 0.01 % gelatin. Standard Brain Heart Infusion (BHI) media was prepared by mixing 37 g or the BHI powder into 1 L of DIW using a magnetic stirrer until a homogenized solution was formed. 1% diluted chicken broth was prepared by diluting 1 mL chicken broth into 99 mL 1X PBS and vortex-mixing the resulting solution. DIW with resistivity of 18 MΩ.cm was used to prepare all the media and chemicals. All buffers and media are sterilized before use.

Screen printed electrodes (SPE) (Zensor) were purchased from CH Instruments, Inc. and used as working, counter, and quasi-reference electrodes. All experiments were performed using a microfluidic flow cell from Metrohm Dropsens.

Methods

Microbiological Methods

Listeria monocytogenes Scott A, a pathogenic strain, was used as the target analyte, whereas *Salmonella enterica* subsp. *Enterica* serovar Typhimurium 291RH (ser. Typhimurium-291RH) and *Escherichia coli* O157:H7 (*E. coli* O157:H7) were used as the non-target pseudo-analytes for specificity studies. Listex P100 bacteriophage (P100 Phage) was purchased from Micreos Food Safety B.V. *L. monocytogenes* Scott A was grown by inoculating a single colony in 3 mL of BHI media and incubating at 37 ^oC for 24 hours at 200 rpm. In this study, ser. Typhimurium-291RH and *E. coli* O157:H7 were grown by the same method as *L. monocytogenes*, while the use of LB media for *E. coli* O157:H7 strain being the only difference. One mL of the mid-log phase bacterial culture was centrifuged at 5000 rpm for 8 min. For detection experiments in buffer, the supernatant was removed and washed twice with 1X PBS buffer to remove any media residue and the pellet was resuspended in 1X PBS buffer. Then, the dilution series was prepared. For detection experiments in 1 % diluted chicken broth the supernatant was removed and

washed twice with 1X PBS buffer to remove any media residue and the pellet was resuspended in 1 % diluted chicken broth. Dilution series was also prepared with 1 % diluted chicken broth as the used media. Enumeration of bacteria was performed by plate-count techniques and expressed in CFU/mL. Plaque assay was carried out with P100 phage and *L. monocytogenes* to measure the phage titer and was expressed in PFU/mL. A soft agar overlay technique was carried out to evaluate the specificity of the P100 phage towards the target (*L. monocytogenes*) and non-target bacteria (ser. Typhimurium-291RH and *E. coli* O157:H7) with the presence and absence of P100 phage.

Electrode Preparation

Quarternized carbon nanotubes (q-CNT) were prepared according to the protocol discussed in appendix C. Screen-printed electrodes (SPE), were rinsed with DIW and dried in room temperature for 2 h prior to modification with q-CNT. Once the electrode dried, 8 µL of the 1 mg/mL q-CNT solution was drop cast on the SPE working electrode and then dried in room temperature. After that, 1-pyrenebutanoic acid succinimidyl ester (PBSE) as a molecular tethering agent was used as a crosslinker for the attachment of the P100 phage to the q-CNT modified electrode. The modified SPE was rinsed with 1X PBS and placed in an ice container, 0.5 µL of 20 mM PBSE solution (in DMSO) was dropped onto it and allow to self-assembly for 15 minutes. Excess PBSE was removed by rinsing twice with 1X PBS prior to phage attachment. One µL of the P100 phage solution was drop cast on the working electrode and was kept overnight at 4 ^{o}C. The P100 phage contain negatively charged capsids and positively charged tail fibers. The strong positive charge on the q-CNT created an oriented phage layer chemically anchored to the surface as was previously discussed in our work [43,206]. After immobilization, the electrode was rinsed with SM buffer and washed with 1X PBS buffer twice. Following the wash, 0.5 µL of 0.1 % BSA solution was deposited on the electrode to block areas that might not have been completely modified for 30 min. Finally, the electrode was incubated in 1X PBS or with 1% diluted chicken broth for 15 min before using

in electrochemical experiments. Farther details about the phage immobilization on the SPE can be found in appendix D.

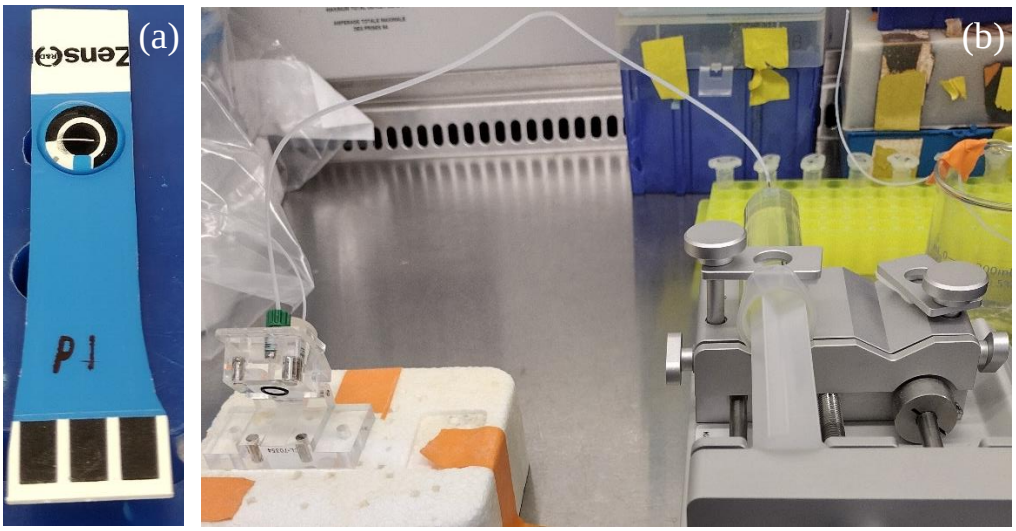

Figure 16. (a) SPE electrochemical biosensor; and (b) Flow-based detection apparatus.

The bacterial solution (100 µL) was drop-cast onto the SPE and incubated for 8 minutes before the measurement. The impedimetric characterization was carried out using CHI-920C Scanning Electrochemical Microscope. The electrochemical system was a 3-electrode SPE as shown in Figure 16 (a), electrochemical impedance spectroscopy (EIS) measurements were done in 5 mM $[Fe(CN)_6]^{4-}/[Fe(CN)_6]^{3-}$ as redox couple, with a frequency range of 1 Hz to 100 kHz with an AC amplitude of 5 mV. All measurements were done at room temperature under standard conditions. The modified SPEs have been tested in 1X PBS buffer and in 1% diluted chicken broth matrices. The negative control contained no bacteria and the test samples contained different concentrations of *L. monocytogenes*. Following incubation with the tested solution, the SPE was rinsed with 1X PBS. A 100 µL of 5mM $[Fe(CN)_6]^{4-}/[Fe(CN)_6]^{3-}$ solution was dropped on the SPE so that it covered the working, counter, and reference electrodes prior to impedimetric measurements. The negative control measurement was used as baseline R_{CT} for each set of measurements presented in this section. Detection experiments under constant

flow were performed using a syringe pump connected to microfluidic flow chamber as shown in Figure 16 (b).

3. Results and Discussion:

Detection of L. monocytogenes in Buffer and Broth:

Initial impedimetric measurements were done with the *L. monocytogenes* suspended in 1X PBS buffer at a concentration range of 10^2 CFU/mL to 10^6 CFU/mL. Triplicates measurements were performed to determine the errors. In Figure 17 (a) a Nyquist plot in presented with data collected form 1X PBS buffer experiments. The calibration data with the baseline boxplot within the inset is shown in Figure 17 (b) along with the linear confidence limits with a confidence level of 95 % that show all points fall within the linear regime. It is visible that at the higher concentrations a larger error is calculated in buffer. The reason is that one of the devices reached saturation at lower concentration than the other two, in addition the rate of signal change from concentration of 10^4 CFU/mL has slowed at different rates. Following the buffer experiments, the detection experiments were done where the negative control and the bacterial solutions were suspended in 1 % diluted chicken broth. The diluted broth was used to reduce the effects of inconsistencies in broth composition. The results of these experiments are shown in Figure 17 (c) and Figure 17 (d). The data suggests that exposure to the 1 % diluted broth causes a significant reduction in the overall values of the R_{CT} even after baseline adjustment, with respect to the corresponding measurements in buffer. Additionally, the 1 % diluted chicken broth measurements showed lower calculated error for all measurements. The lowest concentration measured was 10^2 CFU/mL. In addition, two methods were used to calculate the limit of detection (LOD). The first was using a linear regression method and resulted in 55 CFU/mL in buffer and 10 CFU/mL in broth. The second method was 6σ. Here the LOD is defined as anything higher than three standard deviations of the baseline with confidence level of $\alpha = 0.01$. The value of three standard deviations from the baseline was 38.8 Ω in broth and 126.2 Ω in

buffer. When using these numbers to calculate the limit of detection from the linear equation on the calibration curve the correspond to 10 CFU/mL in broth and 300 CFU/mL in buffer [73]. A possible explanation for the improvement with broth samples is that the different salts and components reduce the charge transfer resistance of the system, in turn lowering readings and making them easier to detect above the noise level also since the broth was diluted to 1%, the LOD in undiluted broth samples would be 10^3 CFU/mL for both methods. In addition, the recovery rate is a parameter that compares the concentration calculated from the calibration curves to the actual concentration placed on the biosensor as shown in Table 6 and farther proves the predictability and accuracy of the biosensor [59].

Table 6. Recovery rate in Broth and Buffer

	Buffer		Chicken Broth	
Actual Concentration Log_{10}(CFU/mL)	Calculated Concentration Log_{10}(CFU/mL)	Recovery Rate	Calculated Concentration Log_{10}(CFU/mL)	Recovery Rate
2	1.97	98%	1.75	88%
3	2.87	96%	2.77	92%
4	3.39	85%	3.78	95%
5	4.44	89%	4.80	96%
6	4.99	83%	5.75	96 %

The recovery rate is calculated according to eq. (17) and (18).

$$(17)\ C_i^{calculated} = \frac{\Delta R_{CT,i} - intercept}{slope}$$

$$(18)\ Recovery\ Rate = \frac{C_{calculated}}{C_{actual}}$$

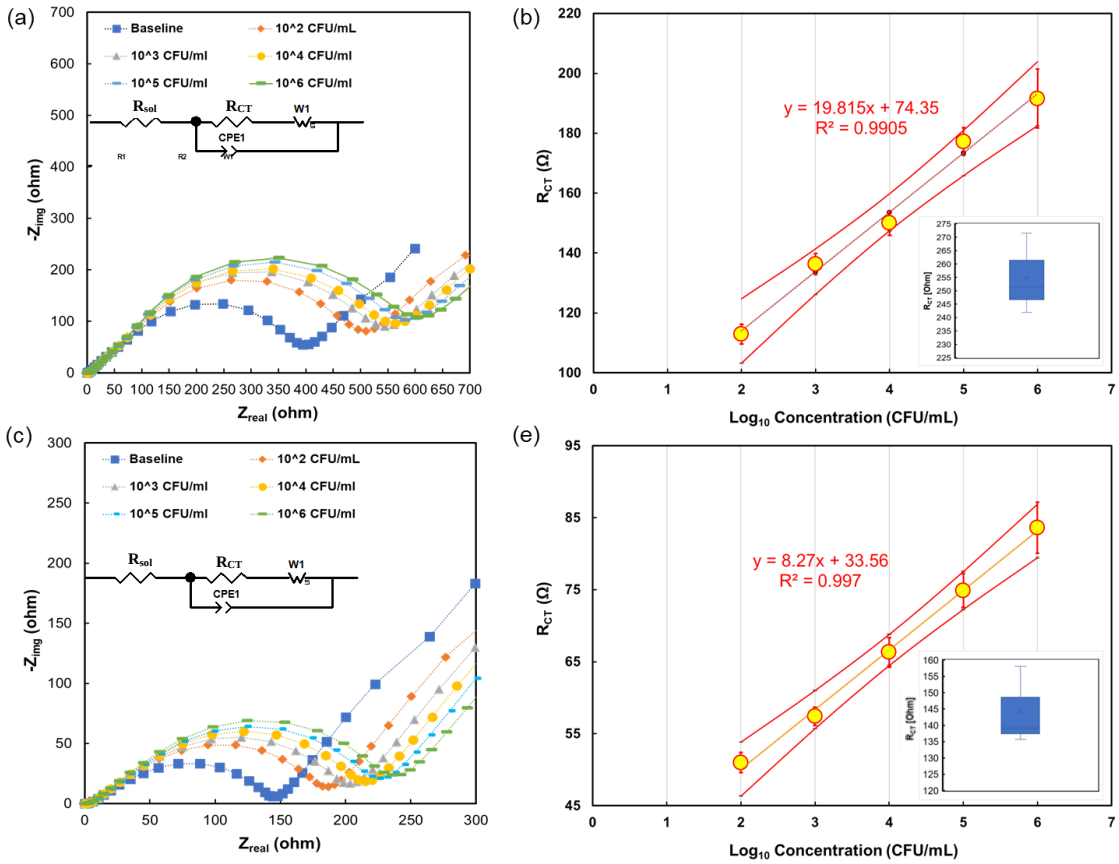

Figure 17: (a) Impedimetric response in 1X PBS to *L. monocytogenes* with the equivalent circuit in the inset; (b) Reliable range of calibration curve in 1X PBS buffer along with linearity confidence interval limits with confidence level of 95% the inset shows a box plot of the baseline measurements; (c) Impedimetric response in 1 % chicken broth to *L. monocytogenes* with the equivalent circuit in the inset; and (d) Reliable range of calibration curve in 1 % chicken broth along with linearity confidence interval limits with confidence level of 95% the inset shows a box plot of the baseline measurements.

Following these results, the biosensor's stability over time was tested. SPEs were prepared at the same time and submerged in 1X PBS at 4 ^{o}C until tested after 1 hour, 1 day, 1 week, and 2 weeks. Per each mentioned time triplicate impedimetric measurements were obtained with 100 CFU/mL *L. monocytogenes* in broth. The variation in impedance signal from the initial value was calculated as the percentage change from the results obtained after 1 h as shown in Figure 18. Since all the electrodes have been prepared at the same time under the same conditions, the results after 1 h were considered as 100 % and all other results have been compared to them. By doing so, it is possible to compare the change in signal over time. The stability measurements showed that after a day, the response was reduced by 10 % but maintained stability. After a week, an overall 30 % reduction was observed and the error became larger, and after 2 weeks the signal was only 40 % of its original value.

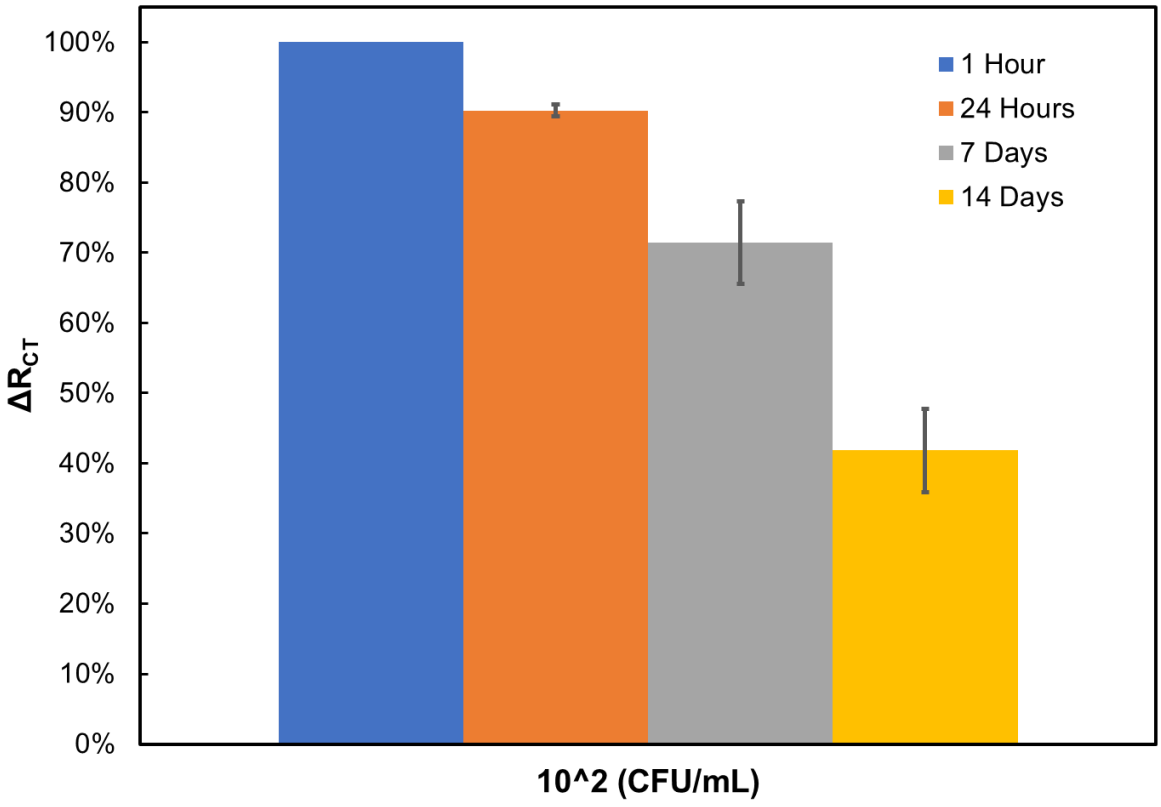

Figure 18: Biosensor stability over time, measured in broth.

Role of Phage as Biorecognition Molecule:

After the positive response of the biosensor to varying concentrations of *L. monocytogenes* in broth, the effect of the P100 bacteriophage as biorecognition molecule was tested to ensure that the impedimetric signal for *L. monocytogenes* detection can be attributed to the presence of biorecognition molecule. Two sets of SPE, one unmodified and the other immobilized with P100 bacteriophage for the same duration. Figure 19 shows the impedimetric response of the biosensor with and without P100 bacteriophage. The response showed that when modified with the phage, there was significantly higher impedance signal which also increased with the concentration analyte, while the SPE without the phage showed almost constant response with little effect from the raising concentrations. The results indicate the impedance signal can be attributed to selective binding of *L. monocytogenes* to the P100 bacteriophage on the SPE.

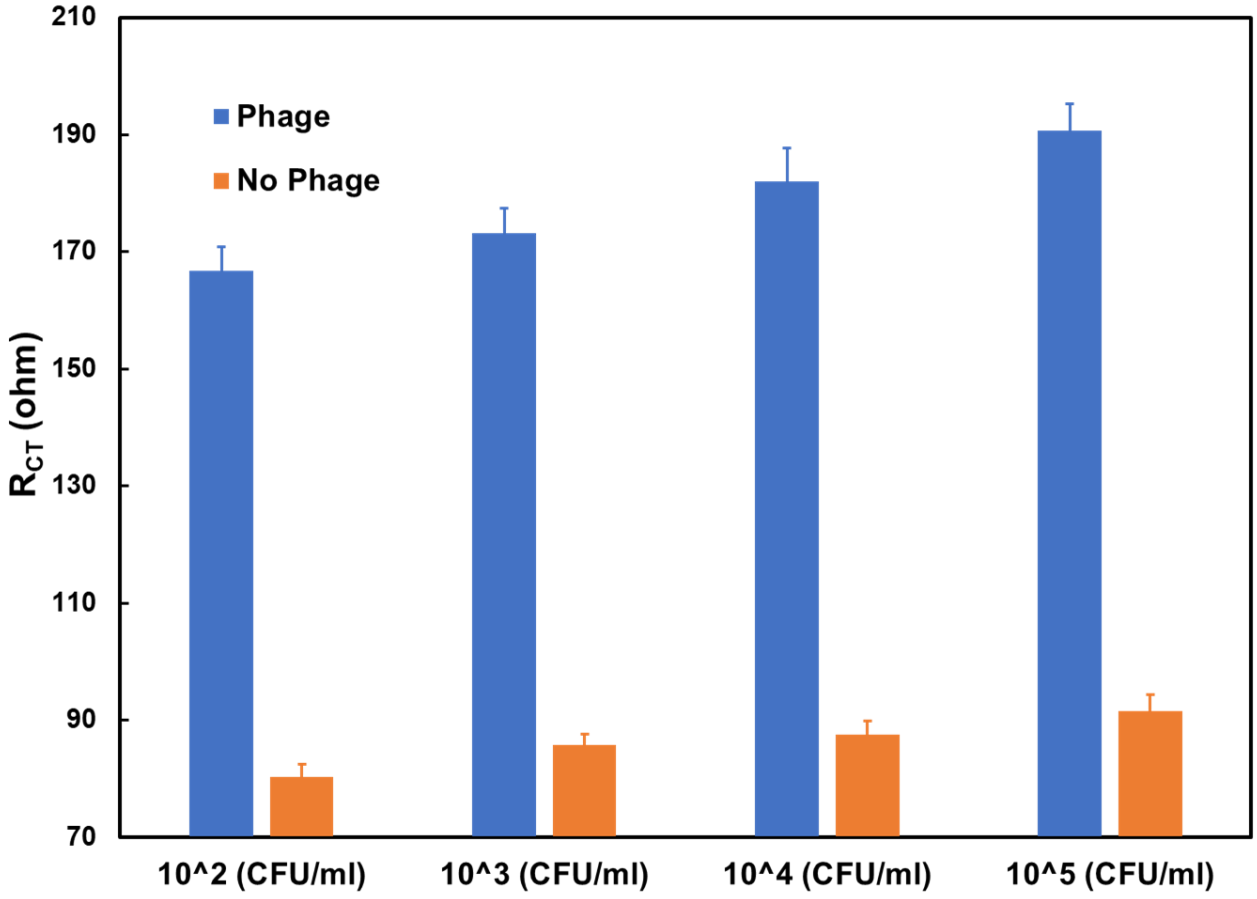

Figure 19: R_{CT} values from measurements of SPE modified with and without P100 bacteriophage

Specificity of the Biosensor:

The specificity of the phage modified biosensor was tested by exposing the SPE with and without P100 bacteriophage to non-target pathogens, *E. coli* O157:H7 and ser. Typhimurium-291RH. In the first set of experiments, 10^2 CFU/mL of single pathogen in broth were tested. In the second set of experiments, a sample containing *E. coli* O157:H7 and ser. Typhimurium-291RH in a concentration of 10^3 CFU/mL each one. In addition, *L. monocytogenes* was added at two different concentrations 10^2 and 10^3 CFU/mL. The impedimetric response to a single pseudo-analyte was 10 - 20 ohm above the response from the negative broth control, while the response to *L. monocytogenes* was 75 ohm above it, as seen in Figure 20

(a), response to pseudo-analytes is 13-26 % of the response to *L. monocytogenes*. This suggests that the biosensor is very specific and a positive response will only originate from bacteriophage-*L. monocytogenes* interaction. The biosensor without phage biorecognition molecule showed 8 - 10 ohm response from all test solutions and the control which further demonstrate the phage effectivity. In the interference study, shown in Figure 20 (b), the biosensor response to a broth sample with both pseudo-analytes with and without *L. monocytogenes* is presented. When *L. monocytogenes* is present even at lower concentration than the pseudo-analytes a clear signal was measured. In these measurements when the biosensor had no phage the response was almost constant without any dependency on the concentration of *L. monocytogenes* which farther emphasizes the specificity of the P100 bacteriophage even in a multi-contaminate environment.

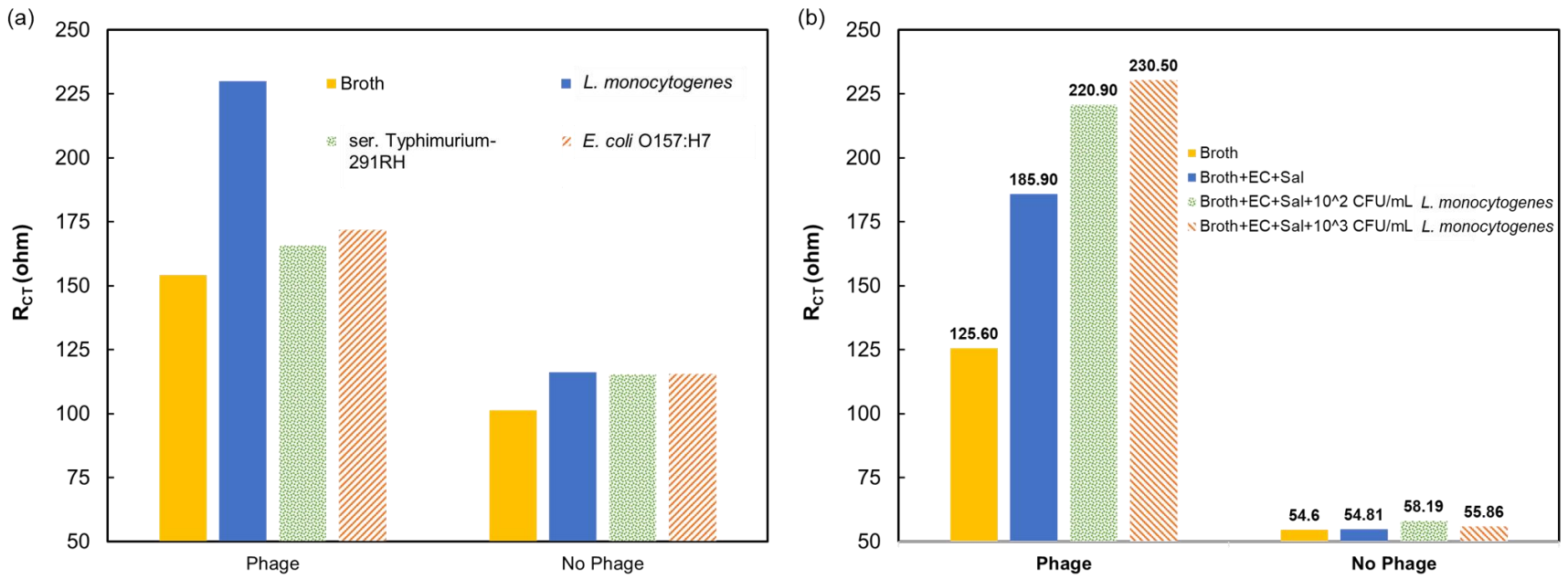

Figure 20: Specificity studies in 1 % chicken broth. (a) Biosensor response to *L. monocytogenes* and non-target pathogens with and without P100 phage; and (b) Interference study where non-target pathogens are kept at 10^3 CFU/mL and L. monocytogenes changes from 0 (negative control) to 10^3 CFU/mL (EC = *E. coli* O157:H7; Sal = ser. Typhimurium-291RH; and Lis = *L. monocytogenes*).

Detection under flow:

The final step was to conduct *L. monocytogenes* measurements in broth at different flow rates. The capbility to detect *L. monocytogenes* in flow conditions is an important proof of concept in the path to portable electrochemical biosensor and to the ability to integrate such a sensor into a production line. Initialy, a 0.01% Tween® 20 solution was flowed through the system. Then, an SPE was inserted into the flow cell and the broth or bacterial sample was flowed on the biosensor's surface for 8 minutes at a flow rate of 0.1 mL/min. After that, 5mM $[Fe(CN)_6]^{4-}/[Fe(CN)_6]^{3-}$ solution was flowed on the SPE surface at a rate of either 0.5 mL/min, 1 mL/min, or 2 mL/min. While the redox couple solution was flowing impedimetric measurements were taken. A Nyquist plot with the results of the 0.5 mL/min flow rate is shown in Figure 21 (a) and the response from all flow rates is presented in the bar chart in Figure 21 (b). The results show that without phage the response is an increase of 1 - 5 ohm and the flow rate did not change them outside of that range. With phage modified SPE the response shows a 10 % decrease in signal every time the flow rate doubles. Even though there was a decrease, the signals all changed with the concentration of *L. monocytogenes*. These results demonstrate that the whole detection process can be accomplished under flow after the SPE is prepared and modified.

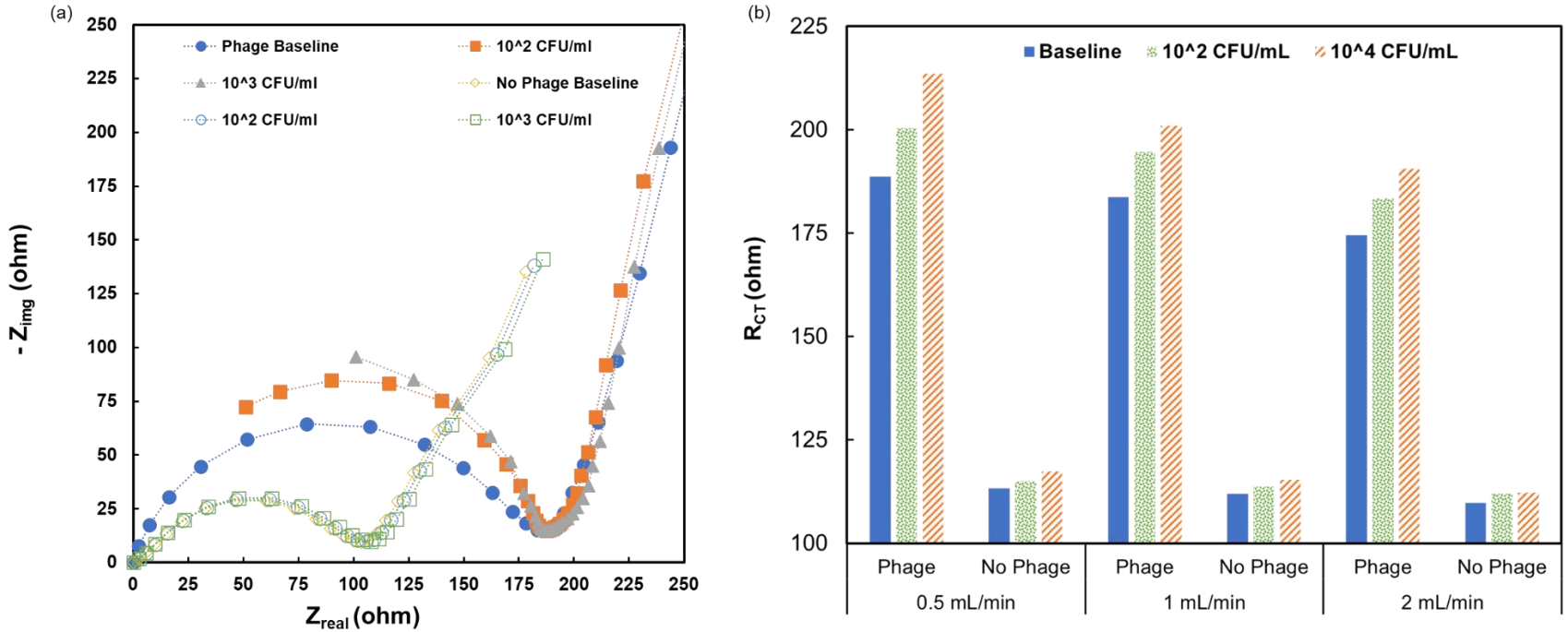

Figure 21: Biosensor's response to *L. monocytogenes* at different concentrations under flow. (a) Nyquist plot of the response with flow rate of 0.5 mL/min; and (b) Bar chart of the response with different flow rates and different *L. monocytogenes* concentrations.

4. Conclusions:

A portable, sensitive, and selective electrochemical biosensors for *L. monocytogenes* was developed and tested in this work. The biosensor demonstrated an ability to detect target bacteria with LOD of 10 CFU/mL which is better than most competing devices and two orders of magnitude more sensitive than PCR. Successful detection measurements were completed in diluted chicken broth with multiple pathogens under flow conditions. The selectivity of the P100 bacteriophage was demonstrated with exposure to a single pathogen and with interference studies. The biosensor has shown stability of up to one week. The use of q-CNT allowed the oriented deposition of P100 phage on the surface of the work electrode. The use of SPEs and microfluidic flow chamber confirmed the portability of the biosensor and its ability to work under complex conditions. These characteristics make the biosensor a suitable platform for industrial food production line and private detection of foodborne pathogens. Future work will be to further examine the biosensor under flow with different food matrices, in addition to add microfluidic sample preparation to allow a singular device for sample collection to detection.

CHAPTER 5

CONCLUSIONS AND FUTURE DIRECTIONS

Developing portable biosensors for foodborne pathogens is an important next step in early detection of infection and the prevention of outbreaks before infected products can reach consumers. Although in most cases the severity of foodborne illness manifest in indigestion, nausea, and diarrhea severe cases may cause hospitalization and even mortality. There are many treatments and medication to treat foodborne pathogen infection, but usually until multiple cases of severe symptoms arise the infection source will not be identified. Current detection standard of bacterial culturing approach requires the use of expensive specialized labs, special equipment, and highly trained personal make these methods expensive and time consuming although very accurate and reliable. The process requires two to five days depending on the target pathogen, its concentration, and the food matrix it is in. All of these factors farther emphasize the need of a rapid, reliable, sensitive, and portable biosensor that will allow early detection of the threat before it reaches the consumers. Biosensors offer a solution to all of these issues, and more specifically electrochemical biosensors due to their sensitivity, time of detection, selectivity, and simplicity of use. Phage-based biosensors offer advantages to other biorecognition elements mostly due to their stability in a wide range of environmental conditions and long shelf lives. Bacteriophages are highly specific due to the receptor binding proteins on their tail fiber that will only attach to a live target.

This dissertation was focused on the development of a phage-based electrochemical impedimetric biosensor on a portable platform for quick and early detection of foodborne

pathogens. The specificity of the biosensor was achieved by utilizing bacteriophage as the biorecognition element. This biosensor can detect its target in both buffer and food samples with very high sensitivity and selectivity. *Listeria monocytogenes* Scott A was chosen as a model analyte and P100 LISTAX bacteriophage as the biorecognition element. To allow the bacteriophage to attach to the surface with its tail fibers in the right orientation, carbon nanotubes with quarternized polyethyleneimine (q-CNT) functionalization were used. P100 bacteriophage has a negatively charged capsule and a positively charged tail, hence due to electrostatic attraction between the phage capsule and the highly positively charged q-CNT. To avoid non-specific binding 0.01 % bovine serum albumin (BSA) blocking agent was used on the surface of the electrode. The results showed active linear range between 10 to 10^4 CFU/mL and a limit of detection of 8.4 CFU/mL with a glassy carbon electrode. When the portable screen-printed electrode was used the limit of detection was 55 CFU/mL in 1X PBS buffer and 10 CFU/mL in 1 % diluted chicken broth, which suggests a detection limit of 10^3 CFU/mL in undiluted broth samples. In addition, the results showed very high recovery rates that farther example the concentration predictability of the biosensor.

Based on the scope of the research discussed in this dissertation, the following paths could be taken for future research on these topics:

1. Sample pretreatment steps like filtration of macro particles, concentration, isolation of target pathogen, and delivery of target pathogen to the detection area of the sensor are currently auxiliary steps that requires the use of additional equipment and add time from sample collection to detection. The utilization of microfluidics can address all of these issues and will be another step towards a point of care lab-on-a-chip device for the detection of foodborne pathogens.

2. The specificity and sensitivity of the biosensor have proved to be very high, but can farther improve by reducing non-specific attachment of pseudo-analytes. This could be achieved by researching alternative surface blocking agents that can repeal the pseudo-analytes or prevent them from interacting with the electrode.

The developed methodology can be used for the detection of almost any bacteria, provided a relevant phage. Investigating this platform with other phage types for the detection of other foodborne bacteria can lead to a multiplexed platform that can detect multiple bacteria from the same sample at the same time or to develop customable kits for the detection of specific foodborne pathogens.

REFERENCES

1. Centers for Disease Control and Preventation Food Safety Available online: https://www.cdc.gov/foodsafety/ (accessed on Nov 3, 2023).
2. Bintsis, T. Foodborne pathogens. *AIMS Microbiol.* **2017**, *3*, 529–563.
3. HOFFMANN, S.; BATZ, M.B.; MORRIS, J.G. Annual Cost of Illness and Quality-Adjusted Life Year Losses in the United States Due to 14 Foodborne Pathogens†. *J. Food Prot.* **2012**, *75*, 1292–1302.
4. World Health Organization Food Safety Available online: https://www.who.int/news-room/fact-sheets/detail/food-safety (accessed on Mar 4, 2023).
5. US Food and Drug Administration Foodborne Pathogens Available online: https://www.fda.gov/food/outbreaks-foodborne-illness/foodborne-pathogens (accessed on Mar 4, 2023).
6. Bacon, T.R.; Sofos, J.N. Characteristics of Biological Hazards in Foods. In *Food Safety Handbook*; Schmidt, R.H., Rodrick, G.E., Eds.; John Wiley & Sons, Inc.: New Jersey, 2003; pp. 157–196 ISBN 0-471-21064-1.
7. Grohmann, G.; Murphy, A.; Christopher, P.; Auty, E.; Greenberg, H. NORWALK VIRUS GASTROENTERITIS IN VOLUNTEERS CONSUMING DEPURATED OYSTERS. *Aust. J. Exp. Biol. Med. Sci.* **1981**, *59*, 219–228.
8. DiGirolamo, R.; Liston, J.; Matches, J.R. Survival of Virus in Chilled, Frozen, and Processed Oysters. *Appl. Microbiol.* **1970**, *20*, 58–63.
9. Murray, C.J.L.; Vos, T.; Lozano, R.; Naghavi, M.; Flaxman, A.D.; Michaud, C.; Ezzati,

M.; Shibuya, K.; Salomon, J.A.; Abdalla, S.; et al. Disability-adjusted life years (DALYs) for 291 diseases and injuries in 21 regions, 1990–2010: a systematic analysis for the Global Burden of Disease Study 2010. *Lancet* **2012**, *380*, 2197–2223.

10. Centers for Disease Control and Prevention Foodborne Outbreaks Available online: https://www.cdc.gov/foodsafety/outbreaks/index.html (accessed on Nov 3, 2023).
11. Hedberg, C.W. Foodborne illness acquired in the United States. *Emerg. Infect. Dis.* **2011**, *17*, 1338–1340.
12. LeDuc, P.; Agaba, M.; Cheng, C.M.; Gracio, J.; Guzman, A.; Middelberg, A. Beyond disease, how biomedical engineering can improve global health. *Sci. Transl. Med.* **2014**, *6*, 1–4.
13. Priyanka, B.; Patil, R.K.; Dwarakanath, S. A review on detection methods used for foodborne pathogens. *Indian J. Med. Res.* **2016**, *144*, 327–338.
14. Feng, P. Impact of Molecular Biology on the Detection of Foodborne Pathogens. *Appl. Biochem. Biotechnol. - Part B Mol. Biotechnol.* **1997**, *7*, 267–278.
15. Foddai, A.C.G.; Grant, I.R. Methods for detection of viable foodborne pathogens: current state-of-art and future prospects. *Appl. Microbiol. Biotechnol.* **2020**, *104*, 4281–4288.
16. Lam, H.M.; Remais, J.; Fung, M.C.; Xu, L.; Sun, S.S.M. Food supply and food safety issues in China. *Lancet* **2013**, *381*, 2044–2053.
17. Chin, C.D.; Linder, V.; Sia, S.K. Lab-on-a-chip devices for global health: Past studies and future opportunities. *Lab Chip* **2007**, *7*, 41–57.
18. Bunney, J.; Williamson, S.; Atkin, D.; Jeanneret, M.; Cozzolino, D.; Chapman, J.; Power, A.; Chandra, S. The Use of Electrochemical Biosensors in Food Analysis. *Curr. Res. Nutr. Food Sci. J.* **2017**, *5*, 183–195.

19. Bhalla, N.; Jolly, P.; Formisano, N.; Estrela, P. Introduction to biosensors. *Essays Biochem.* **2016**, *60*, 1–8.

20. Michelmore, A. Thin film growth on biomaterial surfaces. In *Thin Film Coatings for Biomaterials and Biomedical Applications*; Elsevier, 2016; pp. 29–47.

21. Newman, J.D.; Turner, A.P.F. Home blood glucose biosensors: a commercial perspective. *Biosens. Bioelectron.* **2005**, *20*, 2435–2453.

22. Turner, A.P.F. Biosensors: sense and sensibility. *Chem. Soc. Rev.* **2013**, *42*, 3184.

23. Sethi, R.S. Transducer aspects of biosensors. *Biosens. Bioelectron.* **1994**, *9*, 243–264.

24. Presedence Research Biosensors Market Size, Growth, Trends, Report 2022 to 2030 Available online: https://www.precedenceresearch.com/biosensors-market (accessed on Dec 3, 2023).

25. MARKETSANDMARKETS Biosensors Market Available online: https://www.marketsandmarkets.com/Market-Reports/biosensors-market-798.html (accessed on Dec 3, 2023).

26. Skládal, P. Piezoelectric biosensors. *TrAC Trends Anal. Chem.* **2016**, *79*, 127–133.

27. Eltzov, E.; Cosnier, S.; Marks, R.S. Biosensors based on combined optical and electrochemical transduction for molecular diagnostics. *Expert Rev. Mol. Diagn.* **2011**, *11*, 533–546.

28. Leung, A.; Shankar, P.M.; Mutharasan, R. A review of fiber-optic biosensors. *Sensors Actuators B Chem.* **2007**, *125*, 688–703.

29. Ramanathan, K.; Danielsson, B. Principles and applications of thermal biosensors. *Biosens. Bioelectron.* **2001**, *16*, 417–423.

30. Yakovleva, M.; Bhand, S.; Danielsson, B. The enzyme thermistor—A realistic biosensor

concept. A critical review. *Anal. Chim. Acta* **2013**, *766*, 1–12.

31. Singh, A.; Sharma, A.; Ahmed, A.; Sundramoorthy, A.K.; Furukawa, H.; Arya, S.; Khosla, A. Recent Advances in Electrochemical Biosensors: Applications, Challenges, and Future Scope. *Biosensors* **2021**, *11*, 336.
32. Cesewski, E.; Johnson, B.N. Electrochemical biosensors for pathogen detection. *Biosens. Bioelectron.* **2020**, *159*, 112214.
33. Cho, I.-H.; Kim, D.H.; Park, S. Electrochemical biosensors: perspective on functional nanomaterials for on-site analysis. *Biomater. Res.* **2020**, *24*, 6.
34. Leca-Bouvier, B.D.; Blum, L.J. Enzyme for Biosensing Applications. In *Recognition Receptors in Biosensors*; Springer New York: New York, NY, 2010; pp. 177–220.
35. Newman, J.D.; Setford, S.J. Enzymatic Biosensors. *Mol. Biotechnol.* **2006**, *32*, 249–268.
36. Donahue, A.C.; Albitar, M. Antibodies in Biosensing. In *Recognition Receptors in Biosensors*; Springer New York: New York, NY, 2010; pp. 221–248.
37. Sharma, S.; Byrne, H.; O'Kennedy, R.J. Antibodies and antibody-derived analytical biosensors. *Essays Biochem.* **2016**, *60*, 9–18.
38. Kotsiri, Z.; Vidic, J.; Vantarakis, A. Applications of biosensors for bacteria and virus detection in food and water–A systematic review. *J. Environ. Sci.* **2022**, *111*, 367–379.
39. Hashem, A.; Hossain, M.A.M.; Marlinda, A.R.; Mamun, M. Al; Sagadevan, S.; Shahnavaz, Z.; Simarani, K.; Johan, M.R. Nucleic acid-based electrochemical biosensors for rapid clinical diagnosis: advances, challenges, and opportunities. *Crit. Rev. Clin. Lab. Sci.* **2022**, *59*, 156–177.
40. Glynn, B.; O'Connor, L. Nucleic Acid Diagnostic Biosensors. In *Recognition Receptors in Biosensors*; Springer New York: New York, NY, 2010; pp. 343–363.

41. Zourob, M.; Ripp, S. Bacteriophage-Based Biosensors. In *Recognition Receptors in Biosensors*; Springer New York: New York, NY, 2010; pp. 415–448.

42. Zolti, O.; Suganthan, B.; Ramasamy, R.P. Lab-on-a-Chip Electrochemical Biosensors for Foodborne Pathogen Detection: A Review of Common Standards and Recent Progress. *Biosensors* **2023**, *13*, 215.

43. Zolti, O.; Suganthan, B.; Maynard, R.; Asadi, H.; Locklin, J.; Ramasamy, R.P. Electrochemical Biosensor for Rapid Detection of Listeria monocytogenes. *J. Electrochem. Soc.* **2022**, *169*, 067510.

44. Wang, J. Nanomaterial-based electrochemical biosensors. *Analyst* **2005**, *130*, 421.

45. Zeng, Y.; Zhu, Z.; Du, D.; Lin, Y. Nanomaterial-based electrochemical biosensors for food safety. *J. Electroanal. Chem.* **2016**, *781*, 147–154.

46. Dresselhaus, M.S.; Dresselhaus, G.; Eklund, P.C.; Rao, A.M. Carbon Nanotubes. In *The Physics of Fullerene-Based and Fullerene-Related Materials*; Andreoni, W., Ed.; Springer Netherlands: Dordrecht, 2000; pp. 331–379 ISBN 978-94-011-4038-6.

47. Jiang, Z.; Feng, B.; Xu, J.; Qing, T.; Zhang, P.; Qing, Z. Graphene biosensors for bacterial and viral pathogens. *Biosens. Bioelectron.* **2020**, *166*, 112471.

48. George, J.M.; Antony, A.; Mathew, B. Metal oxide nanoparticles in electrochemical sensing and biosensing: a review. *Microchim. Acta* **2018**, *185*, 358.

49. Fazio, E.; Spadaro, S.; Corsaro, C.; Neri, G.; Leonardi, S.G.; Neri, F.; Lavanya, N.; Sekar, C.; Donato, N.; Neri, G. Metal-Oxide Based Nanomaterials: Synthesis, Characterization and Their Applications in Electrical and Electrochemical Sensors. *Sensors* **2021**, *21*, 2494.

50. Lavagnini, I.; Antiochia, R.; Magno, F. A Calibration-Base Method for the Evaluation of the Detection Limit of an Electrochemical Biosensor. *Electroanalysis* **2007**, *19*, 1227–

1230.

51. Hassibi, A.; Vikalo, H.; Hajimiri, A. On noise processes and limits of performance in biosensors. *J. Appl. Phys.* **2007**, *102*, 014909.

52. BROWN, P.; MUSIL, S.A. AUTOMATED DATA ACQUISITION AND PROCESSING. In *Environmental Monitoring and Characterization*; Elsevier, 2004; pp. 49–67.

53. Ferkany, J.W. RADIOCHEMICAL METHODS | Radioreceptor Assays. In *Encyclopedia of Analytical Science*; Elsevier, 2005; pp. 65–71.

54. Williams, A.J. Foreword. In *Measuring Ocean Currents*; Elsevier, 2014; pp. xi–xviii.

55. Mocak, J.; Bond, A.M.; Mitchell, S.; Scollary, G. A statistical overview of standard (IUPAC and ACS) and new procedures for determining the limits of detection and quantification: Application to voltammetric and stripping techniques (Technical Report). *Pure Appl. Chem.* **1997**, *69*, 297–328.

56. Loock, H.-P.; Wentzell, P.D. Detection limits of chemical sensors: Applications and misapplications. *Sensors Actuators B Chem.* **2012**, *173*, 157–163.

57. Lister, A.S. 7 Validation of HPLC methods in pharmaceutical analysis. In *Separation Science and Technology*; 2005; pp. 191–217.

58. Vashist, S.K.; Luong, J.H.T. Bioanalytical Requirements and Regulatory Guidelines for Immunoassays. In *Handbook of Immunoassay Technologies*; Elsevier, 2018; pp. 81–95.

59. Mohammad-Razdari, A.; Ghasemi-Varnamkhasti, M.; Izadi, Z.; Rostami, S.; Ensafi, A.A.; Siadat, M.; Losson, E. Detection of sulfadimethoxine in meat samples using a novel electrochemical biosensor as a rapid analysis method. *J. Food Compos. Anal.* **2019**, *82*, 103252.

60. Jurado, J.M.; Alcázar, A.; Muñiz-Valencia, R.; Ceballos-Magaña, S.G.; Raposo, F. Some

practical considerations for linearity assessment of calibration curves as function of concentration levels according to the fitness-for-purpose approach. *Talanta* **2017**, *172*, 221–229.

61. Raposo, F. Evaluation of analytical calibration based on least-squares linear regression for instrumental techniques: A tutorial review. *TrAC Trends Anal. Chem.* **2016**, *77*, 167–185.
62. Thompson, M.; Lowthian, P.J. *Notes On Statistics And Data Quality For Analytical Chemists*; 1st ed.; Imperial College Press: London, 2011; ISBN 978-1-84816-616-5.
63. Johnson, E.L.; Reynolds, D.L.; Scott Wright, D.; Pachla, L.A. Biological Sample Preparation and Data Reduction Concepts in Pharmaceutical Analysis. *J. Chromatogr. Sci.* **1988**, *26*, 372–379.
64. Hubert, P.; Chiap, P.; Crommen, J.; Boulanger, B.; Chapuzet, E.; Mercier, N.; Bervoas-Martin, S.; Chevalier, P.; Grandjean, D.; Lagorce, P.; et al. The SFSTP guide on the validation of chromatographic methods for drug bioanalysis: from the Washington Conference to the laboratory. *Anal. Chim. Acta* **1999**, *391*, 135–148.
65. Miah, M.R.; Ohsaka, T. Cathodic Detection of H 2 O 2 Using Iodide-Modified Gold Electrode in Alkaline Media. *Anal. Chem.* **2006**, *78*, 1200–1205.
66. Tsai, W.; Wen, S. Determination of Uric Acid in Serum by a Mediated Amperometric Biosensor. *Anal. Lett.* **2006**, *39*, 891–901.
67. Ricci, F.; Arduini, F.; Tuta, C.S.; Sozzo, U.; Moscone, D.; Amine, A.; Palleschi, G. Glutathione amperometric detection based on a thiol–disulfide exchange reaction. *Anal. Chim. Acta* **2006**, *558*, 164–170.
68. Pereira, F.C.; Moretto, L.M.; De Leo, M.; Boldrin Zanoni, M. V.; Ugo, P. Gold nanoelectrode ensembles for direct trace electroanalysis of iodide. *Anal. Chim. Acta* **2006**,

575, 16–24.

69. Chalk, S.J. limit of detection in analysis. In *The IUPAC Compendium of Chemical Terminology*; McNaught, A.D., Wikinson, A., Eds.; International Union of Pure and Applied Chemistry (IUPAC): Research Triangle Park, NC, 2014; p. 1 ISBN 0-9678550-9-8.
70. Miller, J.; Miller, J. *Statistics and Chemometrics for Analytical Chemistry*; Pearson Education/ Premtice Hall, Ed.; 4th ed.; Pearson Education/ Premtice Hall: Harrow, UK, 2000; ISBN 0-13-022888-5.
71. Asadi, H.; Ramasamy, R.P. Graphene-based Electrochemical Biosensor for Impedimetric Detection of miRNAs as Potential Cancer Biomarkers. *J. Electrochem. Soc.* **2020**, *167*, 167523.
72. Keene, O.N. The log transformation is special. *Stat. Med.* **1995**, *14*, 811–819.
73. Shrivastava, A.; Gupta, V. Methods for the determination of limit of detection and limit of quantitation of the analytical methods. *Chronicles Young Sci.* **2011**, *2*, 21.
74. FDA Foodborne Pathogens Available online: https://www.fda.gov/food/outbreaks-foodborne-illness/foodborne-pathogens.
75. Jahan, S. Epidemiology of foodborne illness. In *Scientific, Health and Social Aspects of the Food Industry*; Valdez, B., Schor, M., Zlatev, R., Eds.; InTech: Rijeka, Croatia, 2012; pp. 321–342 ISBN 978-953-307-916-5.
76. CDC Foodborne Outbreaks Available online: https://www.cdc.gov/foodsafety/outbreaks/lists/outbreaks-list.html.
77. Castle, L.M.; Schuh, D.A.; Reynolds, E.E.; Furst, A.L. Electrochemical Sensors to Detect Bacterial Foodborne Pathogens. *ACS Sensors* **2021**, *6*, 1717–1730.

78. Kumar, H.; Kuča, K.; Bhatia, S.K.; Saini, K.; Kaushal, A.; Verma, R.; Bhalla, T.C.; Kumar, D. Applications of nanotechnology in biosensor-based detection of foodborne pathogens. *Sensors (Switzerland)* **2020**, *20*, 1–19.

79. Lin, C.-Y.; Nhat Nguyen, U.T.; Hsieh, H.-Y.; Tahara, H.; Chang, Y.-S.; Wang, B.-Y.; Gu, B.-C.; Dai, Y.-H.; Wu, C.-C.; Tsai, I.-J.; et al. Peptide-based electrochemical sensor with nanogold enhancement for detecting rheumatoid arthritis. *Talanta* **2022**, *236*, 122886.

80. Colburn, A.W.; Levey, K.J.; O'Hare, D.; Macpherson, J. V. Lifting the lid on the potentiostat: a beginner's guide to understanding electrochemical circuitry and practical operation. *Phys. Chem. Chem. Phys.* **2021**, *23*, 8100–8117.

81. Chen, Q.; Wang, D.; Cai, G.; Xiong, Y.; Li, Y.; Wang, M.; Huo, H.; Lin, J. Fast and sensitive detection of foodborne pathogen using electrochemical impedance analysis , urease catalysis and micro fl uidics. *Biosens. Bioelectron.* **2016**, *86*, 770–776.

82. Wang, R.; Xu, Y.; Sors, T.; Irudayaraj, J.; Ren, W.; Wang, R. Impedimetric detection of bacteria by using a microfluidic chip and silver nanoparticle based signal enhancement. *Microchim. Acta* **2018**, *185*, 1–8.

83. Siller, I.G.; Preuss, J.; Urmann, K.; Ho, M.R.; Scheper, T.; Bahnemann, J. 3D-Printed Flow Cells for Aptamer-Based. *Sensors* **2020**, *20*, 4421.

84. Chiriacò, M.S.; Parlangeli, I.; Sirsi, F.; Poltronieri, P.; Primiceri, E. Impedance sensing platform for detection of the food pathogen listeria monocytogenes. *Electron.* **2018**, *7*, 1–11.

85. Liu, J.; Jasim, I.; Shen, Z.; Zhao, L.; Dweik, M.; Zhang, S.; Almasri, M. A microfluidic based biosensor for rapid detection of *Salmonella* in food products. *PLoS One* **2019**, 1–18.

86. Dzyadevych, S. V.; Arkhypova, V.N.; Soldatkin, A.P.; El'skaya, A. V.; Martelet, C.;

Jaffrezic-Renault, N. Amperometric enzyme biosensors: Past, present and future. *Itbm-Rbm* **2008**, *29*, 171–180.

87. Lopez-Tellez, J.; Ramirez-Montes, S.; Ferreira, T.A.; Santos, E.M.; Rodriguez, J.A. Application of Voltammetric Sensors for Pathogen Bacteria Detection: A Review. *Chemosensors* **2022**, *10*, 424.

88. Dutta, P.; Lu, Y.-J.; Hsieh, H.-Y.; Lee, T.-Y.; Lee, Y.-T.; Cheng, C.-M.; Fan, Y.-J. Detection of Candida albicans Using a Manufactured Electrochemical Sensor. *Micromachines* **2021**, *12*, 166.

89. Fan, Y.-J.; Hsu, Y.-C.; Gu, B.-C.; Wu, C.-C. Voltammetric measurement of Escherichia coli concentration through p-APG hydrolysis by endogenous β-galactosidase. *Microchem. J.* **2020**, *154*, 104641.

90. Mairhofer, J.; Roppert, K.; Ertl, P. Microfluidic systems for pathogen sensing: A review. *Sensors (Switzerland)* **2009**, *9*, 4804–4823.

91. Fernández-la-Villa, A.; Pozo-Ayuso, D.F.; Castaño-Álvarez, M. Microfluidics and electrochemistry: an emerging tandem for next-generation analytical microsystems. *Curr. Opin. Electrochem.* **2019**, *15*, 175–185.

92. Sheen, H.-J.; Panigrahi, B.; Kuo, T.-R.; Hsu, W.-C.; Chung, P.-S.; Xie, Q.-Z.; Lin, C.-Y.; Chang, Y.-S.; Lin, C.-T.; Fan, Y.-J. Electrochemical biosensor with electrokinetics-assisted molecular trapping for enhancing C-reactive protein detection. *Biosens. Bioelectron.* **2022**, *210*, 114338.

93. Zhang, C.; Xing, D.; Li, Y. Micropumps, microvalves, and micromixers within PCR microfluidic chips: Advances and trends. *Biotechnol. Adv.* **2007**, *25*, 483–514.

94. Yoon, J.-Y.; Kim, B. Lab-on-a-Chip Pathogen Sensors for Food Safety. *Sensors* 2012, *12*,

10713–10741.

95. Mei, Y.; He, C.; Zeng, W.; Luo, Y.; Liu, C.; Yang, M.; Kuang, Y.; Lin, X.; Huang, Q. Electrochemical Biosensors for Foodborne Pathogens Detection Based on Carbon Nanomaterials: Recent Advances and Challenges. *Food Bioprocess Technol.* **2022**, *15*, 498–513.

96. Villalonga, A.; Sánchez, A.; Mayol, B.; Reviejo, J.; Villalonga, R. Electrochemical biosensors for food bioprocess monitoring. *Curr. Opin. Food Sci.* **2022**, *43*, 18–26.

97. Curulli, A. Electrochemical Biosensors in Food Safety: Challenges and Perspectives. *Molecules* **2021**, *26*, 2940.

98. Schmidt-Speicher, L.M.; Länge, K. Microfluidic integration for electrochemical biosensor applications. *Curr. Opin. Electrochem.* **2021**, *29*, 100755.

99. Lonchamps, P.-L.; He, Y.; Wang, K.; Lu, X. Detection of pathogens in foods using microfluidic “lab-on-chip”: A mini review. *J. Agric. Food Res.* **2022**, *10*, 100430.

100. Health Protection Agency Guidelines for Assessing the Microbiological Safety of Ready-to-Eat Foods Placed on the Market. *Heal. Prot. Agency, London.* **2009**, 33.

101. Faherty, clinChristina S.; Lampel, K.A. Shigella. In *Food Microbiology*; ASM Press: Washington, DC, USA, 2019; pp. 317–345.

102. Applied Nutrition Center for Food Safety and Of Regulatory Affairs Office CPG Sec 555.320 Listeria monocytogenes Available online: https://www.fda.gov/regulatory-information/search-fda-guidance-documents/cpg-sec-555320-listeria-monocytogenes#policy.

103. Applied Nutrition Center for Food Safety and Of Regulatory Affairs Office CPG Sec. 527.300 Dairy Products - Microbial Contaminants and Alkaline Phosphatase Activity

(CPG 7106.08) Available online: https://www.federalregister.gov/documents/2010/12/23/2010-32232/compliance-policy-guide-sec-527300-dairy-products-microbial-contaminants-and-alkaline-phosphatase.

104. SANITATION PROGRAM NATIONAL SHELLFISH NSSP Guide for the Control of Molluscan Shellfish Available online: https://www.issc.org/Data/Sites/1/media/2009 nssp guide/2009 nssp guide updated 08-08-2011.pdf.

105. United States Department of Agriculture Introduction to the microbiology of food processing: Small plant news guidebook series. **2012**, 1–64.

106. Centers for Disease Control and Prevention Mycobacterium Bovis (bovine tuberculosis) in humans. *Mycobacterium Bovis (bovine Tuberc. humans* **2011**, 2.

107. Ohio Department of Health IDCM Section 3: Vibriosis. In *Infectious Disease Control Manual (IDCM)*; 2019; pp. 1–8.

108. Ohio Department of Health IDCM Section 3: Yersiniosis. In *Infectious Disease Control Manual (IDCM)*; 2019; pp. 1–5.

109. Robilotti, E.; Deresinski, S.; Pinsky, B.A. Norovirus. *Clin. Microbiol. Rev.* **2015**, *28*, 134–164.

110. Smith, H. V Cyclospora. In *Infectious Disease: Foodborne Disease*; Simjee, S., Ed.; Humana Press Inc.: New Jersey, 2007; pp. 277–301 ISBN 9781588295187.

111. Rangel, J.M.; Sparling, P.H.; Crowe, C.; Griffin, P.M.; Swerdlow, D.L. Epidemiology of Escherichia coli O157:H7 outbreaks, United States, 1982-2002. *Emerg. Infect. Dis.* **2005**, *11*, 603–609.

112. Cartwright, E.J.; Jackson, K.A.; Johnson, S.D.; Graves, L.M.; Silk, B.J.; Mahon, B.E. Listeriosis outbreaks and associated food vehicles, United States, 1998-2008. *Emerg.*

Infect. Dis. **2013**, *19*, 1–9.

113. McCrickard, L.S.; Crim, S.M.; Kim, S.; Bowen, A. Disparities in severe shigellosis among adults - Foodborne diseases active surveillance network, 2002-2014. *BMC Public Health* **2018**, *18*, 1–8.

114. Foodborne Diseases Active Surveillance Network *Foodborne Diseases Active Surveillance Network (FoodNet): FoodNet Surveillance Reports for 1996-2020 (Final Reports)*; 2021;

115. Ren, K.; Zhou, J.; Wu, H. Materials for Microfluidic Chip Fabrication. *Acc. Chem. Res.* **2013**, *46*, 2396–2406.

116. Hou, X.; Zhang, Y.S.; Santiago, G.T.; Alvarez, M.M.; Ribas, J.; Jonas, S.J.; Weiss, P.S.; Andrews, A.M.; Aizenberg, J.; Khademhosseini, A. Interplay between materials and microfluidics. *Nat. Rev. Mater.* **2017**, *2*, 17016.

117. Nielsen, J.B.; Hanson, R.L.; Almughamsi, H.M.; Pang, C.; Fish, T.R.; Woolley, A.T. Microfluidics: Innovations in Materials and Their Fabrication and Functionalization. *Anal. Chem.* **2020**, *92*, 150–168.

118. Niculescu, A.-G.; Chircov, C.; Bîrcă, A.C.; Grumezescu, A.M. Fabrication and Applications of Microfluidic Devices: A Review. *Int. J. Mol. Sci.* **2021**, *22*, 2011.

119. Abdullah, A.; Dastider, S.G.; Jasim, I.; Shen, Z.; Yuksek, N.; Zhang, S.; Dweik, M.; Almasri, M. Microfluidic based impedance biosensor for pathogens detection in food products. *Electrophoresis* **2019**, *40*, 508–520.

120. Chand, R.; Neethirajan, S. Microfluidic platform integrated with graphene-gold nano-composite aptasensor for one-step detection of norovirus. *Biosens. Bioelectron.* **2017**, *98*, 47–53.

121. Silva, N.F.D.; Almeida, C.M.R.; Magalhães, J.M.C.S.; Gonçalves, M.P.; Freire, C.; Delerue-Matos, C. Development of a disposable paper-based potentiometric immunosensor for real-time detection of a foodborne pathogen. *Biosens. Bioelectron.* **2019**, *141*, 111317.

122. Jiang, H.; Sun, Z.; Guo, Q.; Weng, X. Microfluidic thread-based electrochemical aptasensor for rapid detection of Vibrio parahaemolyticus. *Biosens. Bioelectron.* **2021**, *182*, 113191.

123. Pinti, M.; Kambham, T.; Wang, B.; Prakash, S. Fabrication of Centimeter Long, Ultra-Low Aspect Ratio Nanochannel Networks in Borosilicate Glass Substrates. *J. Nanotechnol. Eng. Med.* **2013**, *4*.

124. Pawar, P.; Ballav, R.; Kumar, A. Micromachining of Borosilicate Glass: A State of Art Review. *Mater. Today Proc.* **2017**, *4*, 2813–2821.

125. Jung, H.C.; Lu, W.; Wang, S.; Lee, L.J.; Hu, X. Etching of Pyrex glass substrates by inductively coupled plasma reactive ion etching for micro/nanofluidic devices. *J. Vac. Sci. Technol. B Microelectron. Nanom. Struct.* **2006**, *24*, 3162.

126. Chang, T.-L.; Chen, Z.-C.; Lee, Y.-W.; Li, Y.-H.; Wang, C.-P. Ultrafast laser ablation of soda-lime glass for fabricating microfluidic pillar array channels. *Microelectron. Eng.* **2016**, *158*, 95–101.

127. Perrone, E.; Cesaria, M.; Zizzari, A.; Bianco, M.; Ferrara, F.; Raia, L.; Guarino, V.; Cuscunà, M.; Mazzeo, M.; Gigli, G.; et al. Potential of CO2-laser processing of quartz for fast prototyping of microfluidic reactors and templates for 3D cell assembly over large scale. *Mater. Today Bio* **2021**, *12*, 100163.

128. Tang, T.; Yuan, Y.; Yalikun, Y.; Hosokawa, Y.; Li, M.; Tanaka, Y. Glass based micro

total analysis systems: Materials, fabrication methods, and applications. *Sensors Actuators B Chem.* **2021**, *339*, 129859.

129. Aralekallu, S.; Boddula, R.; Singh, V. Development of glass-based microfluidic devices: A review on its fabrication and biologic applications. *Mater. Des.* **2023**, *225*, 111517.

130. Fan, Y.-J.; Huang, M.-Z.; Hsiao, Y.-C.; Huang, Y.-W.; Deng, C.-Z.; Yeh, C.; Husain, R.A.; Lin, Z.-H. Enhancing the sensitivity of portable biosensors based on self-powered ion concentration polarization and electrical kinetic trapping. *Nano Energy* **2020**, *69*, 104407.

131. Iliescu, C.; Taylor, H.; Avram, M.; Miao, J.; Franssila, S. A practical guide for the fabrication of microfluidic devices using glass and silicon. *Biomicrofluidics* **2012**, *6*, 016505.

132. Laser, D.J.; Santiago, J.G. A review of micropumps. *J. Micromechanics Microengineering* **2004**, *14*, R35–R64.

133. Oh, K.W.; Ahn, C.H. A review of microvalves. *J. Micromechanics Microengineering* **2006**, *16*, R13–R39.

134. Ali, U.; Karim, K.J.B.A.; Buang, N.A. A Review of the Properties and Applications of Poly (Methyl Methacrylate) (PMMA). *Polym. Rev.* **2015**, *55*, 678–705.

135. Frazer, R.Q.; Byron, R.T.; Osborne, P.B.; West, K.P. PMMA: An Essential Material in Medicine and Dentistry. *J. Long. Term. Eff. Med. Implants* **2005**, *15*, 629–639.

136. Martynova, L.; Locascio, L.E.; Gaitan, M.; Kramer, G.W.; Christensen, R.G.; MacCrehan, W.A. Fabrication of Plastic Microfluid Channels by Imprinting Methods. *Anal. Chem.* **1997**, *69*, 4783–4789.

137. Xu, J.; Locascio, L.; Gaitan, M.; Lee, C.S. Room-Temperature Imprinting Method for

Plastic Microchannel Fabrication. *Anal. Chem.* **2000**, *72*, 1930–1933.

138. McCormick, R.M.; Nelson, R.J.; Alonso-Amigo, M.G.; Benvegnu, D.J.; Hooper, H.H. Microchannel Electrophoretic Separations of DNA in Injection-Molded Plastic Substrates. *Anal. Chem.* **1997**, *69*, 2626–2630.

139. Chen, Y.; Zhang, L.; Chen, G. Fabrication, modification, and application of poly(methyl methacrylate) microfluidic chips. *Electrophoresis* **2008**, *29*, 1801–1814.

140. Jena, R.K.; Yue, C.Y.; Lam, Y.C. Micro fabrication of cyclic olefin copolymer (COC) based microfluidic devices. *Microsyst. Technol.* **2012**, *18*, 159–166.

141. Nunes, P.S.; Ohlsson, P.D.; Ordeig, O.; Kutter, J.P. Cyclic olefin polymers: emerging materials for lab-on-a-chip applications. *Microfluid. Nanofluidics* **2010**, *9*, 145–161.

142. Pemg, B.-Y.; Wu, C.-W.; Shen, Y.-K.; Lin, Y. Microfluidic chip fabrication using hot embossing and thermal bonding of COP. *Polym. Adv. Technol.* **2010**, *21*, 457–466.

143. Azouz, A. Ben; Murphy, S.; Karazi, S.; Vázquez, M.; Brabazon, D. Fast Fabrication Process of Microfluidic Devices Based on Cyclic Olefin Copolymer. *Mater. Manuf. Process.* **2014**, *29*, 93–99.

144. Gao, H.; Yan, C.; Wu, W.; Li, J. Application of Microfluidic Chip Technology in Food Safety Sensing. *Sensors* **2020**, *20*, 1792.

145. Weng, X.; Kang, Y.; Guo, Q.; Peng, B.; Jiang, H. Recent advances in thread-based microfluidics for diagnostic applications. *Biosens. Bioelectron.* **2019**, *132*, 171–185.

146. Tan, W.; Powles, E.; Zhang, L.; Shen, W. Go with the capillary flow. Simple thread-based microfluidics. *Sensors Actuators B Chem.* **2021**, *334*, 129670.

147. Berzina, B.; Anand, R.K. Tutorial review: Enrichment and separation of neutral and charged species by ion concentration polarization focusing. *Anal. Chim. Acta* **2020**, *1128*,

149–173.

148. Singh, C.; Ali, M.A.; Kumar, V.; Ahmad, R.; Sumana, G. Functionalized MoS2 nanosheets assembled microfluidic immunosensor for highly sensitive detection of food pathogen. *Sensors Actuators B Chem.* **2018**, *259*, 1090–1098.

149. Park, J.; Han, D.H.; Park, J.-K. Towards practical sample preparation in point-of-care testing: user-friendly microfluidic devices. *Lab Chip* **2020**, *20*, 1191–1203.

150. Ghuman, A. BACTERIOPHAGE-ASSISTED MICROFLUIDIC SEPARATION OF PATHOGENS FROM FOOD MATRICES, University of Georgia, 2016.

151. Zhou, Y.; Ramasamy, R.P. Isolation and separation of Listeria monocytogenes using bacteriophage P100- modi fi ed magnetic particles. *Colloids Surfaces B Biointerfaces* **2019**, *175*, 421–427.

152. Tang, M.; Wang, G.; Kong, S.K.; Ho, H.P. A review of biomedical centrifugal microfluidic platforms. *Micromachines* **2016**, *7*.

153. Sivaramakrishnan, M.; Kothandan, R.; Govindarajan, D.K.; Meganathan, Y.; Kandaswamy, K. Active microfluidic systems for cell sorting and separation. *Curr. Opin. Biomed. Eng.* **2020**, *13*, 60–68.

154. Wang, B.; Park, B. Microfluidic Sampling and Biosensing Systems for Foodborne Escherichia coli and Salmonella. *Foodborne Pathog. Dis.* **2022**, *19*.

155. Ngamsom, B.; Lopez-Martinez, M.J.; Raymond, J.-C.; Broyer, P.; Patel, P.; Pamme, N. On-chip acoustophoretic isolation of microflora including S. typhimurium from raw chicken, beef and blood samples. *J. Microbiol. Methods* **2016**, *123*, 79–86.

156. Song, Y.; Li, Z.; Feng, A.; Zhang, J.; Liu, Z.; Li, D. Electrokinetic detection and separation of living algae in a microfluidic chip: implication for ship's ballast water

analysis. *Environ. Sci. Pollut. Res.* **2021**, *28*, 22853–22863.

157. Morani, M.; Mai, T.D.; Krupova, Z.; van Niel, G.; Defrenaix, P.; Taverna, M. Recent electrokinetic strategies for isolation, enrichment and separation of extracellular vesicles. *TrAC Trends Anal. Chem.* **2021**, *135*, 116179.

158. Eun, C.; Koo, B.; Yeong, E.; Yeun, J.; Kim, S.; Shin, Y. Simple and label-free pathogen enrichment via homobifunctional imidoesters using a micro fl uidic (SLIM) system for ultrasensitive pathogen detection in various clinical specimens. *Biosens. Bioelectron.* **2018**, *111*, 66–73.

159. Castillo-león, J.; Svendsen, W.E.; Dimaki, M.; Arima, V.; Akram, M.S.; Miserere, S.; Neuman, C.; Kipling, G.D. *Lab-on-a-Chip Devices and Micro-Total Analysis Systems A Practical Guide*; Castillo-león, J., Svendsen, W.E., Eds.; 1st ed.; Springer Cham: Heidelberg New York Dordrecht London, 2015; ISBN 9783319086866.

160. Wang, R.; Xu, Y.; Sors, T.; Irudayaraj, J.; Ren, W.; Wang, R. Impedimetric detection of bacteria by using a microfluidic chip and silver nanoparticle based signal enhancement. *Microchim. Acta* **2018**, *185*, 184.

161. Shanko, E.-S.; van de Burgt, Y.; Anderson, P.D.; den Toonder, J.M.J. Microfluidic Magnetic Mixing at Low Reynolds Numbers and in Stagnant Fluids. *Micromachines* **2019**, *10*, 731.

162. Gao, X.; Li, Y. Simultaneous microfluidic pumping and mixing using an array of asymmetric 3D ring electrode pairs in a cylindrical microchannel by the AC electroosmosis effect. *Eur. J. Mech. - B/Fluids* **2019**, *75*, 361–371.

163. Li, Y.; Cai, S.; Shen, H.; Chen, Y.; Ge, Z.; Yang, W. Recent advances in acoustic microfluidics and its exemplary applications. *Biomicrofluidics* **2022**, *16*, 031502.

164. Demcenko, A.; Witte, C.; Reboud, J.; Cooper, J.M. Ultrasonic Wave Mixing for Nonlinear Ultrasonics in a Microfluidic Capillary. In Proceedings of the 2019 IEEE International Ultrasonics Symposium (IUS); IEEE, 2019; pp. 284–286.

165. Alexandre, D.L.; Melo, A.M.A.; Furtado, R.F.; Borges, M.F.; Figueiredo, E.A.T.; Biswas, A.; Cheng, H.N.; Alves, C.R. A Rapid and Specific Biosensor for Salmonella Typhimurium Detection in Milk. *Food Bioprocess Technol.* **2018**, *11*, 748–756.

166. Sheikhzadeh, E.; Chamsaz, M.; Turner, A.P.F.; Jager, E.W.H.; Beni, V. Label-free impedimetric biosensor for Salmonella Typhimurium detection based on poly [pyrrole-co-3-carboxyl-pyrrole] copolymer supported aptamer. *Biosens. Bioelectron.* **2016**, *80*, 194–200.

167. Bagheryan, Z.; Raoof, J.-B.; Golabi, M.; Turner, A.P.F.; Beni, V. Diazonium-based impedimetric aptasensor for the rapid label-free detection of Salmonella typhimurium in food sample. *Biosens. Bioelectron.* **2016**, *80*, 566–573.

168. Bhardwaj, J.; Devarakonda, S.; Kumar, S.; Jang, J. Development of a paper-based electrochemical immunosensor using an antibody-single walled carbon nanotubes bio-conjugate modified electrode for label-free detection of foodborne pathogens. *Sensors Actuators B Chem.* **2017**, *253*, 115–123.

169. Hong, S.A.; Kwon, J.; Kim, D.; Yang, S. A rapid, sensitive and selective electrochemical biosensor with concanavalin A for the preemptive detection of norovirus. *Biosens. Bioelectron.* **2015**, *64*, 338–344.

170. Wang, N.; Pan, G.; Guan, S.; Rong, S.; Wang, D.; Gao, Z.; Tian, P.; Li, Q. A Broad-Range Disposable Electrochemical Biosensor Based on Screen-Printed Carbon Electrodes for Detection of Human Noroviruses. *Front. Bioeng. Biotechnol.* **2022**, *10*.

171. Mohammed, M.I.; Haswell, S.; Gibson, I. Lab-on-a-chip or Chip-in-a-lab: Challenges of Commercialization Lost in Translation. *Procedia Technol.* **2015**, *20*, 54–59.

172. Cai, G.; Wang, Y.; Zhang, Y.; Zheng, L.; Lin, J. Magnetorheological elastomer and smartphone enable microfluidic biosensing of foodborne pathogen. *Chinese Chem. Lett.* **2022**, 108059.

173. Qi, W.; Zheng, L.; Hou, Y.; Duan, H.; Wang, L.; Wang, S.; Liu, Y.; Li, Y.; Liao, M.; Lin, J. A finger-actuated microfluidic biosensor for colorimetric detection of foodborne pathogens. *Food Chem.* **2022**, *381*, 131801.

174. Hassan, S.; Tariq, A.; Noreen, Z.; Donia, A.; Zaidi, S.Z.J.; Bokhari, H.; Zhang, X. Capillary-Driven Flow Microfluidics Combined with Smartphone Detection: An Emerging Tool for Point-of-Care Diagnostics. *Diagnostics* **2020**, *10*, 509.

175. Lakhera, P.; Chaudhary, V.; Bhardwaj, B.; Kumar, P.; Kumar, S. Development and recent advancement in microfluidics for point of care biosensor applications: A review. *Biosens. Bioelectron. X* **2022**, *11*, 100218.

176. Joe, C.; Lee, B.H.; Kim, S.H.; Ko, Y.; Gu, M.B. Aptamer duo-based portable electrochemical biosensors for early diagnosis of periodontal disease. *Biosens. Bioelectron.* **2022**, *199*, 113884.

177. Cruz, A.F.D.; Norena, N.; Kaushik, A.; Bhansali, S. A low-cost miniaturized potentiostat for point-of-care diagnosis. *Biosens. Bioelectron.* **2014**, *62*, 249–254.

178. Wang, L.; Hao, L.; Qi, W.; Huo, X.; Xue, L.; Liu, Y.; Zhang, Q.; Lin, J. A sensitive Salmonella biosensor using platinum nanoparticle loaded manganese dioxide nanoflowers and thin-film pressure detector. *Sensors Actuators B Chem.* **2020**, *321*, 128616.

179. Zhang, F.; Luo, L.; Gong, H.; Chen, C.; Cai, C. A magnetic molecularly imprinted optical

chemical sensor for specific recognition of trace quantities of virus. *RSC Adv.* **2018**, *8*, 32262–32268.

180. Yang, S.; Ouyang, H.; Su, X.; Gao, H.; Kong, W.; Wang, M.; Shu, Q.; Fu, Z. Dual-recognition detection of Staphylococcus aureus using vancomycin-functionalized magnetic beads as concentration carriers. *Biosens. Bioelectron.* **2016**, *78*, 174–180.
181. Cheng, C.; Peng, Y.; Bai, J.; Zhang, X.; Liu, Y.; Fan, X.; Ning, B.; Gao, Z. Rapid detection of Listeria monocytogenes in milk by self-assembled electrochemical immunosensor. *Sensors Actuators B Chem.* **2014**, *190*, 900–906.
182. Radhakrishnan, R.; Jahne, M.; Rogers, S.; Suni, I.I. Detection of Listeria Monocytogenes by Electrochemical Impedance Spectroscopy. *Electroanalysis* **2013**, *25*, 2231–2237.
183. Chen, Q.; Lin, J.; Gan, C.; Wang, Y.; Wang, D.; Xiong, Y.; Lai, W.; Li, Y.; Wang, M. A sensitive impedance biosensor based on immunomagnetic separation and urease catalysis for rapid detection of Listeria monocytogenes using an immobilization-free interdigitated array microelectrode. *Biosens. Bioelectron.* **2015**, *74*, 504–511.
184. Chen, Q.; Wang, D.; Cai, G.; Xiong, Y.; Li, Y.; Wang, M.; Huo, H.; Lin, J. Fast and sensitive detection of foodborne pathogen using electrochemical impedance analysis, urease catalysis and microfluidics. *Biosens. Bioelectron.* **2016**, *86*, 770–776.
185. Wang, D.; Chen, Q.; Huo, H.; Bai, S.; Cai, G.; Lai, W.; Lin, J. Efficient separation and quantitative detection of Listeria monocytogenes based on screen-printed interdigitated electrode, urease and magnetic nanoparticles. *Food Control* **2017**, *73*, 555–561.
186. Che, Y.; Li, Y.; Slavik, M. Detection of Campylobacter jejuni in poultry samples using an enzyme-linked immunoassay coupled with an enzyme electrode. *Biosens. Bioelectron.* **2001**, *16*, 791–797.

187. Viswanathan, S.; Rani, C.; Ho, J.A. Electrochemical immunosensor for multiplexed detection of food-borne pathogens using nanocrystal bioconjugates and MWCNT screen-printed electrode. *Talanta* **2012**, *94*, 315–319.

188. Xu, M.; Wang, R.; Li, Y. Rapid detection of Escherichia coli O157:H7 and Salmonella Typhimurium in foods using an electrochemical immunosensor based on screen-printed interdigitated microelectrode and immunomagnetic separation. *Talanta* **2016**, *148*, 200–208.

189. Zelada-Guillén, G.A.; Sebastián-Avila, J.L.; Blondeau, P.; Riu, J.; Rius, F.X. Label-free detection of Staphylococcus aureus in skin using real-time potentiometric biosensors based on carbon nanotubes and aptamers. *Biosens. Bioelectron.* **2012**, *31*, 226–232.

190. Altintas, Z.; Akgun, M.; Kokturk, G.; Uludag, Y. A fully automated microfluidic-based electrochemical sensor for real-time bacteria detection. *Biosens. Bioelectron.* **2018**, *100*, 541–548.

191. Puiu, M.; Bala, C. Microfluidics-integrated biosensing platforms as emergency tools for on-site field detection of foodborne pathogens. *TrAC Trends Anal. Chem.* **2020**, *125*, 115831.

192. Carrell, C.; Kava, A.; Nguyen, M.; Menger, R.; Munshi, Z.; Call, Z.; Nussbaum, M.; Henry, C. Beyond the lateral flow assay: A review of paper-based microfluidics. *Microelectron. Eng.* **2019**, *206*, 45–54.

193. Ramires, T.; Iglesias, M.A.; Vitola, H.S.; Núncio, A.S.P.; Kroning, I.S.; Kleinubing, N.R.; Fiorentini, M.; da Silva, W.P. First report of Escherichia coli O157:H7 in ready-to-eat sushi. *J. Appl. Microbiol.* **2020**, *128*, 301–309.

194. Ford, L.; Wang, Q.; Stafford, R.; Ressler, K.A.; Norton, S.; Shadbolt, C.; Hope, K.;

Franklin, N.; Krsteski, R.; Carswell, A.; et al. Seven Salmonella Typhimurium Outbreaks in Australia Linked by Trace-Back and Whole Genome Sequencing. *Foodborne Pathog. Dis.* **2018**, *15*, 285–292.

195. Desai, A.N.; Anyoha, A.; Madoff, L.C.; Lassmann, B. Changing epidemiology of Listeria monocytogenes outbreaks, sporadic cases, and recalls globally: A review of ProMED reports from 1996 to 2018. *Int. J. Infect. Dis.* **2019**, *84*, 48–53.
196. Georgia Department of Public Health *Listeria Fact Sheet*; 2002;
197. Jin, D.; Luo, Y.; Zhang, Z.; Fang, W.; Ye, J.; Wu, F.; Ding, G. Rapid molecular identification of Listeria species by use of real-time PCR and high-resolution melting analysis. *FEMS Microbiol. Lett.* **2012**, *330*, 72–80.
198. Aznar, R.; Alarcón, B. PCR detection of Listeria monocytogenes: A study of multiple factors affecting sensitivity. *J. Appl. Microbiol.* **2003**, *95*, 958–966.
199. Silva, N.F.D.; Neves, M.M.P.S.; Magalhães, J.M.C.S.; Freire, C.; Delerue-Matos, C. Emerging electrochemical biosensing approaches for detection of Listeria monocytogenes in food samples: An overview. *Trends Food Sci. Technol.* **2020**, *99*, 621–633.
200. Kutter, E.; Sulakvelidze, A.; Summers, W.C.; Guttman, B.; Raya, R.; Ackerman, H.W.; Brussow, H.; Carlson, K.; Fidelma Boyd, E.; Loessner, M.J.; et al. *Bacteriophages: Biology and Applications*; Kutter, E., Sulakvelidze, A., Eds.; 1st ed.; CRC Press in an imprint of Taylor & Francis Group: Boca Raton, FL, 2004; ISBN 13:978-0-203-49175.
201. Chin, B.A.; Suh, S.-J.; Chen, I.-H.; Xi, J.; Liu, Y.; Du, S.; Horikawa, S.; Huang, T.-S. Isolation of highly selective phage-displayed oligopeptide probes for detection of listeria monocytogenes in ready-to-eat food. In Proceedings of the Sensing for Agriculture and Food Quality and Safety X; Kim, M.S., Cho, B.-K., Chin, B.A., Chao, K., Eds.; SPIE,

2018; p. 22.

202. Carnazza, S.; Gioffrè, G.; Felici, F.; Guglielmino, S. Recombinant phage probes for Listeria monocytogenes. *J. Phys. Condens. Matter* **2007**, *19*, 395011.

203. Nanduri, V.; Bhunia, A.K.; Tu, S.-I.; Paoli, G.C.; Brewster, J.D. SPR biosensor for the detection of L. monocytogenes using phage-displayed antibody. *Biosens. Bioelectron.* **2007**, *23*, 248–252.

204. Tolba, M.; Ahmed, M.U.; Tlili, C.; Eichenseher, F.; Loessner, M.J.; Zourob, M. A bacteriophage endolysin-based electrochemical impedance biosensor for the rapid detection of Listeria cells. *Analyst* **2012**, *137*, 5749.

205. Singh, S.; Dhanjal, D.S.; Sonali; Thotapalli, S.; Kumar, V.; Datta, S.; Kumar, V.; Kumar, M.; Singh, J. An insight in bacteriophage based biosensors with focus on their detection methods and recent advancements. *Environ. Technol. Innov.* **2020**, *20*, 101081.

206. Zhou, Y.; Marar, A.; Kner, P.; Ramasamy, R.P. Charge-Directed Immobilization of Bacteriophage on Nanostructured Electrode for Whole-Cell Electrochemical Biosensors. *Anal. Chem.* **2017**, *89*, 5734–5741.

207. Schoch, C.L.; Ciufo, S.; Domrachev, M.; Hotton, C.L.; Kannan, S.; Khovanskaya, R.; Leipe, D.; Mcveigh, R.; O'Neill, K.; Robbertse, B.; et al. NCBI Taxonomy: a comprehensive update on curation, resources and tools. *Database (Oxford).* **2020**, *2020*.

208. Baltimore, D. Expression of animal virus genomes. *Bacteriol. Rev.* **1971**, *35*, 235–241.

209. Patel, D.; Zhou, Y.; Ramasamy, R.P. A Bacteriophage-Based Electrochemical Biosensor for Detection of Methicillin-Resistant Staphylococcus aureus. *J. Electrochem. Soc.* **2021**, *168*, 57523.

210. Zhou, Y.; Ramasamy, R.P. Isolation and separation of Listeria monocytogenes using

bacteriophage P100-modified magnetic particles. *Colloids Surfaces B Biointerfaces* **2019**, *175*, 421–427.

211. Ghuman, A.; Zhou, Y.; Ramasamy, R.P. Selective Isolation and Concentration of Foodborne Bacterial Pathogens in a Microfluidic Device. In Proceedings of the M02 - Nano/Biosensors - Morning; 2019; p. 2278.

212. Sommer, H.Z.; Lipp, H.I.; Jackson, L.L. Alkylation of Amines. A General Exhaustive Alkylation Method for the Synthesis of Quaternary Ammonium Compounds. *J. Org. Chem.* **1971**, *36*, 824–828.

213. Chen, F.C.M.; Benoiton, N.L. A new method of quaternizing amines and its use in amino acid and peptide chemistry. *Can. J. Chem.* **1976**, *54*, 3310–3311.

214. Socrates, G. *Infrared and Raman Characteristic Group Frequencies: Tables and Charts*; 3rd ed.; Wiley, 2004; ISBN 978-0-470-09307-8.

215. Townsend, A.; Strawn, L.K.; Chapman, B.J.; Dunn, L.L. A Systematic Review of Listeria Species and Listeria monocytogenes Prevalence, Persistence, and Diversity throughout the Fresh Produce Supply Chain. *Foods* **2021**, *10*, 1427.

216. Matereke, L.T.; Okoh, A.I. Listeria monocytogenes Virulence, Antimicrobial Resistance and Environmental Persistence: A Review. *Pathogens* **2020**, *9*, 528.

217. Gray, M.L.; Killinger, A.H. Listeria monocytogenes and listeric infections. *Bacteriol. Rev.* **1966**, *30*, 309–382.

218. Mazaheri, T.; Ripolles-Avila, C.; Rodríguez-Jerez, J.J. Cross-contamination of mature Listeria monocytogenes biofilms from stainless steel surfaces to chicken broth before and after the application of chlorinated alkaline and enzymatic detergents. *Food Microbiol.* **2023**, *112*, 104236.

219. McSharry, S.; Koolman, L.; Whyte, P.; Bolton, D. Inactivation of Listeria monocytogenes and Salmonella Typhimurium in beef broth and on diced beef using an ultraviolet light emitting diode (UV-LED) system. *LWT* **2022**, *158*, 113150.

220. Lee, D.-U.; Park, Y.J.; Yu, H.H.; Jung, S.-C.; Park, J.-H.; Lee, D.-H.; Lee, N.-K.; Paik, H.-D. Antimicrobial and Antibiofilm Effect of ε-Polylysine against Salmonella Enteritidis, Listeria monocytogenes, and Escherichia coli in Tryptic Soy Broth and Chicken Juice. *Foods* **2021**, *10*, 2211.

221. Shelef, L.A.; Yang, Q. Growth Suppression of Listeria monocytogenes by Lactates in Broth, Chicken, and Beef. *J. Food Prot.* **1991**, *54*, 283–287.

222. CDC Listeria Outbreaks - Listeriosis Available online: https://www.cdc.gov/listeria/outbreaks/ (accessed on Feb 3, 2023).

223. Zamuz, S.; Munekata, P.E.S.; Dzuvor, C.K.O.; Zhang, W.; Sant'Ana, A.S.; Lorenzo, J.M. The role of phenolic compounds against Listeria monocytogenes in food. A review. *Trends Food Sci. Technol.* **2021**, *110*, 385–392.

224. Mehrannia, L.; Khalilzadeh, B.; Rahbarghazi, R.; Milani, M.; Saydan Kanberoglu, G.; Yousefi, H.; Erk, N. Electrochemical Biosensors as a Novel Platform in the Identification of Listeriosis Infection. *Biosensors* **2023**, *13*, 216.

225. Whittaker, P. Evaluating the Use of Fatty Acid Profiles to Differentiate Human Pathogenic and Nonpathogenic Listeria Species. *J. AOAC Int.* **2012**, *95*, 1457–1459.

226. Taylor, C.; Lough, F.; Stanforth, S.P.; Schwalbe, E.C.; Fowlis, I.A.; Dean, J.R. Analysis of Listeria using exogenous volatile organic compound metabolites and their detection by static headspace–multi-capillary column–gas chromatography–ion mobility spectrometry (SHS–MCC–GC–IMS). *Anal. Bioanal. Chem.* **2017**, *409*, 4247–4256.

227. Spadafora, N.D.; Paramithiotis, S.; Drosinos, E.H.; Cammarisano, L.; Rogers, H.J.; Müller, C.T. Detection of Listeria monocytogenes in cut melon fruit using analysis of volatile organic compounds. *Food Microbiol.* **2016**, *54*, 52–59.

228. Liu, A.; Shen, L.; Zeng, Z.; Sun, M.; Liu, Y.; Liu, S.; Li, C.; Wang, X. A Minireview of the Methods for Listeria monocytogenes Detection. *Food Anal. Methods* **2018**, *11*, 215–223.

229. Vizzini, P.; Braidot, M.; Vidic, J.; Manzano, M. Electrochemical and Optical Biosensors for the Detection of Campylobacter and Listeria: An Update Look. *Micromachines* **2019**, *10*, 500.

230. Gattani, A.; Singh, S.V.; Agrawal, A.; Khan, M.H.; Singh, P. Recent progress in electrochemical biosensors as point of care diagnostics in livestock health. *Anal. Biochem.* **2019**, *579*, 25–34.

231. Zhou, Y.; Ramasamy, R.P. Isolation and separation of Listeria monocytogenes using bacteriophage P100-modified magnetic particles. *Colloids Surfaces B Biointerfaces* **2019**, *175*, 421–427.

232. Zhu, S.; Sun, X.; Gao, X.; Wang, J.; Zhao, N.; Sha, J. Equivalent circuit model recognition of electrochemical impedance spectroscopy via machine learning. *J. Electroanal. Chem.* **2019**, *855*, 113627.

233. Kumar, S.; Ghosh, A.; Tudu, B.; Bandyopadhyay, R. An equivalent electrical network of an electronic tongue: A case study with tea samples. In Proceedings of the 2017 ISOCS/IEEE International Symposium on Olfaction and Electronic Nose (ISOEN); IEEE, 2017; pp. 1–3.

234. Jorcin, J.-B.; Orazem, M.E.; Pébère, N.; Tribollet, B. CPE analysis by local

electrochemical impedance spectroscopy. *Electrochim. Acta* **2006**, *51*, 1473–1479.

235. Tsividis, Y.; Milios, J. A detailed look at electrical equivalents of uniform electrochemical diffusion using nonuniform resistance–capacitance ladders. *J. Electroanal. Chem.* **2013**, *707*, 156–165.

236. Lukács, Z.; Kristóf, T. A generalized model of the equivalent circuits in the electrochemical impedance spectroscopy. *Electrochim. Acta* **2020**, *363*, 137199.

237. del Barrio, J.; Sánchez-Somolinos, C. Light to Shape the Future: From Photolithography to 4D Printing. *Adv. Opt. Mater.* **2019**, *7*, 1900598.

238. Mailly, D. Nanofabrication techniques. *Eur. Phys. J. Spec. Top.* **2009**, *172*, 333–342.

239. Fendler, J.H. Self-Assembled Nanostructured Materials. *Chem. Mater.* **1996**, *8*, 1616–1624.

240. Koziol, K.; Boskovic, B.O.; Yahya, N. Synthesis of Carbon Nanostructures by CVD Method. In *Carbon and Oxide Nanostructures*; Yahya, N., Ed.; Springer Berlin Heidelberg: Berlin, Heidelberg, 2010; pp. 23–49 ISBN 978-3-642-14673-2.

241. Bustillo, J.M.; Howe, R.T.; Muller, R.S. Surface micromachining for microelectromechanical systems. *Proc. IEEE* **1998**, *86*, 1552–1574.

242. Sharma, E.; Rathi, R.; Misharwal, J.; Sinhmar, B.; Kumari, S.; Dalal, J.; Kumar, A. Evolution in Lithography Techniques: Microlithography to Nanolithography. *Nanomaterials* **2022**, *12*, 2754.

243. WATT, F.; BETTIOL, A.A.; VAN KAN, J.A.; TEO, E.J.; BREESE, M.B.H. ION BEAM LITHOGRAPHY AND NANOFABRICATION: A REVIEW. *Int. J. Nanosci.* **2005**, *04*, 269–286.

244. Altissimo, M. E-beam lithography for micro-/nanofabrication. *Biomicrofluidics* **2010**, *4*,

026503.

245. Shen, Y.; Wong, N.; Lam, E.Y. Level-set-based inverse lithography for photomask synthesis. *Opt. Express* **2009**, *17*, 23690.

246. Zhu, S.; Niu, Z.; Zhang, F.; Ma, X.; Zeng, Z.; Cheng, W.; Shi, W.; Huang, H. Programmable pupil correction method for photolithography illumination system. *Optik (Stuttg).* **2020**, *208*, 164072.

247. Zheng, L.; Zywietz, U.; Birr, T.; Duderstadt, M.; Overmeyer, L.; Roth, B.; Reinhardt, C. UV-LED projection photolithography for high-resolution functional photonic components. *Microsystems Nanoeng.* **2021**, *7*, 64.

248. Willson, C.G.; Dammel, R.R.; Reiser, A. Photoresist materials: a historical perspective. In Proceedings of the SPIE 3050, Metrology, Inspection, and Process Control for Microlithography XI; 1997; p. 38.

249. O'Brien, J.; Hughes, P.J.; Brunet, M.; O'Neill, B.; Alderman, J.; Lane, B.; O'Riordan, A.; O'Driscoll, C. Advanced photoresist technologies for microsystems. *J. Micromechanics Microengineering* **2001**, *11*, 353–358.

250. Cui, Y.; Zhong, Z.; Wang, D.; Wang, W.U.; Lieber, C.M. High performance silicon nanowire field effect transistors. *Nano Lett.* **2003**, *3*, 149–152.

251. Thelander, C.; Agarwal, P.; Brongersma, S.; Eymery, J.; Feiner, L.F.; Forchel, A.; Scheffler, M.; Riess, W.; Ohlsson, B.J.; G??sele, U.; et al. Nanowire-based one-dimensional electronics. *Mater. Today* **2006**, *9*, 28–35.

252. Patolsky, F.; Zheng, G.; Lieber, C.M. Nanowire-based biosensors. *Anal. Chem.* **2006**, *78*, 4260–4269.

253. Khanal, D.R.; Wu, J. Gate Coupling and Charge Distribution in Nanowire Field Effect

Transistors. *Nano Lett.* **2007**, *7*, 2778–2783.

254. Bijl, H.J.V.A.N.D.E.R. Sure Unduly .'. *October* **1918**.

255. Baker, R.J.T.A.-T.T.-; Bijl, H.J.V.A.N.D.E.R. CMOS : circuit design, layout, and simulation. *October* **2010**.

256. Cui, Y.; Duan, X.; Hu, J.; Lieber, C.M. Doping and Electrical Transport in Silicon Nanowires. *J. Phys. Chem. B* **2000**, *104*, 5213–5216.

257. Cao, A.; Sudhölter, E.J.R.; de Smet, L.C.P.M. Silicon nanowire-based devices for gas-phase sensing. *Sensors (Basel).* **2013**, *14*, 245–271.

258. Martinez, J.A.; Misra, N.; Wang, Y.; Stroeve, P.; Grigoropoulos, C.P.; Noy, A. Highly efficient biocompatible single silicon nanowire electrodes with functional biological pore channels. *Nano Lett.* **2009**, *9*, 1121–1126.

259. Magasinski, A.; Zdyrko, B.; Kovalenko, I.; Hertzberg, B.; Burtovyy, R.; Huebner, C.F.; Fuller, T.F.; Luzinov, I.; Yushin, G. Toward efficient binders for Li-ion battery Si-based anodes: Polyacrylic acid. *ACS Appl. Mater. Interfaces* **2010**, *2*, 3004–3010.

260. Zheng, G.; Patolsky, F.; Cui, Y.; Wang, W.U.; Lieber, C.M. Multiplexed electrical detection of cancer markers with nanowire sensor arrays. *Nat. Biotechnol.* **2005**, *23*, 1294–1301.

261. Chua, J.H.; Chee, R.E.; Agarwal, A.; She, M.W.; Zhang, G.J. Label-free electrical detection of cardiac biomarker with complementary metal-oxide semiconductor-compatible silicon nanowire sensor arrays. *Anal. Chem.* **2009**, *81*, 6266–6271.

262. Nair, P.R.; Alam, M.A. Design considerations of silicon nanowire biosensors. *IEEE Trans. Electron Devices* **2007**, *54*, 3400–3408.

263. Wang, Y.W.Y.; Lew, K.-K.L.K.-K.; Mattzela, J.; Redwing, J.; Mayer, T. Top-gated field

effect devices using oxidized silicon nanowires. *63rd Device Res. Conf. Dig. 2005. DRC '05.* **2005**, *1*, 2004–2005.

264. Berg, H.C. *Random Walks in Biology expended edition*; Princeton University Press, Ed.; Expended.; Princeton University Press: New Jersey, 1993; ISBN 0-691-00064-6.

265. Leenders, R.T.A.J. Models for network dynamics: A Markovian framework. *J. Math. Sociol.* **1995**, *20*, 1–21.

266. Hassibi, A.; Zahedi, S.; Navid, R.; Dutton, R.W.; Lee, T.H. Biological shot-noise and quantum-limited signal-to-noise ratio in affinity-based biosensors. *J. Appl. Phys.* **2005**, *97*, 084701.

267. Liu, Y. Forward error correction biosensors: Principles, modeling, and fabrication, Michigan State University PP - United States -- Michigan: United States -- Michigan, 2010.

268. Min, J.; Baeumner, A.J. Characterization and Optimization of Interdigitated Ultramicroelectrode Arrays as Electrochemical Biosensor Transducers. *Electroanalysis* **2004**, *16*, 724–729.

APPENDIX A

BUFFER PREPERATION

PBS (pH=7.4) 10X preparation:

1. The following ingredients were dissolved in 800 mL distilled H_2O:
    a. 80 g of NaCl
    b. 2.0 g of KCl
    c. 14.4 g of Na2HPO4
    d. 2.4 g of KH2PO4
2. pH was adjusted to 7.4 using HCl or NaOH.

PBS (pH=7.4) 1X preparation:

1. In a 100 mL glass cylinder the following were mixed:
    a. 10mL of 10X PBS buffer.
    b. 90mL DIW
2. Solution was then poured into a 150 mL glass bottle and mixed.
3. pH was adjusted to 7.4 using HCl or NaOH.
4. Solution was sterilized by autoclaving.

0.01% Tween 20 PBS 1X pH=7.4 solution preparation:

1. The following ingredients were mixed thoroughly:
    a. 10mL PBS 10X
    b. 85mL DIW
2. The solution was poured into a glass cylinder.

3. 10 µL of tween 20 was added to the cylinder and mixed gently.
4. 4.99 mL DIW were added.
5. Solution was sterilized by autoclaving.

Tris-Cl buffer (1M):

1. The following ingredients were mixed in a glass bottle:
    a. 121.8 gr Tris base
    b. 800 mL DIW
2. If the 1 M solution has a yellow shade, it should be discarded.
3. Solution was sterilized by autoclaving.

SM buffer:

1. The following ingredients were mixed in a glass bottle:
    a. 5.8 g of NaCl
    b. 2 g of MgSO4
    c. 50 mL of 1M tris HCL solution (pH = 7.5)
    d. 1 mL of 10% (gr/mL) gelatin in DIW.
2. Solution was sterilized by autoclaving.

APPENDIX B

BACTERIA CULTURE CULTIVATION

Brain Heart Infusion (BHI) Media:

BHI media was prepared by mixing 37 g of BHI powder into 1 L of DIW and adjusting the pH to 7.4 ± 0.2 by using HCl or NaOH. For hard or soft agar solution 1.5 g or 0.5 g of agar powder was added to every 100 mL of BHI media. The media solution was then autoclaved at 121 ^{o}C for 30 min, under pressure of 18 psi.

Luria-Bertani (LB) Media:

LB media was prepared by mixing 10 g of tryptone, 5 g yeast extract, and 10 g of NaCl in 1 L of DIW and adjusting the pH to 7.0 ± 0.2 by using HCl or NaOH. For hard or soft agar solution 1.5 g or 0.5 g of agar powder was added to every 100 mL of BHI media. The media solution was then autoclaved at 121 ^{o}C for 30 min, under pressure of 18 psi.

***Listeria monocytogenes*:**

Hard agar plate culture:

A single freshly isolated *Listeria monocytogenes* colony was scooped with a sterile loop and streaked again on a new BHI agar plate. The plate was again incubated for 18 hours at 37 ^{o}C. The plates were stored in a fridge at 4 ^{o}C for a maximum duration of 2 months.

Liquid culture:

A single colony of *Listeria monocytogenes* was scooped from an agar plate and mixed into 3 mL of liquid BHI media. The liquid media with the single colony was then incubated in a shaker

for 18 hours and 200 RPM, at a temperature of 37 ^{o}C. The liquid culture was stored in a fridge at 4 ^{o}C for a maximum duration of 1 week.

***Salmonella enterica* subsp. *Enterica* serovar Typhimurium 291RH (ser. Typhimurium-291RH)**:

Hard agar plate culture:

A single freshly isolated ser. Typhimurium-291RH colony was scooped with a sterile loop and streaked again on a new BHI agar plate. The plate was again incubated for 18 hours at 37 ^{o}C. The plates were stored in a fridge at 4 ^{o}C for a maximum duration of 2 months.

Liquid culture:

A single colony of ser. Typhimurium-291RH was scooped from an agar plate and mixed into 3 mL of liquid BHI media. The liquid media with the single colony was then incubated in a shaker for 18 hours and 200 RPM, at a temperature of 37 ^{o}C. The liquid culture was stored in a fridge at 4 ^{o}C for a maximum duration of 1 week.

Escherichia coli O157:H7:

Hard agar plate culture:

A single freshly isolated *Escherichia coli O157:H7* colony was scooped with a sterile loop and streaked again on a new LB agar plate. The plate was again incubated for 12 hours at 37 ^{o}C. The plates were stored in a fridge at 4 ^{o}C for a maximum duration of 2 months.

Liquid culture:

A single colony of *Escherichia coli O157:H7* was scooped from an agar plate and mixed into 3 mL of liquid LB media. The liquid media with the single colony was then incubated in a shaker for 12 hours and 200 RPM, at a temperature of 37 ^{o}C. The liquid culture was stored in a fridge at 4 ^{o}C for a maximum duration of 1 week.

APPENDIX C

PREPARATION OF QUATERNIZED POLYETHYLENIMINE CARBON NANOTUBES

The first step was to create polyethyleneimine modified carbon nanotubes (PEI-CNT). Initially, 2 mg of COOH-functionalized CNTs were dispersed in 1 mL of dimethylformamide and sonicated for 5 minutes. 6 mL of $SOCl_2$ was added to the suspension to acylate the carboxylic acid, and the $SOCl_2$ acylated the carboxylic group. The suspension was refluxed for 24 hours with constant stirring under 120 ^oC. The suspension was centrifuged at 10000 rpm for 8 minutes following the reflux to form a pellet. The pellet was washed with anhydrous tetrahydrofuran (THF) and dried at room temperature under a vacuum for 2 hours. 5 mL dimethylformamide (DMF) was used to resuspend the pellet and then stirred in an N_2 environment at 90 ^oC. 100 mg of PEI was then added and reacted for three days. It was then centrifuged at 10000 rpm for 8 minutes, washed with methanol, and dried at a temperature of 70 ^oC. The second step was to quarternize the amine groups on the PEI molecule by adding 8 mg of PEI-CNT powder to a 5 mL round bottom flask. 2 mL of methylene chloride was added to the flask using a micropipette. 20 wt% of iodomethane was pipetted into the flask sealed by a septum and vented using a 23G needle. The heterogeneous mixture was then stirred at room temperature for three days before the solvent and excess reactant was evaporated with gentle heating over one hour.

APPENDIX D

PHAGE IMMOBILIZATION TECHNIQUES

Phage immobilization on the working electrode have been carried out in two methods both uses surface charge to orient the phage so that its tail fibers will be faced outwards to improve attachment probability to the target bacteria.

Phage Immobilization Trough Electrodeposition on Glassy Carbon Electrode:

q-CNT electrodes were prepared as described in appendix C. The q-CNT were dispersed in 3 mL deionized water (DIW) at concentration of 1 mg/mL and ultra-sonicated using ultrasonic homogenizer for 60 minutes. The sonication was carried out at 5 minutes intervals with 2 minutes break between each interval to avoid damaging the sonication probe and overheating the dispersion.

A 3 mm GC working electrode was polished on a polishing pad using 0.3 µm alumina powder, rinsed with DIW, bath sonicated for 5 minutes, and rinsed with DIW one more time to achieve a mirror like finish. The electrode was then dried in an oven for 1 hour at 70 ^{o}C to dry the electrode and was then cooled at room temperature. 2 µL of the q-CNT dispersion were drop cast onto the glassy carbon electrode and then dried in an oven at 70 ^{o}C. This drop cast repeated 8 times and overall, 16 µg of q-CNT were deposited on the GC electrode's surface. The electrode surface was rinsed with DIW to remove any unattached q-CNT from the surface and was visually inspected to verify there are no areas on the electrode that were not covered.

After q-CNT deposition, the GC electrode was rinsed with dimethylformamide (DMF). A 4 mg/mL solution of 1-pyrenebutanoic acid succinimidyl ester (PBSE) in DMF (10mM) was

prepared and thoroughly mixed by vortex at high setting for 1 minute. The electrode was placed in an ice container and 4 µL of the PBSE solution were drop cast on it. The PBSE and the q-CNT on the electrode surface were reacting for 15 minutes. Following that, the electrode was rinsed with DMF to remove any unattached PBSE molecules from the surface. The PBSE was used as a molecular tethering agent.

A Listex P100 bacteriophage solution was made by diluting 0.5 mL of the stock solution into 2 mL of 1X PBS without mixing. The GC working electrode was then rinsed with 1X PBS twice and was submerged in the phage solution. The electrode was connected to an electrochemical potentiostat along with Pt wire counter electrode and Ag/AgCl reference electrodes. As seen in Figure 22, the reference and the working electrodes were kept close while the counter was placed opposing them bothFigure *22*.

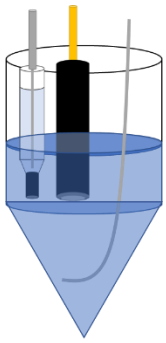

Figure 22: Illustration of the working (middle), counter (right), and reference (left) electrodes in an electrochemical cell with phage solution.

The electrochemical potentiostat program was set to amperometric I-t curve with 0.5V constant potential for 2 hours. The reason for the location of the electrodes was to create an electric gradient between the counter and the working electrode, where the positive terminal is the working electrode. Due to the overall negative charge of the bacteriophage, the potential assist with transporting the bacteriophage towards the working electrode where they are covalently bond with the PBSE. The q-CNT and its high positive charge, causing the negatively charged capsid on the

phage to be facing the electrode while leaving the capturing tail fibers oriented towards the solution.

The working electrode was then rinsed with SM buffer and 1X PBS to remove any unattached bacteriophage from the surface. 6 µL of 0.01 % BSA solution was deposited on the electrode to block areas that might not have been completely covered by the bacteriophage and the electrode was kept submerged in 1X PBS until used.

Phage Immobilization Trough Charge Direction on a Screen-Printed Electrode:

A screen-printed electrode (SPE) that included a planar working, counter and quasi-reference electrodes was cleaned by rinsing it with DIW, bath sonicating for 5 minutes, and rinsing with DIW one more time. The electrode was then dried in room temperature for 1-3 hours. 1 µL of the q-CNT dispersion was drop cast onto the SPE's working electrode and then dried in room temperature. This drop cast repeated 8 times and overall, 8 µg of q-CNT were deposited on the SPE's working electrode surface. The electrode surface was rinsed with DIW to remove any unattached q-CNT from the surface and was visually inspected to verify there are no areas on the electrode that were not covered.

After q-CNT deposition, the SPE was rinsed with 1X PBS, the SPE is very sensitive to chemical solvents like DMF and dimethyl sulfoxide (DMSO) and cannot be used for rinsing, since one of them is needed for dispersing the PBSE tethering agent, DMSO was used on the working electrode only. A 8 mg/mL solution of PBSE in DMSO (20mM) was prepared and thoroughly mixed by vortex at high setting for 1 minute. The electrode was placed in an ice container on a glass substrate, and 0.5 µL of the PBSE solution were drop cast on its working electrode only. The PBSE and the q-CNT on the electrode surface were reacting for 15 minutes. Following that, the

electrode was rinsed with 1X PBS twice to remove any unattached PBSE molecules from the surface.

The SPE was moved to a cold room with a controlled temperature of 4 ^{o}C. 1 µL of the Listex P100 phage stock solution was drop cast on the working electrode, the SPE was covered with a beaker and was left to immobilize overnight. The SPE was then rinsed with SM buffer and 1X PBS to remove any unattached bacteriophage from the surface. 0.5 µL of 0.01 % BSA solution was deposited on the SPE's working electrode to block areas that might not have been completely covered by the bacteriophage and the SPE was kept submerged in 1X PBS until used.

APPENDIX E

ELECTROCHEMICAL IMPEDIMETRIC EXPERIMETNS

The impedimetric biosensors in this dissertation, have been used to detect Listeria monocytogenes by utilizing a three-electrode system and analyzing the open circuit potential and polarization curves.

1. Three-Electrode System:

As its name suggests, the first electrode in the three-electrode system is the working electrode where the electrochemical interaction that is measured happen. The working electrode is where the detection of Listeria monocytogenes is happening after the immobilization of q-CNT and P100 phage.

The second electrode in the system is the reference electrode. This electrode, has a stable potential and acts as the reference potential for the process measured on the working electrode. There is also a quasi-reference electrode that cannot maintain a constant potential but rather supply predictable potential under specific conditions like pH or temperature. When operating outside of the quasi-electrode predictable range its behavior is no longer predictable. In this work both a reference and a quasi-reference electrode were in use.

The third electrode is the counter electrode. This electrode is used to finish the electric circuit of the system. The electric parameters are not measured on this electrode and it is usually placed at a farther distance from the other two electrodes. These electrodes will usually be made from inert materials like Au, Pt, or Carbon to avoid interference with the conditions of the experiments.

For the system to operate as it should, all three electrodes are connected to a potentiostat on one end and their work area is submerged in the electrolyte solution. An electrochemical method is then chosen and the system can conduct its purpose.

2. Open Circuit Potential:

Open circuit potential (OCP) is an electrochemical technique that measures the intrinsic potential difference between the work electrode and the counter electrode in a three-electrode system or between the cathode and the anode in a two-electrode system while no current is passing between them and no external load is applied.

3. Amperometric I-t Curve:

Amperometric I-t curve is an electrochemical technique that measures the current that runs through the system under constant potential load for a specific time span. The I-t curve presents the current at steady state and in this work was used for charge directed phage immobilization.

4. AC Impedance:

Impedance is the resistance and reactance in an alternating current system. It is the ratio between the complex representation of a sinusoidal potential to the complex representation of the current under one or more frequencies. The impedance, unlike regular resistance, show the magnitude of the resistance in addition to phase change of the current. In the case of the impedimetric biosensor of this work, the impedance measures the charge transfer resistance at the surface of the work electrode as an indication of an attachment between the biorecognition molecule and the target analyte.

5. Equivalent Circuit Parameters and Analysis:

The electrochemical equivalent circuit, known also as the Randles circuit, is a way to electrically model electrochemical impedimetric systems and includes at least the electrolyte solution active resistance (R_S) connected in a series to the capacitance of the double layer (C_{DL}) or a constant phase element (CPE), a charge transfer resistance on the working electrodes surface (R_{CT}) and the Warburg diffusion element (Z_w) that represent an impedance element with a constant phase angle of 45 ^{o} regardless of the frequency and a magnitude that is inversely proportional to the square root of the frequency. A basic model with these components is shown in Figure 23.

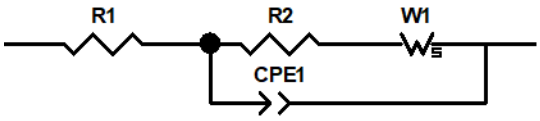

Figure 23: A simple equivalent circuit model that was used in the experimental work in this dissertation.

Here R1 is the solution resistance, R2 is the charge transfer resistance, CPE1 is the constant phase element, and W1 is the Warburg diffusion element. The major use of the Randles circuit is to interpret of the impedimetric spectrum and extract specific values from experimental results [232,233].

The mathematical approach to describe a simple impedimetric system can start by assuming finite values of R_{CT} that is tied to a number of simple reduction-oxidation (REDOX) reactions and can be formulated as seen in eq (19) [234,235].

$$(19)\, Z(\omega) = R_s + \frac{R_{CT}}{1+i\omega\tau}$$

Where Z(ω) is the angular frequency dependent impedance value, i is $\sqrt{-1}$, ω is the angular frequency, and τ is the time constant. Eq. (17) can model the values of simple systems with slow charge transfer resulting in a perfect semi-circle Nyquist diagram. In most real cases the measured

impedance shows distortions that result in depressed semicircles. The addition of a constant phase element as was shown in Figure 23 and described by eq (20).

$$(20)\, Z(\omega) = R_s + \frac{R_{CT}}{1+(i\omega\tau)^{1-\beta}}$$

Where β is a positive constant phase parameter that is much smaller than 1. This equation is correct but it does not allow the separation of the linear coefficients for the charge transfer and the capacitance. To separate them, the equation can be rewritten as eq (21).

$$(21)\, Z(\omega) = R_s + \frac{R_{CT}}{Y_{CT}+Q(i\omega\tau)^{1-\beta}}$$

Where Y_{CT} is the compensated admittance of the charge transfer ($Y_{CT} = \frac{1}{R_{CT}}$) and Q is a fractional coefficient relating to the capacitance. Both Q and β are relating to physical properties as dielectric constant and thickness [232,236].

6. Three electrode Systems Used in This Dissertation:

In this work two different electrochemical three-electrode systems were in use. The first consist of a glassy carbon electrode with a diameter of 3 mm and a cylindrical shape, a Ag/AgCl sat. KCl reference electrode with an equilibrium potential of 0.197 V with respect to standard hydrogen electrode (SHE). Last, a Pt wire counter electrode.

The second was a portable screen printed three-electrode system with working and counter carbon ink electrodes and a Ag quasi-reference electrode. All three electrode were printed on a planer paper based holder with lamination to prevent damages from aqueous solution exposure.

APPENDIX F

PHOTOLITHOGRAPHY

The fabrication of well-defined geometries at micro- and nano- scales is required for research and industry in multiple fields such as, micro-optics, integrated circuits, micro- and nano-fluidics, microelectromechanical systems (MEMS), and many more [237,238]. There are many approaches to create micro- and nano scale structures, among them self-assembled materials [239], chemical vapor deposition [240], micromachining [241], and the most common and well established method is Lithography [242]. Lithography is an umbrella term that consist of many irradiation-based printing techniques that vary according to the type of radiation used, like X-ray lithography, electron beam lithography, ion beam lithography and photolithography. The choice of the right technique depends on the cost, resolution, registration accuracy of multiple layers, and the time limitations for the fabrication. The conventional and most widely used method of lithography is photolithography that uses ultra-violet light exposure at wavelengths of 190-430 nm. Photolithography is the most established method that is in used since 1952 and has the quickest fabrication time with relatively easy and accurate registration of multiple layers although its resolution is not as small as some of the other techniques [243,244].

Photolithography technique requires a patterning mask, optical exposure system, photoresist, development and washing chemicals, and a substrate. A patterning mask is made from a substrate that is transparent to UV radiation with areas that are covered with a Cr or Fe_2O_3 UV-absorbing film. The patterning mask will allow the UV light to pass through a design to the UV sensitive coating on the substrate according to the wanted design. The photomask can be light

field, which means that most of the light passes through and the design is blocked, or dark field by making the light pass only through the design [245].

The optical exposure system consists of a light source with a specific wavelength or a range at a needed intensity. The UV light waves are then passing through a condenser lens that deflects the UV light waves towards the photomask. Originally the optical exposure system was used for contact printing, which means that the mask was in direct contact with the substrate and the system can print the pattern in a 1:1 size ration between the mask and the substrate. The advantages of contact lithography are simplicity, low cost, quick exposure of the whole wafer, and no interference patterns. Its disadvantages are mask wear causes defects and limited resolution. The minimal size that can be made with contact system is calculated according to eq. 22:

$$(22)\, X_{min} = \frac{3}{2} \times \sqrt{\frac{\lambda z}{2}}$$

Where X_{min} is the smallest possible feature, λ is the wavelength, and z is the thickness of the photoresist. To farther reduce the dimensions of the pattern projection lithography was invented by adding an aperture which limits the amount of UV waves that passes to prevent possible interference effects on the substrate, and to form an exposure function as close to a square function at the areas the user wants to expose. After the aperture the UV waves passes through a projection lens that focuses the waves and allows the formation of features at a ratio of up to 1:10 of the original mask features. The resolution of an optical exposure system defines the smallest feature it can create and the depth of focus will define the maximal resist thickness that will allow a sharp image on the substrate, both characteristics are defining the quality of the system but higher the depth of focus the larger is the resolution hence a tradeoff is required. The equations for the resolution and depth of focus are shown in eq. (23) and (24) [246,247].

$$(23)\ R = \frac{k_1 \lambda}{NA}$$

$$(24)\ DOF = \frac{k_2 \lambda}{NA^2}$$

Where R is the resolution, k1 and k2 are Rayleigh constants and NA is the numerical aperture. The schematics of both optical exposure systems is shown in Figure 24.

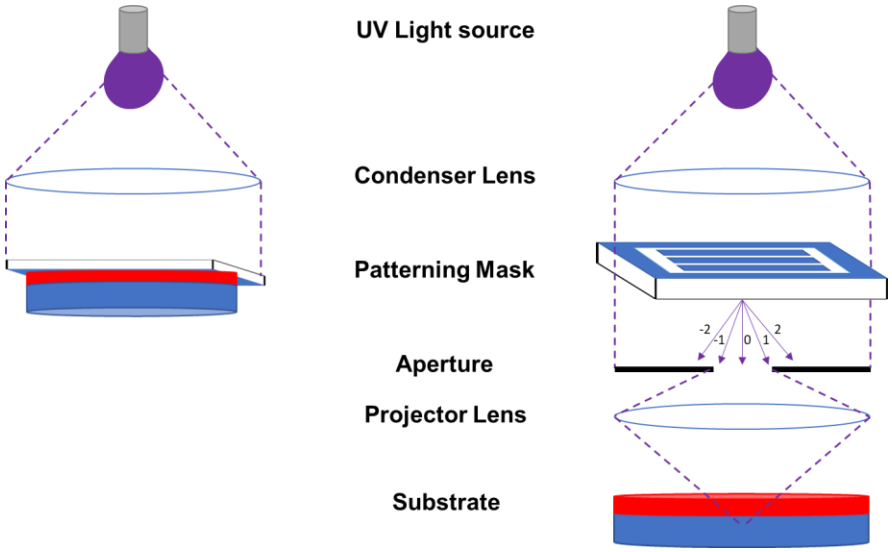

Figure 24: Schematic of contact (left) and projection (right) photolithography optical exposure systems

Photoresists are photosensitive materials that upon exposure to radiation at specific wavelength and intensity will either form crosslinking bonds and polymerize, also known as negative photoresist, or break crosslinking bonds and depolymerize, also known as positive photoresist, both are shown in Figure 25. The substrate can be coated with photoresist in different methods like spray coating, meniscus coating, or spin-coating. The conditions of the coating will determine the homogeneity and thickness of the coating. To improve the adhesion of the photoresist to the surface of the substrate, following the coating, a pre-expose bake step at temperatures of up to 180 ^{o}C that will evaporate the solvents in the resist and stabilize it prior to UV exposure. Additionally, better adhesion can also be improved by using chemical pretreatments

like hexamethyldisilazane (HMDS), its NH_3 group interact with the moisture and removes it from the surface. As a result, the surface energy is decreasing and the adhesion and coverage are improving. Following the exposure, the substrate will be submerged in a developing solution that will remove all the non-polymerized photoresist and leave the wanted pattern on the surface [248,249].

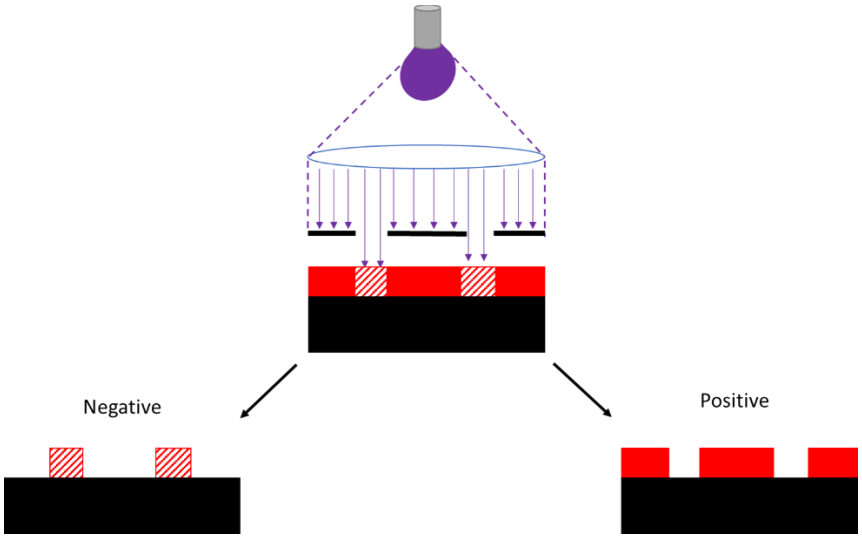

Figure 25: Positive and negative resist.

APPENDIX G

MICROFLUIDIC CHANNELS FABRICATION AND COMPUTATIONAL WORK

For filtration of food macroparticles, a filtering microfluidic channel was fabricated from polydimethylsiloxane (PDMS) using soft lithography technique. Prior to its fabrication, it was designed and flow simulations were done to validate its ability to work.

Listeria monocytogenes bacteria is a rod-shaped bacterium with its length dimension between 0.5-2 μm, and an approximate cross-sectional area of up to 2 μm^2 for the rectangular cross section and up to 0.8 μm^2 for the circular cross section as seen in Figure 26.

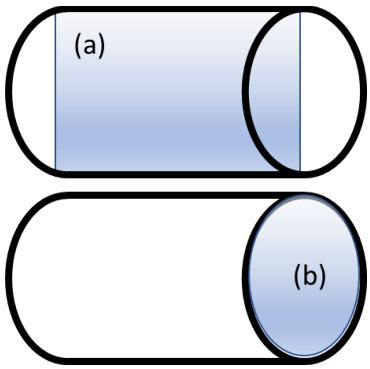

Figure 26: relevant cross-sectional areas of *Listeria monocytogenes* bacteria modeled as a rod.

The microfluidic filter will need to allow the bacteria to flow through and block any food particle that might clog the flow chamber and interfere with the flow of the carrying fluid. For that a design of multiple filters with diminishing cross-sectional area from 5000 to 1250 μm^2 were chosen. The filter should be easily unclogged with inverse flow and the channel is fed through a 1 mm diameter tube. The design is shown in Figure 27.

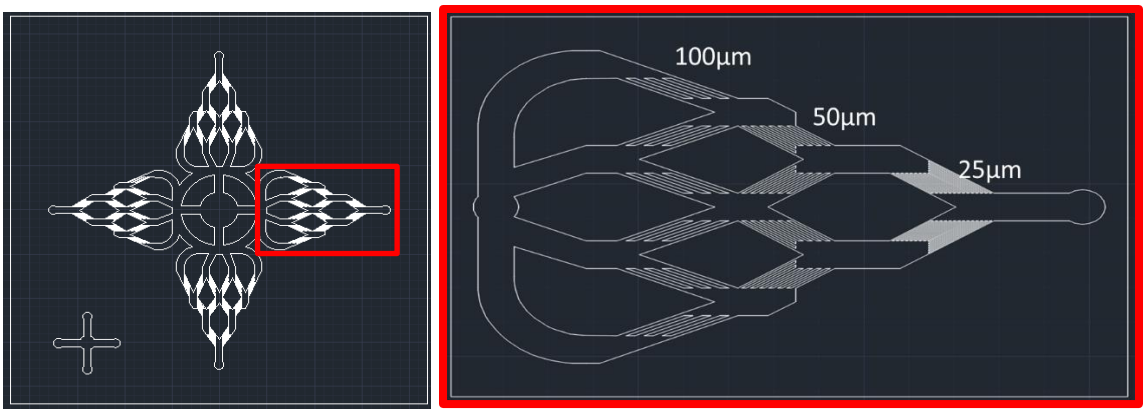

Figure 27: Microfluidic filter design. (a) the whole filter and (b) zoom in with filter width dimensions. Channel height was set to 50 um and width as shown in the zoomed in image.

After the design a series of flow simulations was carried out, using Ansys to characterize the channel and predict the flow vectors, velocity, and pressure field. The meshing of the channel had 315,050 nodes and $1.68*10^5$ elements. The volumetric flow through the channel was set to 10^{-3} L/min and an outlet pressure of 1 atm (standard). The flow medium was set to water and the assumptions for this computational work were:

- Flow is steady and does not change.
- There are no particles (simulation software did not support particle simulation).
- Channel walls will not compress or inflate during the flow.

The channel design mesh and simulation results are shown in Figure 28. As seen from these simulations, the pressure within the channel is low and stay between 1 to $1.125 *10^5$ Pa. The velocity vectors are not predicting areas of back flow and the streamlines seem discreet without areas of turbulence.

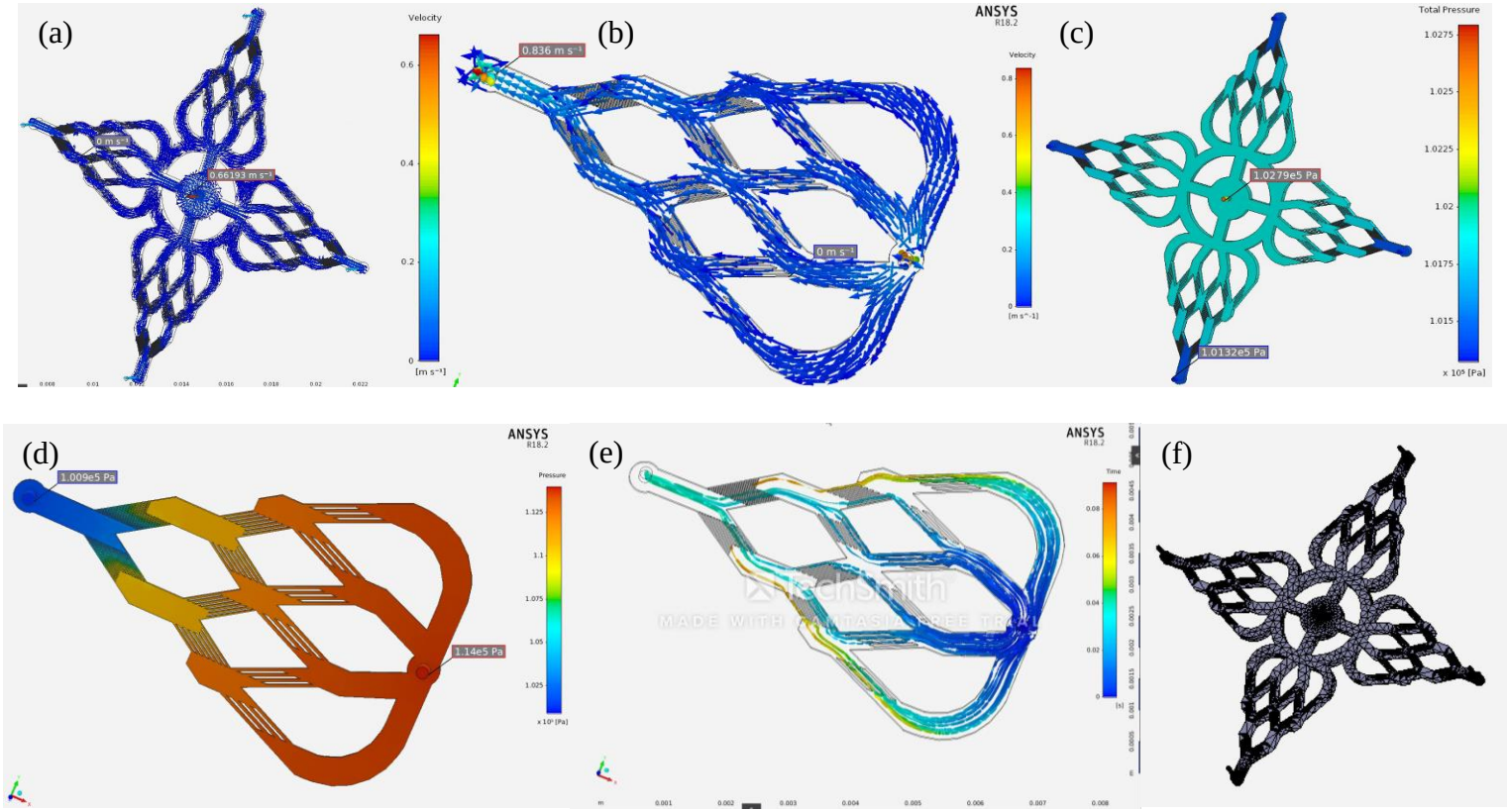

Figure 28: Flow simulation results. (a) Full design velocity vectors; (b) Velocity vectors in a zoomed in area; (c) Pressure field across the full design; (d) Pressure field in a zoomed in section; (e) zoomed in area flow lines; and (f) the design's mesh.

Following the computational experiment results, the channel was fabricated using a soft lithography method. A 3 in Si wafer was cleaned by rinsing with acetone, isopropanol, and ethanol. The wafer was then treated with oxygen plasma to farther remove any organic residues from its surface. SU-8 3035 negative photoresist was spin coated on the wafer at 2000 RPM for 30 seconds after initial homogenizing at 500 RPM for 5 seconds to achieve a height of 50 μm. The wafer with the resist was then baked on a hot plate at a temperature of 95 ^{o}C for 15 minutes to remove solvents and stabilize the resist on the wafer. A photolithography mask with the design was used in the Suess MA-6 photolithography machine at contact exposure setting, and the photoresist was exposed with a dose of 167 mJ/cm^2. The exposed wafer was then baked again for 5 minutes at a temperature of 95 ^{o}C. Following the post expose bake, the pattern was developed in SU-8 developing solution for 10 minutes with slight agitation to promote the development. The wafer was rinsed with isopropanol, dried with N_2, and was stored until the next step. More information about photolithography can be found in appendix F.

After the master mold was ready, the PDMS was made by mixing Slygard 184 and a curing agent at a ratio of 10:1. The two components were thoroughly mixed for 3 minutes, and degassed under vacuum until all the air bubbles disappeared. The master mold was treated with chlorodimethylsilane as a mold release by placing 0.5 mL in covered glass petri dish near the wafer until all the solution evaporates. The petri dish cover was then removed and the degassed PDMS was slowly poured on the mold to avoid forming bubbles. After the PDMS was poured the petri dish is baked in an oven for 3 hours at a temperature of 80 ^{o}C.

The PDMS with the microfluidic channel was cut out with a scalpel and the inlets and outlets were punched out with a 1 mm biopsy puncher. It was rinsed with isopropanol and was treated with oxygen plasma for 5 minutes alongside its glass cap that was cleaned by rinsing it

with acetone, isopropanol, and ethanol before entering the plasma treatment. The glass cap was placed on the channel, 1 mm silicon tubing were connected and it was tested with DIW to verify there are no leaks. The prepared channel is shown in Figure 29.

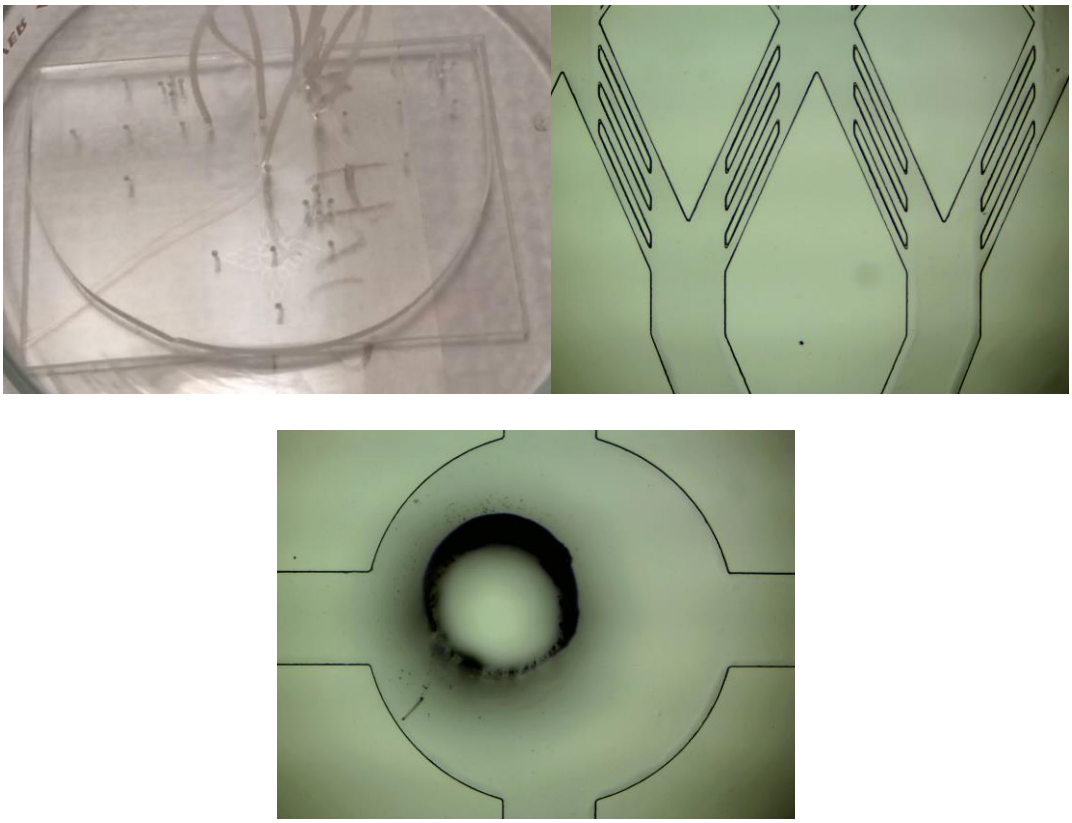

Figure 29: The fabricated filtering microfluidic channel. (a) the channel with the tubing; (b) A microscopy image of the 25 um filter area; and (c) the inlet with the 1 mm punch hole.

APPENDIX H

FET-BIOSENSORS

Nanomaterials like Si nanowires (SiNW), single wall CNT (SWCNT), graphene sheets, and others are attractive components for present and future nano-electronics because they exhibit a wide range of device functions. They can be prepared with single crystal structures, dimensions as small as several nanometers, one or more atomic layers, and controllable hole or electron doping, thus represent powerful building blocks for nano-electronic devices, like field effect transistor (FET). Among the many possibilities, the FET stands out as being the modern workhorse of the semiconducting industry. The basic approach to fabricate such devices is by depositing the nanomaterials on an insulating substrate, making source and drain electrodes on opposite ends, and configuring a top or bottom gate electrode. These devices serve as the basis for hybrid electronic systems, consisting of nanoscale building blocks integrated with planar circuitry. The nanomaterial that is used for FET fabrication should be semiconducting, where the dopant type and concentration can be controlled during its synthesis. nanomaterials can deliver currents comparable with standard planar Si devices. Energy band gap engineering of the nanomaterial channel adds a new degree of freedom in tuning the performance of the resulted FET device [250,251]. Schematics of a nanomaterial-based FET devices are shown in Figure 30.

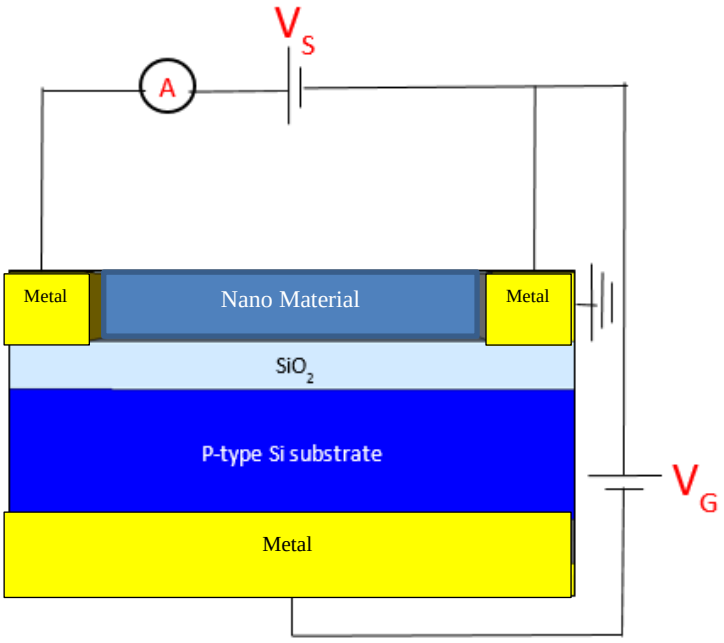

Figure 30: FET schematics with electrical connections.

In typical MOS-FET technology the semiconductor is connected to metallic source and drain electrodes through which a current is injected and collected. The conductance of the semiconductor between the source and the drain is switched on and off by a gate electrode, that its electrical capacity is coupled through a thin dielectric layer. For example, when using a p-type semiconductor, using a positive gate voltage depletes the charge carriers and reduces the conductance, and vice versa for negative gate voltage which leads to accumulation of charge carriers and therefore increases the conductivity [252]. The ON-OFF behavior is controlled by the gate electrode, which induces the carriers within the nanomaterial channel. When the induced carriers are of the same type as the original doped carriers in the accumulation regime, there will be a measurable enhancement in electrical conductance. In the linear regime the conductance is expressed as:

$$(25)\ \frac{\partial I_{SD}}{\partial V_{SD}} = \mu \frac{C(V_{gate} - V_{threshold})}{L^2}$$

Where μ is the majority carrier mobility, C the gate-NW capacitance, L the gated nanomaterial channel length, V_{gate} is the gate voltage, $V_{threshold}$ is the threshold voltage of the device, V_{SD} is the source-drain voltage and I_{SD} is the current flowing through the nanomaterial. In addition, the capacitance of the device, for typical FET geometries as presented in Figure 30, is calculated according to the shape of the nanomaterial, in case of nanotubes or nanowires it can be modeled as:

$$(26)\frac{C}{L} = \frac{2\pi\varepsilon_0\varepsilon_r}{cosh^{-1}\left(\frac{(R+h)}{R}\right)}$$

Where h is the gate oxide thickness, R is the nanomaterial's radius, ε_0 is the vacuum permittivity, ε_r is the oxide relative dielectric constant, L is the gated nanomaterial length and C is the capacity [253].

In order to characterize the FET device, one should examine the I-V and the Trans-Conductance (TC) curves. I-V curve is typically made of two regions, the linear and the saturation. The linear region suggests that the electrical contacts are ohmic in nature, implying there are no contact issues between the nanomaterial and the metallic source-drain electrodes (Schottky barrier). The saturated region shows the maximal current that can flow through the nanomaterial for a specific gate voltage. By measuring the I-V curve at different gates the response will demonstrate the conductance type of the nanomaterial as p - or n - type. The TC curve is essentially a measure of the current response with respect to the gate voltage. The TC has four regions: the 'off' region where the device has the minimal current for a given V_{SD}, the subthreshold regime where the current changes exponentially with the change in V_G, the linear regime where the change in V_G changes the current linearly and the saturation regime where the current through the nanomaterial is constant and at its maximum value [254,255]. It is possible to estimate the charge carrier mobility from the TC according to:

$$(27)\frac{\partial I_{SD}}{\partial V_G} = \mu\frac{CV_{SD}}{L^2}$$

Where I_{SD} is the current through the nanomaterial, V_G is the gate voltage, μ is the charge carrier mobility, C is the capacitance, V_{SD} is the source-drain voltage and L is the gated nanomaterial length [256]. The gate dependence of the nanomaterial FET can be explained by the potential effect on the energy bands of the junctions between the nanomaterial and the metallic contacts. When $V_G > 0$, the bands are lowered, which deplete the holes in the p-type nanomaterial and suppresses conductivity, but leads to accumulation of electrons in the n-type nanomaterial and enhance the conductivity. Conversely, when $V_G < 0$ the bands in the p-type will raise and the conductivity will increase, where as in the n-type the bands will decrease and conductivity will decrease [256]. An example for electron transport measurements, I-V and TC curves, are shown in Figure 31.

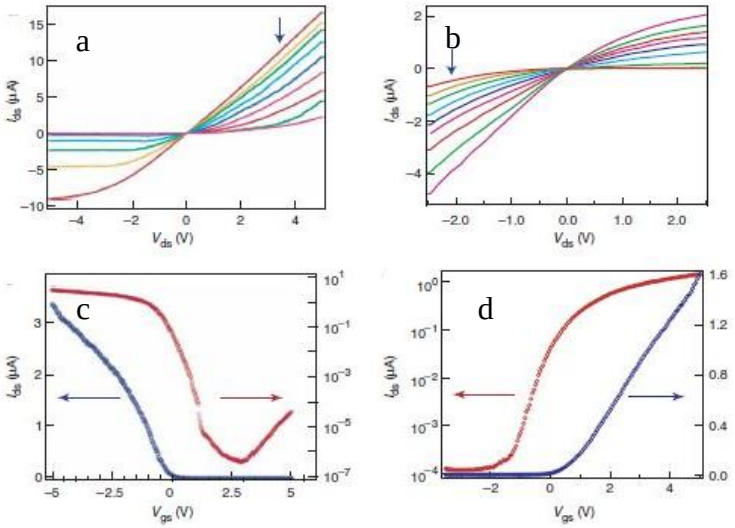

Figure 31: Transport measurements of nanomaterial FET devices in air (a) I-V curves of a p-type channel at different V_G; (b) I-V curve of an n-type channel at different V_G. The gate voltage values from the arrow down are {-5V, -4V, -3V, -2V, -1V, 0V, 1V, 2V and 3V}; (c) TC chart for p-type channel and (d) TC chart for n-type channel. For both the red line show the response in logarithmic scale and the blue line in linear scale.

These transport properties are determined by various important factors such as structure, dimensions, surface condition, doping level and orientation [256]. FET sensor devices have caught the interest as a general platform for ultra-sensitive electrical detection of different chemical and biological species [257]. They have been employed for various sensing applications due to their biocompatibility [258], convenient surface modification [259], exceptionally high surface-to-volume ratio and small cross-section. This enables an increase of sensitivity, fast response and good reproducibility [260,261].

Selectivity denotes the ability of receptors to bind with the desired target in the presence of various molecules. The time taken by a sensor to produce a stable signal change defines the settling time, the time to capture a certain amount of analyte molecules, which is determined by their concentration, diffusion coefficient through the carrying medium and their association affinity to the receptors on the FET sensor's surface. Sensitivity corresponds to the relative change in sensor characteristics upon the binding of analyte molecules on the nanomaterial's surface [262]. The methodology of FET sensors is based on the local change in charge density, which characterizes the recognition event between a target molecule and the surface receptor. That change in surface chemical potential is detected as an applied gate voltage to the NW, and affects the current within it. The binding of the analyte to the NW surface will cause a depletion effect if its charge is positive, and accumulation if the charge is negative for p-type nanomaterial channel [263]. The fingerprinting of such sensors is achieved by exploiting the kinetic and thermodynamic properties of the surface receptors and analyte association, through pattern recognition. The kinetics will influence the slope of the current-time chart—binding and releasing dynamics will keep a constant ratio K for every analyte-receptor couple (equation 1.7). The thermodynamics of the binding process will influence the height of the signal. By taking these factors into

consideration, it is possible to create a library of analytes fingerprints. The schematics of these sensing steps are shown in **Error! Reference source not found.**.

$$(28)\, K = \frac{S_{bind}}{S_{release}}$$

Where K is the slopes ratio, S_{bind} is the slope during the adsorption and $S_{release}$ is the slope during desorption. The slopes values are determined by the best linear compatibility factor (R^2)

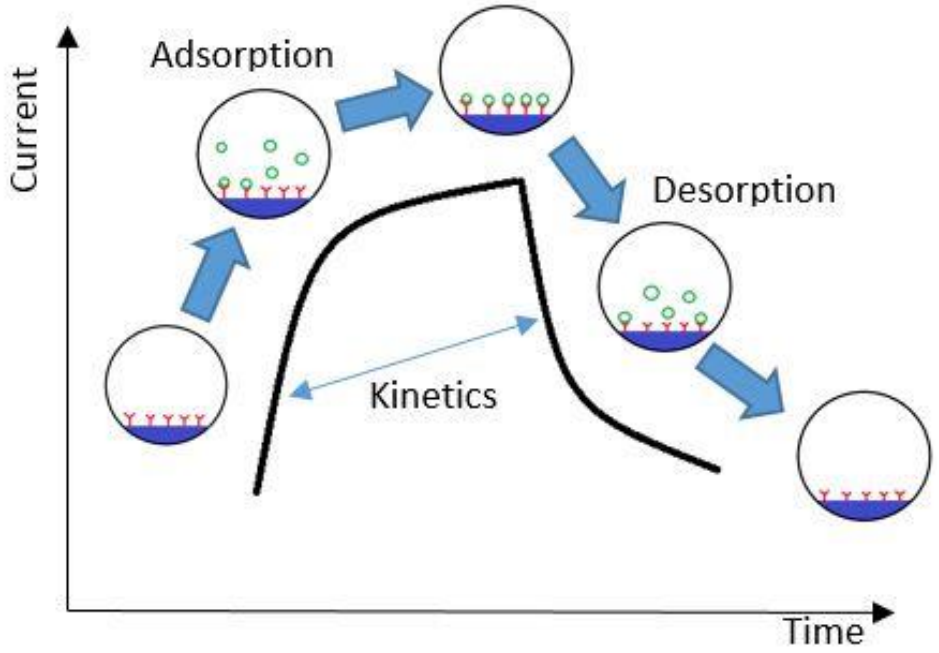

Figure 32: Signal schematics of the adsorption and desorption of chemical species on the NW surface and their effect on the FET current.

One of the initial approaches of this work was to fabricate an SWCNT FET-biosensor for the detection of different biological agents in the food and agriculture industries. The SWCNT had to be with a zigzag chirality to assure semiconducting behavior. The fabrication was done according to the schematic in Figure 33.

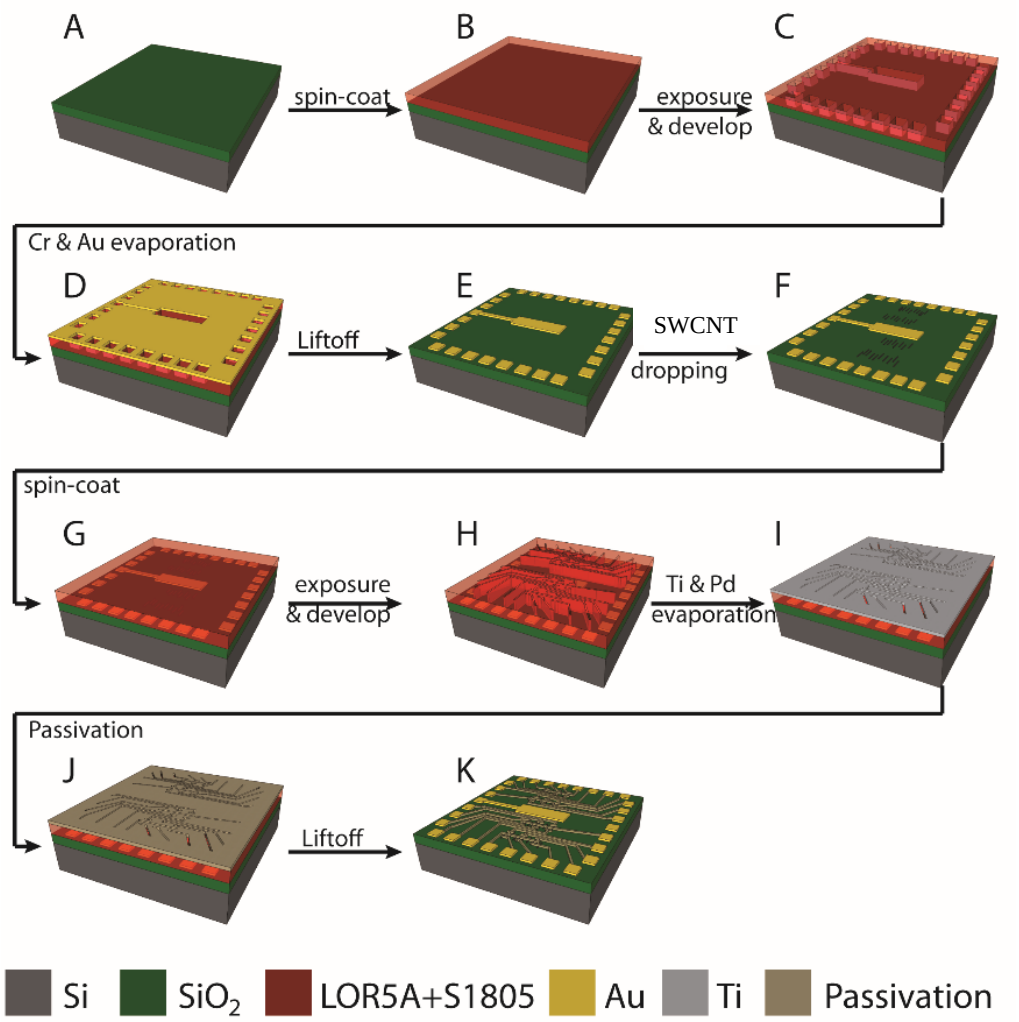

Figure 33: Fabrication method of the SWCNT-FET biosensors.

The concept was to fabricate a common source, with four drains at a distance of 2 µm between them. The gate potential will be transferred via deionized water due to their polar nature and their high resistivity of 18.8 MΩ. The design, microscopy image, and fabricated chips are shown in Figure 34.

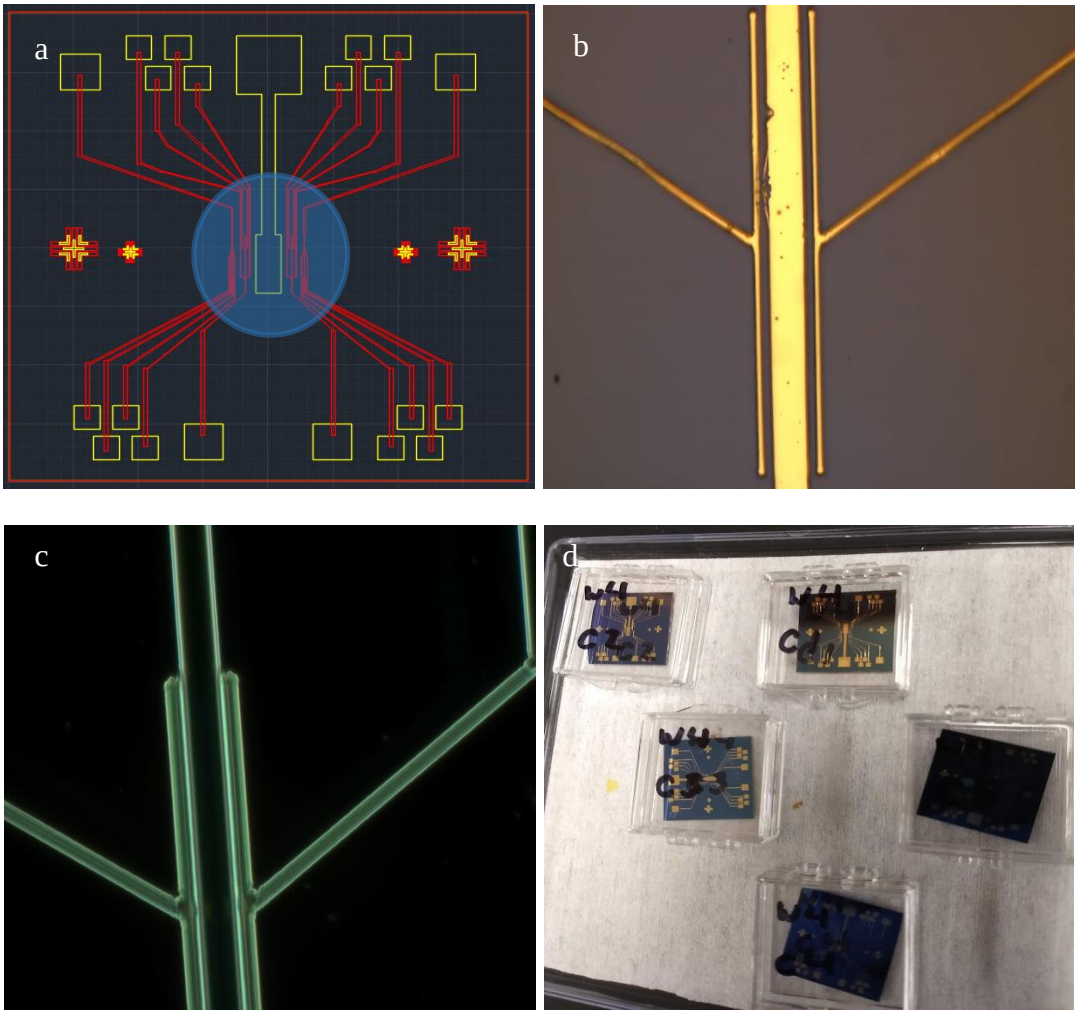

Figure 34: CNT-FET device. (a) Design; (b) Bright field microscopy image of the source and the drain; (c) A dark field microscopy image of the source and the drain; and (d) the fabricated SWCNT FET-Biosensor.

Following the fabrication, the devices were characterized as previously described. I-V curves and TC charts were measured and prepared to better understand the capabilities and working potentials of the devices as seen in Figure 35. The device exhibited a bi-polar behavior around VG = 0 V, as showed from its TC chart in Figure 35 (a). Current increased under both negative and positive potentials to the same order of magnitude and that suggests that the working gate potential should be set to the minimum point since any change will be very noticeable. There is a slightly higher current and slope on the positive side and a saturation asymptote on the negative

side, which suggests that the SWCNT was behaving more as an n-type. The I-V curve in Figure 35 (b), showed parallel linear slopes, where the higher curves belonged to the more positive gate potentials as was expected from an n-type device and the V_{SD} should be between 0.1 V to 0.3 V so that the sensor will have the ability to have higher and lower I_{SD} as a result of successful surface attachment.

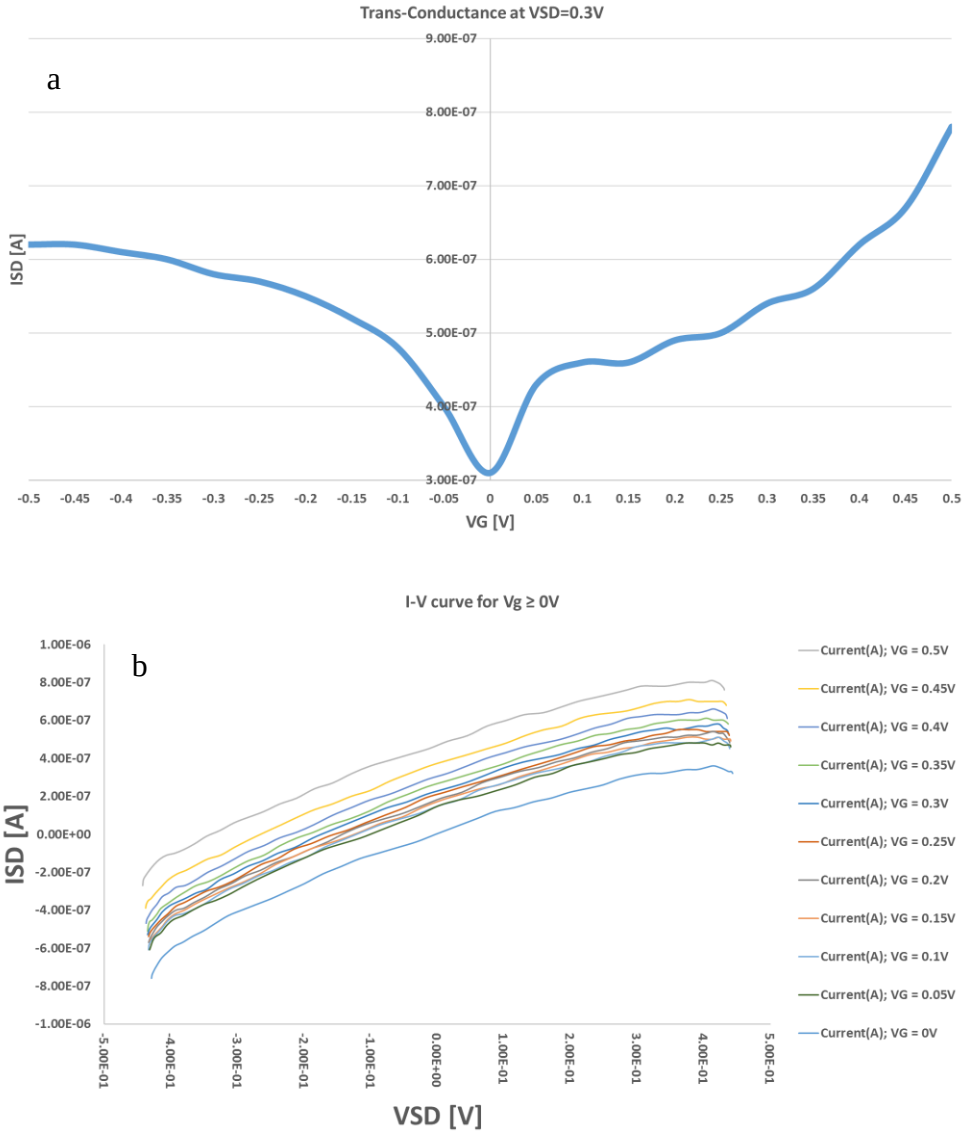

Figure 35: The characteristic charts of the FET-Biosensor. (a) TC chart and (b) I-V curves.

These devices can be used for detection experiments after surface immobilization of a biorecognition molecule and an experimental adjustment of the VSD the increase the sensor's sensitivity.

APPENDIX I

SIGNAL TO NOISE CALCULATION

The electrochemical biodetection uses recognition molecules to determine the presence of their target analyte within a specific sample. From their structure and mode of operation ECBS are susceptible to thermal fluctuations from the environment and chemical or electrochemical reactions. Also, due to their electric nature, ECBS are affected by electromagnetic fields that exist in the vicinity of any active electric circuit with non-ideal isolation. All of these in addition to mechanical forces and human handling inconsistencies are sources of variability within the ECBS response to the analyte which is commonly known as measurement or statistical noise and exampled in Figure 36 [51,264].

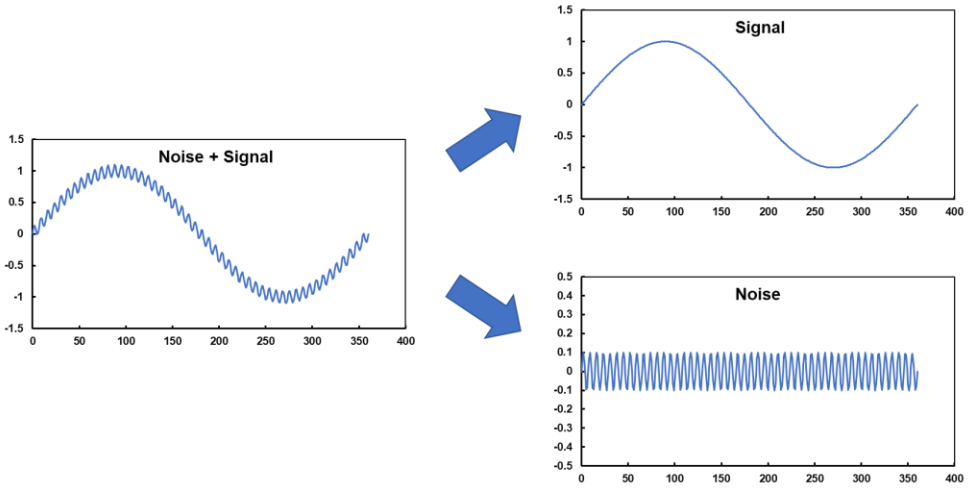

Figure 36: Signal and noise

The liquid sample that contains the target analyte, contains in addition many other salts, organisms, and biomolecules. All of these are susceptible to thermal fluctuations that induces Brownian motion and diffusion. Statistically, since the movement is random, it reduces the amount

of biorecognition element collisions with the target analyte within the sample. This characteristic will also increase the non-specific interaction between other components of the sample and the working electrode's surface. Using the Markov model for probabilistic motion creates the probabilities of a particle to move from one place to another in a given time. The state transition probability from state i to state ii for coordinates R_i and R_{ii} can be written as seen in eq. (1):

$$(29)\, m_{i,ii} = \Pr[R(\Delta t) = R_{ii} | R(t = 0) = R_{ii}]$$

Where R(t=0) and R(Δt) are the sets of coordinates for the location of the analyte at time 0 and t respectively. Due to the relative high number of target analyte particles in a sample and that the analyte movement is independent of the biorecognition molecule it is safe to assume a homogeneous Markov process. It is therefore possible to model special distribution of target analyte particles as seen in eq. (2):

$$(30)\, X(t) = nx(k\Delta t) = n[M(\Delta t)]^k x(0) = [M(\Delta t)]^k X(0)$$

Where X(t) is the concentration distribution of the target particles, n is the number of analyte particles, x(kΔt) is the probability distribution, k is an integer, M(Δt) is the transition matrix, x(0) is the probability distribution at t=0, and X(0) is the initial concentration of the analyte [265–267].

After the collision probability was described, next is to model their interaction between the biorecognition element A and the target analyte B. The assumption of this model is that all receptors are capable of attaching, each biorecognition molecule can interact with only one target analyte molecule, A and B have an association rate k_1 and disassociation rate k_{-1} as seen in eq. (3) and (4):

$$(31)\, A + B \overset{k_1, k_{-1}}{\longleftrightarrow} AB$$

$$(32)\frac{\mathrm{dC(AB)}}{\mathrm{dt}} = \mathrm{k_1 C(A)C(B)} - \mathrm{k_{-1} C(AB)}$$

Here C regarding the concentration of the element within the brackets. Combining eq. (4) with eq. (1) and (2) it is possible to model the probability of the capture of a target analyte by a biorecognition molecule as seen in eq. (5):

$$(33)\, m_{1,captured} = \alpha k_1 \Delta t$$

Here $m_{1,captured}$ is the association transition probability and α describes the immobilization of the biorecognition element and the distance between the analyte and the biorecognition element [266]. The last part of the biosensor to model is the transduction. The output signal of the transduction process can be modeled according to eq. (6):

$$(34)\ s(t) = TX(t) + u_T(t)$$

Where s(t) is the output signal, T is a matrix of detectable results, and $u_T(t)$ describes the random process of the noise added by the transducer itself. X(t) is assumed to be an expected behavior by using the average concentration distribution ($\overline{X(t)}$) eq. (6) will transform into eq. (7):

$$(35)\ s(t) = T\left[\overline{X(t)} + u_X(t)\right] + u_T(t)$$

Where $U_X(t)$ describes the deviation of the actual concentration distribution from the average value. To make the performance of different transducers comparable, mainly due to the large variability between different transducers, the equivalent signal should be used. The equivalent signal ($s_{eq}(t)$) is composed of assumed concentration distribution and its uncertainty. To do so eq. (7) will be divided by the effective gain of the biosensor as seen in eq. (8):

$$(36)\, T_\Sigma = \frac{\Delta s(t)}{\Delta n} = \frac{T\overline{X(t)}}{n}$$

Where T_Σ is the expected output signal change according to the concentration of the analyte. The master equation for the biosensor that is only dependent on the amount of target analyte can now be described by eq. (9):

$$(37)\, s_{eq}(t) = n + (T_\Sigma^{-1}T)u_x(t) + T_\Sigma^{-1}u_T(t)$$

This equation displays the obtained signal and the major noise sources in the system. The noise level will cause variability in response around its average value and might mask small reactions that are in the same order of magnitude. The parameter of a biosensor that will determine its resolution is the signal-to-noise ratio (SNR). The higher the SNR is the higher the lower the threshold (change from baseline) and the resolution (change between different concentrations) will be [51,56,267,268].